Sheffield Hallam University

A Sheffield Hallam University thesis

Effects of the Weld Thermal Cycle on the Microstructure of Alloy 690

James Robert Tuttle

A thesis submitted in partial fulfilment of the requirements of Sheffield Hallam University for the degree of Master of Philosophy

July 1997

Collaborating Organisation:

Health & Safety Executive; H.M. Nuclear Installations Inspectorate

'Vulgo enim dicitur: Icundi acti labores.' (for it is commonly said: completed labours are pleasant) - Cicero (106-43 B.C.) De Finibus Bk. 2 Ch. 105.

Declaration

During the period of registration for the Sheffield Hallam University degree of M.Phil. the candidate has not been registered for any other Sheffield Hallam University award or for a University degree.

The results and theories presented in this thesis are original except where reference is made to previous work.

Signed: Date: 14th July 1997

Acknowledgements

James Robert Tuttle

July 1997

Associated Studies and Work

During the course of the research studies the student has attended and successfully completed the following units from the MSc course in Materials Process Engineering at Sheffield Hallam University:

High Strength Alloys

Energy Management Studies parts I & II

Attended and successfully completed an examination to pass with credit level on the following short course:

Royal Microscopical Society (RMS) Spring School in Electron Microscopy - University of Leeds - 5-10 April 1992

Attended the following short course:

Thermocalc - Computer Modelling of Materials Thermodynamic Systems - Imperial College - 19-21 April 1993

Attended the following conferences:

Materials Selection for Design and Manufacture - Institute of Materials, London - November 1991

International Metallographic Society Lectures Session - Micro '92 Exhibition - Ramada Inn, London - 10 July 1992

Presented the technical papers detailed below:

'The Effect of the Weld Thermal Cycle on the Microstructure and Corrosion Resistance of Alloys 690, 600 and 800'; A Smith, R Stratton, R Tuttle - Sixth International Symposium on Environmental Degradation of Materials in Nuclear Power Systems: Water Reactors - Bahia Resort Hotel, San Diego, USA - 1-5 August 1993.

'The Effect of the Weld Thermal Cycle on the Corrosion Resistance of Alloy 690'; R Tuttle - Junior Euromat '92 - Swiss Federal Institute of Technology, Lausanne, Switzerland - 24-28 August 1992.

'Is Alloy 690 the Answer?'; R Tuttle - International Workshop on PWR Steam Generator Research - Hallamshire Business Park, Sheffield - 8 April 1992.

Abstract:

Alloy 690 has been introduced as a material for use as the heat exchanger tubes in the steam generators (SGs) of pressurised water reactor (PWR) nuclear power plant. Its immediate predecessor, alloy 600, suffered from a number of degradation modes and another alternative, alloy 800, has also had in-service problems. In laboratory tests, alloy 690 in both mill annealed (MA) and special thermally treated (STT) condition has shown a high degree of resistance to degradation in simulated PWR primary side environments and other test media.

Limited research has previously been undertaken to investigate the effects of welding on alloy 690, when the material is used in SG applications. It was deemed important to increase knowledge in this area since fabrication of PWR SGs involves gas tungsten arc welding (GTAW) of the heat exchanger tubes to a clad tubeplate. For this research investigation welded samples of alloy 690 have been produced in the laboratory using a range of thermal cycles based around recommended weld parameters for SG fabrication. These samples have been compared with archive welds from PWR SG manufacturers. A number of welds incorporating alloy 600 and a number using alloy 800 tubing material have also been fabricated in the laboratory for comparative purposes. Two experimental melts have been produced to study the effects of Nb substitution for Ti in alloy 690 type materials.

Welded and unwelded specimens have been studied, analysed and tested using a variety of methods and techniques. A method of metallographic sample preparation for transmission electron microscope (TEM) thin foil specimens has been developed and documented which ensures foil perforation in a specific region. The effects of Nb substitution for Ti have been discussed. Chemical balances and microstructures in the fusion zone of welds manufactured from alloy 690 tubing incorporating alloy 82 weld consumable have been shown to be non-ideal. Within the heat affected zone (HAZ) of both laboratory produced and archive welds the microstructures have been identified as detrimentally altered from the STT condition original tubing material(s). A number of conclusions have been drawn and recommendations have been made for future work.

James Robert Tuttle - BEng CEng MIMechE

Table of Contents

APPENDIX

List of Figures

List of Tables

1. Introduction

1.1. Background and Motivation

The work in this thesis is concerned with the materials used in heat exchanger tubes in Pressurised Water Reactors. There are currently three Nickel-Chromium-Iron (Ni-Cr-Fe) materials being used for the heat exchanger tubes in Pressurised Water Reactor (PWR) nuclear power plant steam generators (SGs) - alloys 600, 800 and 690. Alloy 690 is the specified steam generator tubing material for the first British Pressurised Water Reactor (Sizewell B PWR). Sizewell B has been constructed using the standard Westinghouse 'four loop' system. Each loop has a steam generator (heat exchanger) between the primary circuit of the reactor core and the secondary circuit of the steam turbines/generators. Figure 1 shows a schematic diagram of a typical PWR system.

As the literature survey in this thesis will show, there has been a wide range of degradation problems associated with PWR steam generator tubing on both primary and secondary sides. Continued efforts to reduce, or eliminate, these degradation problems has led to a number of modifications in SG design, materials selection and the methods of materials processing used for this application. The latest material used for PWR SG tubing is alloy 690, which it is hoped will provide long-term reliability up to PWR service life of around forty years. This work is concerned with an examination of problems which might occur with alloy 690 tubing as a result of fusion processes. During SG fabrication the heat exchanger tubes on the primary side of the tubesheet are welded at both ends. Any alterations to tube microstructure and/or composition in the weld and adjacent area could affect the resistance of the

1

material to degradation in operating environments and thus the reliability and efficiency of the SG.

As the work in this thesis is concerned with certain aspects of the PWR's it is appropriate at this point to outline briefly the modus operandi of the particular PWR with which the work is concerned. The principle of operation of the Sizewell steam generator is detailed at length by Sylvester *et al* [1]. A summary of the operational parameters is now given.

1.2. Sizewell B Steam Generator Mode of Operation

The steam generators for the Sizewell station are based on the Westinghouse Model F steam generator design, with minor modifications to comply with United Kingdom Safety Legislation [1]. The steam generators are substantial structures, being over twenty metres in height and approximately four and a half metres diameter across the top steam separator section of the component. Figure 2 shows details of the Sizewell B nuclear steam supply system whilst figures 3 and 4 show the Westinghouse model F steam generator dimensions and internal structure respectively. The steam generators are the second largest components in the PWR nuclear steam supply system, being exceeded in size only by the reactor itself.

The Model F is a vertical U-tube heat exchanger design which uses high temperature pressurised water on the primary side, which flows around the reactor core and, via heat transfer through the SG tube walls, the secondary side water is boiled. This eventually produces dry saturated steam on the secondary side. In this manner the SG tubes form the interface between the continually re-circulating, pressurised, primary side coolant and the secondary side fluid where boiling produces steam which subsequently drives the turbines that generate electricity.

1.2.1. Primary side

The primary PWR water, which is heated in the reactor vessel, enters the steam generator tubes at a temperature of 326°C and is maintained at a pressure of 155 bar to prevent boiling. The water is relatively pure with boric acid additions for neutron absorption together with lithium hydroxide for control of primary circuit dose rates. To further inform the reader, details of a simulated PWR primary water chemistry as used by Skeldon *et al* [2] for their investigations is shown below:

Simulated PWR Primary Water [Skeldon *et al*]		
H_3BO_3	(ppm)	6000
Li^+	(ppm)	2
Oxygen	(ppb)	<2
Hydrogen	(cm3kg^{-1}STP)	0-50
Cl^-	(ppb)	<50
F^-	(ppb)	<50
So_4^{2-}	(ppb)	<30

The water flows through the U-tubes, where heat transfer takes place, and exits from the opposite side of the divided channel head. The primary and secondary sides are separated by a thick forged plate called the tubesheet. The U-tubes are held firmly in the tubesheet by tube expansion and welding, and are supported laterally along their length by tube support plates. In the U-bend area, support is provided by a series of anti-vibration bars.

1.2.2. Secondary side

On the secondary side, feedwater enters through a feedring and is directed downward by inverted J-tubes. The feedwater, mixed with the recirculating water from the moisture separators, flows down the annulus between the tube bundle wrapper and the lower shell and enters the tubesheet bundle just above the tubesheet. The secondary side water is purified and treated river, lake or sea water. A flow distribution baffle enhances horizontal sweeping velocities across the top of the tubesheet, so minimising any lower flow zone at the centre. The steam-water mixture (wet steam) produced rises through the tube bundle whilst heat is transferred from the primary side fluid, through the tube walls, to the secondary side fluid.

The wet steam that leaves the tube bundle then passes through a centrifugal moisture separator followed by a secondary moisture separator, to produce dry saturated steam at a temperature and pressure of 285°C and 69 bar, respectively, with a final moisture content of less than 0.25% by weight. Steam then exits through a nozzle in the upper head. The steam nozzle incorporates an integral flow limiter that restricts the flow during any possible steamline break. Water that is separated from the steam is mixed with the entering feedwater and recirculated through the steam generator. The steam exiting the upper head is fed to the main turbine generators. The overall power train at Sizewell B incorporates two turbine-generator units, each of 630 MW nominal output and each machine draws one half of the steam flow generated via the four steam generators by the 3425 MW(Th) PWR reactor.

1.3. Tube-to-tubesheet section

At Sizewell B the SA508 Class 3 ferritic tube baseplate (normally referred to as the tubesheet) is clad on its primary side face with the Ni-Cr-Fe weld metal alloy 82 to a

4

minimum depth of 5mm. The specification and selection of this material, as opposed to SA 533 Grade A Class 2 and other SA 508 materials previously used, is as recommended by the United Kingdom Atomic Energy Authority (UKAEA) study report [3]. The reasons for this change of material are documented in detail elsewhere [1] but to summarise, the material exhibits a satisfactory fracture toughness for its duties and the lower carbon together with the higher manganese/sulphur ratio make the material less susceptible (than previously employed materials) to liquation cracking during the weld cladding overlay operations. Further analysis and tensile requirements for the SA 508 Class 3 and its comparison to SA 508 Class 2A is to be found in the paper of Sylvester *et al* [1]. The tubes, 5,200 per steam generator, are placed in position through the clad and drilled tubesheet where they are hydraulically expanded before being autogenous Gas Tungsten Arc Welded (GTAW) into place at either end of each tube to the clad primary side tubesheet. Further details of the Westinghouse welding specifications for PWR steam generator tube welding are to be found in the experimental methods section of this thesis. Thus 10,400 tube-to-tubesheet welds exist in each steam generator making a total of 41,600 tube-to-tubesheet welds in a four-leg PWR system such as the Sizewell B plant.

1.4. Tube Manufacture

The successful manufacture of SG tubing requires the use of a combination of both mechanical and thermal processes under highly controlled conditions. Each process is important and can affect the microstructure, and will be examined where appropriate at a later stage. A summary of the typical material processing route as used by the French tube manufacturers, Vallourec, [4] is as follows:

⇒ Alloy Melting (Vacuum Induction Process).

⇒ Bar Forging.

⇒ Hot Extrusion to Hollow Shell .

5

⇒ Cold Reduction to Final Dimensions via Cold Pilgering Process Multiple Step Operation with Intermediate Mill Anneals.

⇒ Final Cold Reduction to Finished Size via Drawing Process for Strictest Dimensional Requirements.

⇒ Final Mill Anneal.

⇒ Roll Straightening.

⇒ Surface Preparation (Shot Blasting Inside Diameter and Grinding Outside Diameter).

⇒ Special Thermal Treatment (STT).

⇒ Bending to U-Section.

⇒ Stress Relieving of Tight U-Bends.

⇒ Final Inspection and Packing.

1.5. Thesis Scope and Objectives

A study of the effects of the weld thermal cycle on the microstructure of alloy 690 was chosen for the research project presented in this thesis. Emphasis is given to the microstructural aspects, whilst recognising the importance of corrosive attack in life-cycle considerations. Corrosive attack has, historically, been a major limiting factor in PWR steam generator operations and any microstructural alterations from the effects of welding might effect the material resistance to this mode of degradation. To this end alloy 690 material has been subjected to weld thermal cycles typical of those expected weld procedures specified for PWR fabrication. For comparison purposes alloys 600 and 800 have also been welded to PWR specifications. A range of heat inputs has also been examined for alloy 690 and a number of samples have been subjected to two weld thermal cycles, in order to simulate weld repair.

Two experimental alloy 690 type melts, with Nb substitution for Ti, were produced in a vacuum furnace then cold rolled, heat treated, welded to PWR SG specifications

and the effects studied. A number of the welded samples were subjected to Modified Huey testing in order to ascertain if 'sensitisation' was present. Alloy 690 samples (in both welded and as received form) are studied to failure under Constant Extension Rate Tests (CERT) in an argon environment. By using weld thermal cycles based upon established industrial practice and then studying the effects of changes in weld parameters together with the associated tests undertaken in this project, the work updates current knowledge on SG tubing materials. Conclusions are drawn as to the effect of the weld thermal cycle on alloy 690 and recommendations made for future investigations.

1.6. Thesis Layout

The thesis is comprised of seven chapters and its layout and presentation conform with the regulations of the Research Degrees Committee and the Research Office of Sheffield Hallam University. The contents of each chapter are summarised as follows:

Chapter 1, the current chapter, introduces the reader to the project. The research is discussed within the context of the Sizewell B PWR and typical operating methods are given.

Chapter 2 presents a summary of previous research, relevant literature and discussion in areas related to the thesis. In particular, research on the three main materials currently, or recently, used for SG tubing (namely alloys 690, 600 and 800), historical failures and failure modes of SG tubing and issues related to the welding of the tubing materials together with any associated weld consumables.

Chapter 3 introduces the experimental techniques used for the research - including details of the materials, equipment, test conditions and methodology. The welding parameters selected for the purposes of these investigations is also detailed together with the reasons for these choices.

Chapter 4 incorporates the experimental results obtained during laboratory investigation. Where appropriate, the reader is directed towards the necessary figures and tables which accompany the laboratory investigations and results.

Chapter 5 presents discussion on the issues highlighted both by the literature and the experimental results. Particular focus has been placed upon the microstructural changes within the heat affected zone(s) following welding. Also highlighted are differences in chemical composition of the fusion zone(s) before and after the application of a weld thermal cycle.

Chapters 6 and 7 summarise the conclusions drawn and state the principal research contributions of the thesis. Recommendations for further research are also indicated in this section.

Details of the references used within the thesis are listed immediately following chapter 7.

The appendix is at the rear of the thesis. It is in this section that the majority of the figures and tables relating to literature, experimentation, results and discussion have been placed together, for the convenience of the reader.

Having discussed the specific operation of the Sizewell B PWR, outlined the fabrication route for the SG tubes and detailed the thesis scope and organisation, it is appropriate at this stage to review relevant literature on steam generator tubing materials and the welding of such alloys. Also reviewed are details of general operating experience with PWR plant, together with such laboratory investigations and testing of SG materials as have been published

2. Literature Review

2.1. Materials Performance in PWR Service

PWR design has evolved rapidly since the first PWR power plant was commissioned in Shippingport USA in 1957, and over two hundred reactors have now been ordered in over twenty countries. Steam generator operating experience with PWR power stations over the past thirty seven years has shown steam generators to be a major area for failures due to problems associated with the corrosion of the internal heat exchanger tubes.

One such problem has been denting of the tubes, induced by constriction resulting from the accumulation of by-products of corrosion of the steel support plate. The denting arose from plastic deformation of the tubes at the support plate intersections due to squeezing of the tubes by the build-up of corrosion products in the gaps between the tubes and the tube support plates. Furthermore, this plastic deformation of the tubes induces high residual tensile stresses at the inside surface of the tube which could result in stress corrosion cracking.

The current practice, as in the Westinghouse model F, of employing tube support plates with a broached quatrefoil hole rather than a drilled cylindrical hole has largely alleviated the denting problem in modern PWR plant. The quatrefoil hole provides four flow areas in the plate surrounding each tube thus offering a resistance to chemical concentration, the tube contact area is minimised and flow along the outer tube surface is therefore increased. Thus the potential for dryout and any subsequent

impurity concentration is reduced, whilst a high structural load carrying capability is maintained. A diagram of a typical broached quatrefoil hole is shown below:
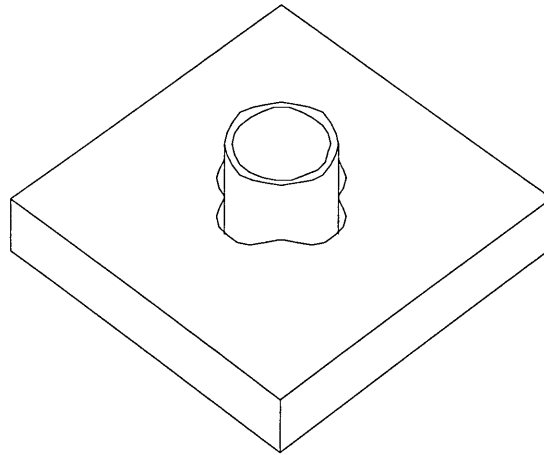
Quatrefoil hole for tube with tube inserted

In other cases, experience has shown that thinning and wastage of the tubes has occurred. This is a localised dissolution of the tube wall on the secondary-side caused by a chemical attack from acid phosphate residues, concentrated in low flow velocity areas adjacent to the tubesheet and in those same areas when a tubesheet sludge pile has created a crevice effect. In order to minimise this form of tube degradation a number of remedial measures have been used, including: crevice flushing, boric acid soaks (off-line); on-line boric acid addition(s), temperature reduction; sludge pile removal (by chemical cleaning or water lancing) and (in severe cases of degradation) by tube sleeving.

Stress corrosion cracking (SCC) on the primary side tubing inner surface and the secondary side tubing outer surface of PWR SG has frequently occurred. Stress corrosion cracking occurs in areas where high stresses exist. The term Caustic Stress Corrosion Cracking (CSCC) refers to the special case of SCC where a corrosion agent of a caustic nature has been identified as being present. The CSCC form of

tube degradation has been observed on the secondary side in the roll transition zone of the tubes. Specifically this has been found to occur in the crevice between the tubes and tubesheet in the case of partial rolling, and at the tubesheet surface level when there has been full depth tube-to-tubesheet expansion. Where the aggressive agent cannot be identified the phenomenon is referred to as Secondary Side Stress Corrosion Cracking (SSCC). SSCC has been observed in the same areas as CSCC.

Primary Side Stress Corrosion Cracking (PSSCC) refers to stress related corrosion of the tubes on the primary side, where the water chemistry environment is highly controlled. This form of corrosion has been observed on alloy 600 in several regions of the SG, in particular in the tube rolling transition zone, in the tube section within the tubesheet, at the apex of the small U-bent inner tubes of the tube bundle and also at the transition between the straight and bent portions of the tubes.

The failure phenomena discussed above are now well documented and have been attributed to a combination of factors which are necessary in order for failure to occur. These factors are:

◊ Corrosive environment:-

On the primary side this relates simply (and perhaps surprisingly) to dearated, doped water at high temperature; whilst on the secondary side this relates to salt concentrations at lower temperatures.

◊ High stresses:-

The presence of high stress levels with a surface tensile component.

◊ Material susceptibility:-

A material which is chemically and/or is microstructurally inappropriate for the PWR service conditions encountered.

11

Thus, correct material selection is of great importance in PWR steam generator design, since the materials are being submitted to high temperature and high pressure operating conditions over considerable periods of time. Further, it appears likely that the welding of the tubes into position may alter the chemical composition from the preferred one in the weld fusion zone and in addition alter the, previously optimised, microstructure within the weld heat affected zone (HAZ). The welding process itself will leave residual stress within the section. This is primarily due to the fusion zone melting and then contracting on solidification and subsequent cooling from the melting point to room temperature whilst being constricted in its movement by lesser affected and unaffected adjacent areas of material.

Any residual stresses from the weld thermal cycle are often reduced by a post weld heat treatment (PWHT). Domain *et al*, [5] during their investigations into the effect of microstructure on the stress corrosion cracking resistance of alloy 600, comment on the advantages of a simulated PWHT (18hrs @ 621°C). However, the weld procedure data sheets for the Sizewell B SG tube-to-tubesheet welds indicate that no PWHT was applied.

In the HAZ the weld thermal cycle can affect the microstructure of that region. In the area of the HAZ immediately adjacent to the fusion line the peak temperature will be close to the melting point, T_m, of the material. At these temperatures grain coarsening can occur, even at the short time of exposure typical of a weld thermal cycle. Also, at the temperatures experienced during welding, the grain boundary carbides formed by the expensive and time consuming STT could be taken back into solution and thus negate the beneficial effects of the STT [5], [13] and increase the material susceptibility to SCC.

Hence, the requirements for possible failure by SCC exist within the fusion and/or heat affected zones following the weld thermal cycle. This, together with the associated steam generator life-cycle requirements, and the dire consequences of any catastrophic failures, show the research undertaken to be appropriate since materials degradation within the steam generators is still a major limiting materials issue in PWRs at the present time [6], [7], [8], [9].

2.2. Materials used in steam generator tubing

The three materials currently in use for steam generator heat exchanger tube are, as previously stated, alloys 690, 600 and 800. The chemical compositions of these materials is to be found in the appendix, table 1. The materials are fully austenitic in nature. Alloys 690 and 600 are thermally treated for PWR applications, to produce a carbide morphology of semicontinuous chains of carbide precipitates at the grain boundaries. The alloy 800 tube samples used in this research programme contained a grain boundary carbide morphology consisting of an equal mixture of semicontinuous chains and discrete carbides. Alloy 600 was, to all intents and purposes, the predecessor of alloy 690 in Nuclear PWR applications. Steam generators tubed with Alloy 600 are susceptible to corrosive attack in environments of primary and secondary water circuits as has been demonstrated by laboratory studies and service experience [5]. Further, it has been shown that Alloy 800, an alternative material for use as steam generator tubing, is also susceptible to corrosion under certain conditions and environments [10], [11].

Alloy 690 has ostensibly better corrosion resistance than alloys 600 or 800 [12] in the primary side PWR steam generator environment. This resistance has been attributed to its chemical composition and its microstructure [12], [13]. The material is subjected to time consuming and expensive thermal treatments in order to optimise

13

the microstructure and promote the grain boundary carbide precipitation which has been shown to be critical in corrosion control [13]. The carbon morphology has a pronounced influence on the corrosion resistance of these alloys in both primary and secondary side PWR environments [14] with a semi-continuous precipitation of chromium carbides being preferred. The heat treatments applied to the alloy 690 tubes of the steam generators prior to assembly, in order to obtain the preferred morphology, are typically in the form of a short high temperature mill anneal at 925-1100°C for 2-5 minutes, followed by a special thermal treatment (STT) of 700-750°C, in a vacuum, for 5-15 hours. Manufacturing practices differ in the actual time periods used for the STT, but detailed investigations by Smith on commercial alloy 690 tubing [13] revealed no discernible change in corrosion resistance for a given composition and corrosive environment for thermal treatment times greater than 1 hour. For alloy 600, at least 14 hours are needed to replenish the depleted region around the grain boundaries with chromium from the bulk material [14] but it is argued that since alloy 690 has *circa* 10% higher chromium content, a shorter thermal treatment may be adequate. The STT promotes the formation of the semi-continuous grain boundary network of chromium carbides and also allows sufficient time at temperature for the back diffusion of chromium to the denuded grain boundary regions.

2.3. Welding of SG Tubes

During the final stages of manufacture, and indeed after the STT has been completed, the tubes are positioned through the tubesheet then welded in place by autogenous GTAW. This process causes alterations to the ideal composition in the fusion zone and the microstructure, which has been previously optimised by use of the STT, is altered in the weld heat affected zone (HAZ) [14].

The tube-to-tubesheet welds on the Sizewell B plant are unlikely to be exposed to secondary side water environment since there has been full depth hydraulic expansion to eliminate a crevice and thus minimise any potential concentration zone (i.e. the crevice) on the secondary side of the tubesheet [4]. The 'full depth expansion' is accomplished hydraulically using high pressure water to expand the tube. In this context, 'full depth expansion' refers to expansion of the tube through the full depth of the tubesheet. This method of fabrication is designed to minimise the residual stresses placed in the expanded to unexpanded transition zone so lowering the probability of SCC occurring.

There is also the previously mentioned potential problem of grain growth in the heat affected zones of the welds which may give a region of lower proof or yield stress and an increased susceptibility to failure by mechanical overload. Whilst this is a theoretical failure mode, the design of the Westinghouse SG model F is such that the heat exchanger tubes (and therefore the welds also) are expanded into and supported by the adjacent tubesheet and therefore the welds cannot be subjected to any large radial strain.

The three candidate materials under investigation will now be examined separately, with particular emphasis on alloy 690.

2.4. Alloy 690

The continued failures and repairs on steam generators tubed with alloy 600 led to the development of alloy 690 as a suggested alternative material for this application. Alloy 690 contains nominally 10% higher Cr than alloy 600, with an associated lowering of the Ni content. Alloy 690 is characterised by a fully austenitic structure, with small amounts of inclusions and precipitates. The thermal treatments (STT)

15

given to the material for steam generator applications induce the precipitation of semi-continuous chains of Cr-rich carbides at the grain boundaries. A small number of Ti(CN) particles formed from the melt have been found to be distributed in the matrix.

Smith [13] undertook detailed investigations of alloy 690 (STT) and confirmed that the grain boundary carbides were exclusively of $M_{23}C_6$ form. During the investigations of intergranular precipitation on alloy 600 and alloy 690 undertaken by Stiller [15], a similar grain boundary carbide formation of semi-continuous chains of $M_{23}C_6$ to that revealed by Smith, was found in thermally treated alloy 690. In addition, one single M_7C_3 carbide was also found. It is important to note that both Smith and Stiller were investigating commercially produced alloy 690 samples.

The observation by Stiller of an M_7C_3 precipitate in thermally treated 690 confirms that this type of precipitate is thermodynamically stable in 690 material. If a driving force exists for M_7C_3 to convert to $M_{23}C_6$, then the single M_7C_3 found by Stiller also has the potential for in-service transformation. Should this occur in sufficient numbers, further Cr denudation of areas adjacent to the grain boundary would result which could leave these regions more susceptible to corrosive attack. Indeed, this was shown in work on alloy 600 by Hall and Briant [16] using laboratory tests with acidic environments. Hall and Briant also discuss the fact that in Ni-Cr-C alloys M_7C_3 is formed at temperatures above 1000°C, but below this temperature M_7C_3 may form initially but with increasing annealing time should transform to $M_{23}C_6$.

The hypothesis that $M_{23}C_6$ particles form from converted M_7C_3 particles was postulated by Lewis and Hattersley [17] as a precipitation carbide formation mode during their investigations on austenitic stainless steels. Angeliu and Was commented on the possibility of this conversion mode in Ni-Cr-Fe systems during

16

their investigations on high purity samples of alloy 690 type specimens [18]. There is evidence that such a conversion is possible in both austenitic steels and Ni-Cr-Fe alloy systems [19]. But the facts that no M_7C_3 particles were found by Smith [13] and the knowledge that, in stainless steels, with increasing Cr content the thermodynamic driving force is towards carbides of larger Cr content leads one to the conclusion that the formation of different carbide phases is most dependent upon Cr and C content with the possibility of some intermediate carbide formation being unproven.

The general sequence of carbide formation in stainless steel systems has been shown to be [20] of the simplified form:

$$(Fe,Cr)_3C \rightarrow (Cr,Fe)_7C_3 \rightarrow (Cr,Fe)_{23}C_6$$

with each increasing stage becoming the preferential formation with increasing wt% of Cr, assuming sufficient C is available for free carbide formation. Sarver *et al* [21] investigated the carbide distribution and stress corrosion cracking behaviour of alloy 690 and compared it with alloy 600. Amongst other findings, the studies of Sarver *et al* showed that with the higher Cr content of alloy 690 to that of alloy 600 and the associated lower solubility for C there would be an increased tendency for carbide precipitation. This again suggests direct formation of $M_{23}C_6$ in the high Cr alloy 690 system with no intermediate carbide formation.

The composition of the carbides formed depends in part upon alloying additions other than chromium as can be seen from detailed diffraction pattern analysis of the actual carbide structures found by Stiller [15]. The composition of typical grain boundary precipitates seen in the alloy 690 (STT) samples investigated by Stiller [15] were found to be as follows:

$$M_{23}C_6 = (Cr_{0.915}Ni_{0.050}Fe_{0.029}Ti_{0.006})_{23} (C_{0.981}B_{0.015}N_{0.004})_6$$
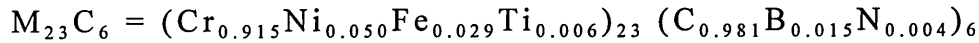
with the single M_7C_3 grain boundary precipitate found being of the form:

$$M_7C_3 = (Cr_{0.70}Ni_{0.25}Fe_{0.05})_7 (C_{0.81}B_{0.04}N_{0.15})_3$$
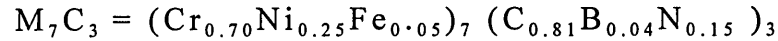
It is, however, unclear from the paper of Stiller [15] whether the composition values quoted were average values or derived from just one carbide in each case.

Detailed analysis of the effect of microstructure on corrosion resistance of alloy 690 by a number of researchers has shown that, when thermally treated, the material exhibits a high corrosion resistance in a range of environments [12], [13], [21], [22]. Airey *et al* [12] found alloy 690 (STT) to be less susceptible to stress corrosion cracking than alloys 600 and 800 in simulated PWR primary side environment. Sarver *et al* [21] showed that thermally treated alloy 690 (thermal treatments of between 1 and 15 hours at various temperatures between 607°C and 871°C) was more resistant to stress corrosion cracking, in a caustic environment (deaerated 10% NaOH) than alloy 600 with the specified post mill annealed thermal treatment (i.e. 704°C for 15 hours) [21]. Page and McMinn [22] investigated the corrosion susceptibilities of alloys 600 and 690 in a simulated Boiling Water Reactor (BWR) environment and also found alloy 690 to have superior resistance to both IGSCC and SCC in such a medium.

Thus, comprehensive comparative evaluation has shown that thermally treated alloy 690 was superior as a PWR steam generator material to alloy 600 in a simulated PWR primary side environment. The use of alloy 690 in PWR steam generator applications began with the incorporation of it in replacement steam generators delivered by Westinghouse to two United States facilities in 1988. It was selected as the tubing material for the Sizewell B project [4] in preference to the initial selection

of alloy 600 (STT) [23]. This change of selected material reflected the superior performance consistently demonstrated by alloy 690 in corrosion testing and other laboratory evaluations.

Alloy 690 (STT) is now being widely incorporated into steam generator design. In fact it is the material recommended by Framatome in French PWR construction following successful comparative testing with alloy 600 in a variety of environments [24]. Further, it has been announced by the same company that, following the discovery of cracks in the alloy 600 vessel head penetrations [25], all new reactor pressure vessel heads manufactured by Framatome for domestic needs (i.e. for French reactors) in the foreseeable future will incorporate alloy 690 [26]. Continued discussion and reference to the problems of cracking on the vessel head penetrations is to be found later in the literature survey.

During this decade between twenty one and forty nine steam generators are expected to need replacing in the USA due to the corrosion problems associated with alloy 600 tubing and by the year 2020 a further thirty US replacements could be needed [27]. Many of these replacements have already specified that alloy 690 (STT) is to be used [28], [29] and it is expected that this will be the case for the other similar utilities in the USA.

2.5. Alloy 600

Alloy 600 is characterised by a fully austenitic structure, with small amounts of inclusions and precipitates. Gane [30] undertook detailed investigations of alloy 600 and confirmed that the thermal treatments given to the material for steam generator applications induce the precipitation of both M_7C_3 Cr-rich carbides and $M_{23}C_6$ Cr-rich carbides on the grain boundaries. In addition a small number of Ti(CN) particles

19

formed from the melt are distributed in the matrix. The same carbide morphology was reported by Was [31]. Both Gane and Was [30], [31] also stated that, prior to thermal treatment, the alloy 600 precipitates found were primarily of M_7C_3 Cr-rich carbide form with $M_{23}C_6$ occurring only sporadically on the grain boundaries and in the matrix. This may again indicate that the $M_{23}C_6$ particles either preferentially form during the thermal treatments or 'mutate' from previously formed M_7C_3 [17], [18], [19] but, as discussed earlier, this is unlikely and in any case is unproven.

Alloy 600 was originally supplied for steam generator applications in the mill annealed (MA) condition and this was considered sufficient to withstand corrosive attack. In the event many failures in steam generator tubes of 600 MA ensued and the consequences are still being felt in modern operating nuclear plants [32]. The main mechanisms of tube deterioration were denting, pitting, secondary side intergranular attack and both primary and secondary side stress corrosion cracking. Following these initial problems, alloy 600 steam generator tubes were supplied in the STT condition which was shown to enhance its corrosion resistance in both simulated primary side PWR and caustic environments [33], [34]. Laboratory testing and research showed that thermally treated alloy 600 had a greater resistance to intergranular attack than MA alloy 600, so promising increased service life when used in thermally treated condition. However, failures of such tubes by corrosive attack continue to occur in operating plant. Scott published a detailed review [35] in which it is stated that the thermal treatment discussed ($\approx$700°C for $\approx$16 hours) would eliminate any 'sensitisation'. Based on a typical 'sensitisation' test such as modified Huey this will be true, but Hall and Briant have shown that there will still be a Cr denuded area close to the grain boundary [16].

Klein *et al* [36] investigated thermally treated alloy 600 (and alloy 690) in simulated secondary-side and simulated primary-side environments and the results were compared with those from mill-annealed alloy 600. The materials used were

20

processed under production conditions to meet the chemical and mechanical property requirements of the ASME SB163 and Code Case N-20 standards and so are directly comparable to in-service history. It was concluded that compared with the mill annealed material the thermal treatment (nominally 704°C for 15 hours) provided enhanced SCC resistance, under the environments tested.

Economy *et al* undertook [37] laboratory testing of alloy 600 SG tubing in both water and steam above 360°C and found increased exposure times before the alloy cracked with the thermally treated materials and that they also exhibited an increased resistance to IGSCC. After 2,800 hours exposure to 400°C steam with hydrogen at 76KPa, IGSCC had initiated in 92% of the MA test specimens but only in 3% of the thermally treated specimens. An important point made by Economy in the same paper, based upon other experiments, is that for the thermal treatment(s) to be of maximum benefit it is necessary for the final mill anneal treatment on the material to be of a sufficient temperature and duration to dissolve the majority of the carbon in the alloy into solid solution. For heats given a low mill anneal (insufficient to dissolve all the carbon) the benefit of the subsequent thermal treatment was not so great.

2.6. Alloy 800

The Ni-Cr-Fe alloy 800 is characterised by a fully austenitic structure, with small amounts of inclusions and precipitates. The composition of the alloy 800 sample(s) used in this research programme are to be found in the appendix, table 1. The thermal treatments given to the material for steam generator applications induce the precipitation of $M_{23}C_6$ Cr-rich carbides at the grain boundaries and a small number of gamma prime (Ni$_3$[Al,Ti]) particles are distributed in the matrix [42]. Alloy 800 was originally developed, by Huntingdon Alloy Products, in 1949, to fill a gap created

during a period of restricted availability of nickel. The intention was to provide an easily fabricated and heat resistant alloy for domestic appliance use, but the market potential created by the added benefit of high corrosion resistance led to its wide use in the petrochemical industry and subsequently as boiler and superheater tube material for power plants.

Alloy 800 is currently used extensively in PWR steam generators in Germany and Belgium, and was chosen for use in the steam generator replacement programme for the Doel 3 reactor which was undertaken in 1993. The reasons for this choice are documented by Stubbe *et al* [43]. A comparative evaluation between alloys 690 and 800 focused on the service behaviour and corrosion resistance of the materials. The final decision in favour of alloy 800 was due to the fact that it had a longer service history.

2.7. Grain Boundary Chromium Depletion

All three alloys have been shown to form Cr rich grain boundary carbides which are encouraged to nucleate and grow during thermal treatment. The diffusivity of carbon, which diffuses as an interstitial element, is much higher than that of chromium which must diffuse substitutionally. This difference in diffusivities permits the formation of the Cr carbides which then produces a chromium depleted region surrounding the grain boundary. The, so called 'sensitised', chromium depleted region continues to exist even when the thermal treatment is for such a duration as to allow sufficient time at temperature for some back diffusion of Cr ('desensitisation') to this denuded grain boundary region [16].

The 'sensitised' structure is normally detrimental to the corrosion resistance of stainless steels and Ni-Cr-Fe alloys in acidic environments [52]. This is not

necessarily the case in high temperature deaerated water environments, such as those encountered on the primary side of a PWR. Indeed, under such conditions this 'sensitisation' has been shown in some laboratory investigations to slightly improve the corrosion resistance of alloy 600 [33]. Kai *et al* [53] have conducted tests on alloy 600 and 690 and concluded that alloy 690 is a superior material to alloy 600 as a PWR steam generator tubing material and that when 'sensitised' both materials offered a superior corrosion resistance in pure deaerated water. Not all researchers agree on the 'sensitisation' issue in Ni-Cr-Fe alloys in PWR primary water, however, and reports are contradictory as Scarberry *et al* discuss in a paper on precipitation reactions in alloy 600 [54].

Some researchers have proposed a range of critical percentage Cr, by weight, needed to be retained within the Cr depleted area in order for corrosion resistance to be maintained in Ni-Cr-Fe materials. Airey *et al* [55] suggested between 9.8% and 11.7% - however, this was for cracking in polythionic acid to occur, hence its relevance to PWR environment is questionable. During Kai's investigations [53] a minimum Cr weight value of approximately 8% was proposed to prevent stress corrosion cracking failure following constant load and constant extension rate tests on alloys 600 and 690 in a sodium thiosulphate solution.

Was *et al* [18] developed an interactive computerised thermodynamic model for alloy 600, called DEPLETE, and extended the work by establishing a further model known as DEPLETE690 for alloy 690, which attempts to predict the amount of chromium depletion in the denuded areas close to the grain boundaries. This research showed that both models correlated well with experimental data, but the tests were conducted on a high purity melt and not on as received commercial materials. Also, the kinetic model on which the DEPLETE computer programme is built is based upon a number of assumptions by Was and Kruger which, whilst simplifying the model, are possible sources of error [56]. The assumption is that the metallic content of the carbides is

100% Cr and that the carbide forms a continuous film of uniform thickness along the grain boundary limit the model.

For the DEPLETE model it is further assumed that the only carbide present is in the form M_7C_3, this was altered for the DEPLETE690 programme [18] to take account of the lower solubility of carbon in alloy 690 [57] and to assume the only carbide present to be of $M_{23}C_6$ form. Since Stiller has already shown the carbides in alloy 690 type alloys to be complex, it would appear that further errors are built into the model [15]. This may well be a reason why these interactive computer models have not been more widely used in research and industry for Cr depletion prediction.

Briant and Hall [16], [58] propose a simple empirical formula to quantify the effect of C% and Cr% concentrations on 'sensitisation' and its likely in-service corrosion resistance. Their research indicated that there was a grain boundary Cr level requirement of 12% weight, minimum, for immunity to corrosion. The formula proposed was originally successfully developed for use in predicting the corrosion resistance of stainless steels and has been adapted for use in Ni-Cr-Fe systems. The formula used is based on the supposition that the two most important factors in determining whether significant Cr depletion will occur are the amounts of C and Cr in the alloy.

The formula suggested by Briant *et al* is of the form:

$$Cr^{eff} = Cr_{bulk} - AC_{bulk}$$

where Cr^{eff} represents the amount of depletion that should occur, Cr_{bulk} and C_{bulk} are the bulk concentrations of Cr and C respectively and A is a multiplication factor. Based on their experimental data, Briant and Hall propose A = 200. It is concluded that a Cr^{eff} figure larger than 12-15 will result in little, or no, corrosion.

The model appears to work well, but is inadequate to correctly predict corrosion susceptibility for several reasons. The complete heat treatment cycle undergone by the material has been shown to be important in determining the corrosion resistance of Ni-Cr-Fe alloys and no account is taken in the formula of this processing. Neither are the effects of minor elemental traces within the materials on the amount of chromium depletion considered [59]. Also, the possible consequences of changes to water chemistry on the SG tubing primary side environment and subsequent corrosion resistance are not accounted for [60], [61]. The testing environment used was 25% boiling nitric acid, which is known as a Modified Huey Test and is primarily used to indicate 'sensitised' materials or for comparative purposes, thus the model used appears only to predict likely corrosion parameters in this medium and no attempt was made to compare this to PWR operating environment data. Further, the multiplication factor attached to the carbon content, A, in the proposed formula remains unaltered for different Ni-Cr-Fe alloys which seems incompatible with the varying carbon solubility of the alloys available for SG tubing.

2.8. Tubesheet Cladding Materials

Now, briefly considering the candidate cladding materials for the tubesheet. Alloy 82 is the weld consumable used to clad the tubesheets in the Sizewell B PWR. This alloy was first developed for use with alloy 600 and has similar levels of Cr and Ni. It is conceivable that its continued use with the change of steam generator tubing to alloy 690 may result in undesirable changes in chemical composition within the fusion area of PWR steam generator welds [14]. Furthermore, and somewhat disturbing, operating experience and experimental research has shown alloy 82 to crack under stress in primary PWR water [62]. The material has also been found to be susceptible to corrosive attack in several independent laboratory tests [63], [64].

The work undertaken by Briant and Hall [63], in which they considered the microstructural causes of IGC in alloys 82 and 182, used Huey testing (25% boiling nitric acid for 48 hours) for comparison of the various samples. Some of the welded samples were given a low temperature ageing (LTA) treatment of 400°C for 200 hours followed by an air cool. This treatment has subsequently been used by Povich [65] to produce the same microstructural changes as could occur during extended (greater than 20 years) service at reactor operating temperatures. The LTA treated samples showed slightly increased corrosion, when compared to untreated samples, during the testing. This indicated increased susceptibility to corrosion after time, though some caution is needed, since the Huey corrosion test does not simulate service environments in water reactors. The work by Povich in which the LTA was originally used was undertaken on austenitic stainless steel when investigating low temperature 'sensitisation'. So some care is needed before too readily interpreting the results as comparable to the Ni-Cr-Fe materials under investigation and typical PWR operating environments.

There is also conflicting opinion as to the usefulness of data obtained from accelerated ageing of materials by using forms of thermal treatment. In order to investigate the possible effects of the weld thermal cycle over time it was deemed important to conduct some such testing in the current research programme. It is recognised that the accelerated ageing method could alter the mechanism of the natural degradation process of alloy 690. But since the material has only been used in PWR steam generators since 1988 historical data is unavailable. Therefore one would expect and hope that such testing of welded specimens will increase knowledge of accelerated ageing on such materials.

Research on experimental Ni based weld metals R-135 and R-127 with high Cr content undertaken by Briant and Hall [66] has shown the good weldability of such materials. Other investigators too have been undertaking laboratory testing of similar

Ni based weld metals in both pure water and boiling water reactor (resin intrusion) environments. Again, the experimental weld metals R-135 and R-127, with Cr contents of approximately 30%, gave good results with regard to immunity to stress corrosion cracking in pure water, as did welding alloy 72 (43% Cr), when investigated by Page and McMinn [67] for the Electric Power Research Institute (EPRI). From these studies the commercially available weld/cladding consumable alloy 52 has recently been developed which has Ni and Cr ratios in similar proportions to those found in alloy 690 [68]. This new alloy has recently superseded alloy 82 as the recommended weld consumable for use with alloy 690 [69]. Therefore, it is likely that future SG tubesheets manufactured to incorporate alloy 690 tubes will be clad with alloy 52 material.

2.9. Welds and Welding in PWRs

A number of specific weld associated issues should also be mentioned and expanded upon at this point.

Autogenous, gas tungsten arc welding (GTAW) is the exclusive method used for joining the heat exchanger tubes to the clad tubesheet in PWR steam generator fabrication. The tubesheet weld cladding material specified for use with alloy 690 for the Sizewell B project was alloy 82. Alloy 82 weld consumable has Ni and Cr compositions in similar weight percentages to alloy 600 and was developed primarily for use with this alloy. Naturally, alloy 82 was used in the construction of SGs with alloy 600 tubing. As previously discussed, alloy 52 is now the recommended cladding material for use with alloy 690 tubing.

Looking at the welding of alloy 800, Lambert [47] studied the welding behaviour of twenty six commercial casts of alloy 800. Welding techniques conforming to PWR

weld parameters were used in order to investigate the effects that cast material compositional variation has on the physical characteristics of the weld. Lambert concluded that slight changes (of the order of +0.003 weight %) in sulphur and calcium levels could alter the weld width whilst maintaining similar weld pool and arc characteristics.

More detailed work on microstructural changes to alloy 800 due to the weld thermal cycle was undertaken by Romig *et al* [48]. Considerable attention was focused on the weld cracking susceptibility of alloy 800 within the HAZ. The results from these tests indicated that alloy 800 was not highly susceptible to HAZ cracking. Earlier research [49] into the effects of welding on the material properties of alloy 800 did, however, show that hot tearing was a potential problem area.

Resistance heating (Gleeble test) was used by Romig *et al*, during their investigations, to simulate a weld thermal cycle applied to alloy 800 specimens. Although the use of the Gleeble test is a recognised laboratory test method for weld history simulation, there is continued debate as to the ability of the test to simulate all weld parameters accurately. It is considered by many that the actual thermal history of any weld cycle can be reproduced by this method when computer-controlled [50]. Dolby and Widgery have shown that differences in both microstructural and mechanical properties can occur between simulated and real welds [51].

A variety of environmental considerations such as humidity, shield gas temperature, gas pressure and arc characteristics, which may affect the final structure of a weld are not easily taken into account during a Gleeble cycle test. However this is not necessarily a problem as these variables could be sources of error when analysing experimental results. Based on literature and discussions the author considers that Gleeble simulation of weld thermal cycles is an extremely useful and highly

controllable investigative laboratory method, but that the results should, where possible, be collated with real-time welds or historical data for corroboration. Before any results from Gleeble weld simulations are used to recommend welding standards and/or practices, further testing and investigation is necessary in order to verify the simulation findings with empirical welding data. Without such careful data comparison there is clearly a danger that unsuitable specifications could become contained in welding procedures and safety regulations.

There have been problems associated with welds and weldments of the Inconel alloys used in nuclear reactor environments. The most recent problem to emerge, and potentially one of the most damaging to the PWR programme world wide, is the previously mentioned cracking of PWR vessel head control rod drive mechanism (CRDM) penetration weldments [25], [26], [38], [39], [40], [41]. Examination of PWR reactor vessel head penetrations (control rod drive mechanism (CRDM) penetrations) in France have found penetration cracks along the alloy 600 sleeve/alloy 82 cladding weld interface on the top face of the vessel head(s) [25]. The plant operators, manufacturers and regulatory authority were immediately concerned that this could be a generic problem for many PWRs of the same design and indeed this has subsequently been found to be the case [38].

The materials used in the reactor vessel head penetrations area are of a similar nature to those found in the steam generator tube-to-tubesheet weld using alloy 600 tubing and have undergone a similar weld thermal cycle. The main difference in the material aspects of the CRDM penetration is that in SG tubes the microstructure and chemical composition has been carefully controlled whereas the penetrations are machined from alloy 600 bars produced by press or hammer forging [39]. The bars are heat treated in order to soften the material, thus resulting in a wide scatter of microstructures, chemical compositions and mechanical properties (yield strengths between 260 and 500 MPa).

29

The discovery of these cracks has had major implications for the PWR programme world wide. Similar faults were later found in a Swedish reactor [40] and have since been discovered in Spanish PWR plant also [41]. It is expected that the same degradation problems will ultimately be found in operating PWR plant in the USA [11] and appropriate exploratory inspections are being carried out. Further details of the problem are now given.

2.9.1. Vessel Head Penetration Cracking

The cracking on the CRDM penetrations was first detected in September 1991 when the French PWR at Bugey 3 was undergoing a mandatory hydrotest as part of the ten year inspection of French reactors. During the test, conducted at 133% of normal operating pressure, a slight leak was detected acoustically. The leak was confirmed by visual inspection. A special inspection programme on the other 1st generation French PWRs resulted in cracks being found on eleven vessel head penetrations [70]. It was at first thought that this problem was restricted to the older French PWR stations but subsequent inspection revealed similar cracks in newer plant [25]. Figures 5-7 show details of the vessel head penetrations and the typical cracking mode found[1]

The problem is not restricted to France. The investigations eventually led to identification of the cause of the degradation being primary water stress corrosion cracking (PWSCC) of the alloy 600. Thus PWRs of the same design were assumed to be susceptible to this generic problem [38]. Following these preliminary inspections

---

[1] Figures 5-7 reproduced by kind permission of AEA Technology, Corporate and Marketing Communication Service, Didcot, Oxfordshire

and the associated testing programme into the causes and effects of the problem, the PWSCC of the CRDM penetrations has been linked to four main factors:

⇒ The high temperature of the vessel head during operation (315°C).

⇒ High residual stresses from the welding process between peripheral penetrations and vessel head.

⇒ Susceptibility of the forged alloy 600 used for CRDM penetration manufacture.

⇒ Cold working, introduced by fabrication

Electricité de France (EdF) sent information about the problem to all operators having reactors built to a similar Westinghouse design and have subsequently published the findings to date [38]. Because other countries routinely carry out their hydrotests at only 110% of normal operating pressure it was clearly possible that cracks such as those discovered in France had not been detected. Cracks were subsequently detected in similar situations in other countries [40], [41].

For the UK PWR programme the CRDM penetration cracking problem is highly significant since it only came to light after the manufacture of the reactor pressure vessel head for the Sizewell B power station. The head had been produced using the alloy 600 penetrations and I82 buttering and welding materials which are themselves suffering in-service cracking problems. Thus, the dilemma for the UK PWR operators is that Sizewell B station will begin operating with a crack initiation problem which has been found to be of a generic nature already in place. Inspection of the CRDM penetrations is therefore of the utmost importance in order that any crack initiation and propagation is properly monitored.

2.9.1.1. Inspection and Repair of CRDM

A major problem is inspection of the affected area. The initial inspection programme was carried out using semi-automatic systems which performed well but were costly in dosimetric terms and require the CRDM to be removed. Framatome, EdF and Westinghouse have been developing robots capable of in-service inspection and prototypes of these are being tested. The second problem is one of repair. For the older French units EdF has decided to replace the vessel heads with penetrations made of alloy 690 [70]. With the newer French units the underhead temperature is being reduced by 25°C since one of the major factors favouring stress corrosion cracking is known to be temperature [71].

The international perspective on the CRDM penetration cracking issue put forward in a detailed report by the international environmental group Greenpeace International [72] is one of "a global catastrophe waiting to happen". Greenpeace claim that the PWR operators do not understand the cause of the cracking and that, even worse, the possibility of circumferential cracking cannot be excluded. According to Greenpeace, circumferential cracking could result in a penetration rupture leading to non-isolatable leaking of the primary water circuit, therefore making plant susceptible to a loss-of-coolant accident (LOCA) resulting in a reactor core melt-down. Their drastic recommendation is that all reactors in which CRDM penetration cracking has been detected should immediately be shut-down. The Greenpeace report is well written but many of its arguments seem to be unsubstantiated or referenced out of context. Furthermore, it does not mention the sophisticated control systems built into modern PWR plant [73], [74] which are designed to shut-down reactors safely long before any catastrophic LOCA could occur. Also the high cost calculations of temporary plant shutdown(s) due to CRDM penetration inspections is statistically correct but uses reference costs based on coal fired power plant [75]. Not surprisingly therefore, the nuclear industry has countered this by stating that the Greenpeace report was

32

excessive. They insist that current safety standards, coupled with detailed inspection criteria and leak detection systems which can "sniff even a few molecules of boron that might be leaking from a penetration" justifies continued plant operation and a low profile approach to the penetration cracking problem [76]. It must be said though, in all fairness to Greenpeace, that their "China Syndrome" urge to extreme caution philosophy does err on the side of safety for the general public.

2.9.2. Tube repair - welded sleeving

Once a steam generator tube fails then it can be taken out of service by tube plugging. This operation will, by its very nature, reduce the efficiency of the SG and eventually will necessitate replacement as it is general agreement amongst PWR operators that a steam generator must be changed when fifteen percent of its tubes are plugged [77]. Therefore, if the tube can be repaired in some manner and allowed to remain in service the life of the SG is extended.

One method of repairing leaking SG tubing is to introduce a sleeve inside the tube so that it spans the corroded area and then to seal the tube at both ends by welding. This method of repair was not particularly successful when used in the Doel 2 reactor in Belgium, on around 200 sleeved tubes. Within a few months more than 50% of the sleeved tubes had to be plugged as they were cracking circumferentially just behind both ends of the sleeve. This had the desirable result that it prompted research work by the Belgian utilities and also joint work with other European partners [78].

The research programme in Belgium was designed to study a number of tubes with different weld techniques (GTAW, laser and kinetic welding were used) followed by a PWHT. It was found that nearly all the specimens which had not been subjected to a PWHT developed cracks when tested in caustic environments (10% NaOH

deaerated solution at 350°C). The thermally treated samples had variable results, although the time-to-failure increased significantly and cracking still occurred within the weld area. The service life of SG tubes repaired in this manner was also calculated by comparing with roll transition data. The conclusion drawn was that the life expectancy of tubes repaired by sleeving could be estimated at between 3 and 6 years when post-weld-heat-treated.

As always, some degree of caution is necessary in extrapolating such conclusions from laboratory testing. Also, in the research paper referenced, no mention is made of the fact that these results are in direct contradiction to operational experience since over 50% of the sleeved tubes at Doel 2 had failed within months. Nickel electroplating of cracked SG tubes has also been successfully undertaken in Belgium, France and elsewhere as a repair method for ruptured tubes [79].

Sleeving still remains a possible repair method. For example, in circumferential cracking of tubes. In Japan, where plugging was originally the only repair method used, laser welding of sleeved tubes was used effectively as a maintenance method in 1989 to repair tubes at Kansai Electric's Ohi 1 PWR [80]. Since the experience with tube sleeve weld repair in Japan is far better than that in Belgium, the laser welding technique used may well be preferable. Certainly the deep penetration afforded by this method of welding together with the narrow weld bead and HAZ widths will limit any detrimental effects due to the welding process itself.

It does however remain to be seen how long the laser welded tubes at Ohi 1 will remain in serviceable condition as they are currently coming to the end of their life (3 to 6 years), according to the predictions based upon the research in Belgium. Kansai Electric are additionally investigating the previously mentioned nickel plating of

tubing as a method of repair and research work in this area being conducted by Framatome is jointly funded by the Japanese PWR plant operators and themselves.

2.9.3. Further Welding Effects

Yamauchi *et al* [81] undertook research showing that, in the alloy 600 type materials tested, there was an enhanced susceptibility to IGSCC, in high temperature (288°C) oxygenated pure water (8ppm oxygen), resulting from welding. This is an important concern in nuclear power plant component construction. The investigations state that chromium depletion at the grain boundary in the weld HAZ is a major factor influencing this increased susceptibility and in order to improve the IGSCC resistance Yamauchi proposes the addition of niobium to suppress the precipitation of chromium carbides by the stabilisation of carbon as niobium carbides (NbC).

Whilst the increase in IGSCC susceptibility from the weld thermal cycle is not challenged, it is unclear how Yamauchi reaches the conclusion on 'sensitisation'. No attempt is made either in the paper or the associated research methods to qualify or quantify the morphology and distribution of any inter or intra granular carbides within the weld HAZ. There has not even been any microscopy to show the presence or otherwise of any precipitates following welding. Payne *et al* [82], and several others [13], [30], [31] have shown that carbide formation during thermal treatments affect the 'sensitisation'. This, it must be said, is a major omission from the Yamauchi work.

Failure of welded alloy 600 at the heat exchanger primary cooling loop inlet and outlet pipes was also detected in a nuclear reactor in Israel. Work by Kohn *et al* [83] on the failed sections showed the failures to be due to IGSCC in the weld HAZ, thus substantiating the conclusions of Yamauchi on IGSCC failure following welding.

Grain growth in the HAZ is given as a probable contributing factor for the failure, together with stresses resulting from the weld thermal cycle and the weight of the pipe itself.

Discontinuities in Inconel GTA welds for nuclear applications were investigated by Patterson *et al* when studying alloy 600 [84]. During this work, cracking in the fusion zone was encountered and this is stated to result from a hot cracking susceptibility. The issue of grain growth from the weld thermal cycle is also mentioned by Patterson, with a further recommendation to avoid any large recrystallised grain sizes and also an associated recommendation to use low average heat input welding parameters. Interestingly, this research showed niobium enrichment, resulting from the decomposition of niobium rich carbides in the fusion zone during the weld thermal cycle, to be a contributing factor to any fusion zone cracking and shrinkage porosity. This has major implications on the validity of the recommendation by Yamauchi [81] to add substantial amounts of niobium (2 to 3% weight were used in the research) for stabilisation and resistance to IGSCC following welding.

Work by Lippold [85] on HAZ cracking in alloy 800 revealed titanium enrichment as a probable major influence on HAZ hot cracking susceptibility and cited the same reasons as Patterson for niobium enrichment from dissolved Nb rich carbides in alloy 600 (i.e. titanium from dissolved Ti rich MC carbides). The research of Lippold substantiates the discussions of Rothwell *et al* [49] that HAZ cracking was a potential problem in alloy 800.

The literature survey has clearly identified microstructure and composition of SG tubing materials and their associated weld metal consumables. The nature and distribution of any carbide precipitates and inclusions are seen as major factors in assessing SG tubing material suitability. This is critical for optimum PWR power

plant in-service materials performance requirements. The same factors are influenced by the weld thermal cycle applied during SG fabrication. The theme of this investigation is, therefore, to explore the effects of the weld thermal cycle specifically on the microstructure of alloy 690, with comparisons to alloys 600 and 800, and in doing so to increase knowledge in this area.

3. Experimental Methods

In this chapter the methods and equipment used in this research are described. The materials investigated are listed and classified, with references where appropriate.

3.1. Materials for Laboratory Investigations

A range of materials were acquired for the experiments and weld thermal cycle simulations undertaken, these being:

◊   Commercially produced steam generator tubing.

◊   Standard weld consumable (tubesheet cladding) materials.

◊   Experimental melts.

3.1.1. Commercial Materials

Inconel alloys 690, 600 and 800, in commercially manufactured steam generator tubing form, were acquired. The alloy 690 tubing was supplied by Sandovik, the material was from the `cast F' used in the manufacture of the tubing for the Sizewell `B' project. The alloy 600 and alloy 800 tubing material samples were supplied from what was the CEGB laboratories in Leatherhead. The alloys 690 and 600 had been subject to STT following mill annealing. The thermal history of the alloy 800 tubing material was unknown. The commercial tubing materials were subjected to a full chemical analysis to ascertain their chemical compositions. The results are shown in Table 1.

3.1.2. Weld Consumables

Although the weld process used for the laboratory weld sample generation was an autogenous one it was necessary to use weld consumable(s) to simulate tubeplate primary side cladding. Two weld consumable materials were acquired, namely alloy 82 and alloy 52. Alloy 82 is the material incorporated as the primary side cladding for the SG tubesheets when manufacturing the Sizewell `B' plant [86], and has been used extensively as the recommended weld consumable for use with alloy 600. The alloy 82 was used for the majority of the laboratory welds. Following the increasing use of alloy 690 as SG tubing material alloy 52 has now been adopted as the recommended weld consumable for use with alloy 690. Eighteen samples were therefore welded using alloy 52 for the cladding. The chemical compositions of the two as-received welding materials are given in table 2.

3.1.3. Experimental Melts

In addition to the commercially available materials, two experimental melts were produced. These two casts were designed to be of alloy 690 type composition but with niobium (Nb) substitution for titanium (Ti). Study of these experimental melts was seen to be relevant following the work of Yamauchi *et al* on the use of Nb in alloy stabilisation [81], and also the conclusions reached by Patterson *et al* on the detrimental effects of Nb carbide decomposition on Inconel GTA welds [84].

The compositions of the experimental melts are shown in table 3, from which it can be seen that the amounts of Nb used constitutes minor alloying additions as a direct substitution, by weight %, for Ti. The quantities of Nb used by Yamauchi were far larger (up to 10 times greater) where it became a major constituent of the melt. The

39

justification for use of such amounts is detailed in the Yamauchi paper [81] but it was felt this would be likely to cause weld defect problems if used for the purposes of this project.

3.1.3.1. Production of Experimental Alloys

The experimental alloys were manufactured as 5kg melted cast ingots using a Consarc vacuum furnace. The ingots produced were hot rolled into solid bar from a temperature of approximately 1150°C using a number of reduction passes with intermediate re-heats to 1150°C to prevent cracking. The final hot rolled bars were of a diameter of approximately 21mm. These bars were then turned and bored into SG tube form and dimensions, 17.5mm external diameter with a nominal wall thickness of 1.1mm. The resulting tubes were then cut into 50mm lengths, mill annealed and thermally treated in accordance with typical alloy 690 SG tubing manufacture specifications, based on those used by the French producers, Vallourec Industries [4]. The procedures used are detailed below:

◊ The tube sections were sealed in silica glass tubes under a partial pressure of argon (approximately 100mm Hg) in order to prevent any oxidation during high temperature treatment.

◊ A short high temperature mill anneal accomplished by placing the samples, in their silica tubes, in a furnace set at a temperature of 1100°C for 4 minutes followed by a water quench, the silica tubes breaking under the water due to thermal shock.

◊ Re-seal samples in new silica tube, as previously described, and thermally treat by placing in a furnace at 720°C for a soaking time of 15 hours followed by a water quench. The silica tubes fracturing under the water.

40

3.2. Production of Specimens for Welding

In order to manufacture specimens for welding with comparable parameters to those encountered during SG production a number of preliminary steps were taken:

◊ Sections of bright drawn mild steel (bdms) bar with a diameter of 75mm were cut and then faced off on a centre lathe to a length of 94mm. The dimensions of the bdms bar were chosen in order to act as an infinite heat sink in the same manner as the clad tubesheet within an SG.

◊ The sections of bdms bar were clad, to a minimum thickness of 6mm, with alloy 82 weld metal applied in layers by the gas metal arc welding (GMAW) process. A limited number of sections were clad with the alternative weld consumable, alloy 52. All the clad sections were then faced off in a centre lathe to 100mm length and centrally bored with a 17.5mm diameter hole for insertion of samples of SG tube material.

◊ Six holes of 1.5mm diameter were machined into the cladding using electro-discharge machining (spark erosion) through to the centre bored hole at a distance of 0.1mm to 0.6mm from the top face of the cladding, in steps of 0.1mm. For the duration of the welding operation, thermocouples would be placed into the holes through to the SG tube material and thus the temperature profiles down the tube from the fusion zone could be monitored.

◊ 75mm long samples of the tubing materials (alloy 690, alloy 600, alloy 800, VMA & VMB) were placed in the holes in the alloy 82 clad bdms sections to a slight interference fit; the tubes were aligned with the top of the cladding. Additionally, a number of alloy 690 tube samples were placed in the alloy 52 clad bdms sections.

3.3. Welding of Laboratory Specimens

The SG weld simulations were carried out using a Kempotig AC/DC 250 dedicated welding unit. The welding unit was attached to an Abio TIGMATIC 150 series controller and turntable with speed, dwell time(s) and reverse controls. The samples for welding were placed in the turntable jaws which were then tightened. The GTAW torch unit and shield was swung into position on a fixed length arm which allowed for arc gap adjustment and reproducibility of position.

For temperature data acquisition an OPUS PC IV with a Keithley Instruments K500 series interface card on-board was connected to a 575 Measurement and Control System. The input to the 575 system was six analogue temperature signals from the K-series thermocouples placed in the holes on the samples detailed previously and connected via three pairs of linearising amplifiers to the measurement and data control system. The signals from the thermocouples were then digitised and sent to the PC as calibrated millivolt readings. The sampling rate was set to 1,000 readings per second for a duration time of 45 seconds in order to ensure that all relevant thermal data from the welding process was collected. The three sections of hardware (welder, turntable and computer) were all connected through a foot switch to allow simultaneous start-up of the equipment.

To investigate the effects of various heat inputs three different sets of weld parameters were chosen. These were designed to simulate:

◊ The weld thermal cycle to Westinghouse SG PWR specifications.

◊ The weld thermal with increased heat input rate.

◊ The weld thermal with decreased heat input rate.

The majority of the specimens were welded using the Westinghouse welding parameters for PWR SG fabrication. Only alloy 690 samples with alloy 82 cladding (i.e. the materials used in the Sizewell `B' SG fabrication) were subjected to the weld thermal cycles incorporating increased and decreased heat input. During fabrication of the Sizewell `B' SGs, the specifications allow a second weld thermal cycle should the original weld fail inspection. To simulate the effects of such weld repairs during fabrication, a number of the alloy 690 with alloy 82 cladding samples were welded to Westinghouse PWR specifications, allowed to cool to ambient temperature ($\approx$20°C) and then subjected to a repeat weld thermal cycle.

The calculations were made using the formula:

$$heat\ input\ rate\ per\ unit\ length = \frac{\eta VI}{v} = \frac{q}{v}$$

where:

η = efficiency (i.e. the proportion of arc energy transferred to work piece as heat)

V = Arc Voltage

I = Arc Current

v = welding velocity

q = heat input

Altering the heat input rate could have been accomplished by altering the amperage, voltage or travel speed. Since alterations to the amperage or voltage could affect the stability of the arc during welding, control of heat input rate was achieved by altering the travel speed.

The travel speed was progressively increased until a point was reached where weld integrity could not be assured. At this point the speed was decreased slightly. This

43

speed was then used for welding with decreased heat input rate. All other weld parameters remained unaltered.

The travel speed was then progressively decreased until a point was reached where weld integrity again could not be assured. The speed was then increased slightly. This speed was then used for welding with increased heat input rate. All other weld parameters remained unaltered.

The Weld Thermal Cycles used are listed below, the final heat input rate assuming 100% efficiency (i.e. η=1):

	Westinghouse PWR Specification	Decreased Heat Input	Increased Heat Input
Weld Method	Gas Tungsten Arc	Gas Tungsten Arc	Gas Tungsten Arc
Amp Range	69±1	69±1	69±1
Volt Range	12±1	12±1	12±1
Gas Shield	Argon	Argon	Argon
Gas Flow Rate	8.5 to 10 litres min^{-1}	8.5 to 10 litres min^{-1}	8.5 to 10 litres min^{-1}
Gas Pre-flow	5 seconds	5 seconds	5 seconds
Gas post purge	5 seconds minimum	5 seconds minimum	5 seconds minimum
Electrode used	2.4mm diameter, 2% thoriated tungsten	2.4mm diameter, 2% thoriated tungsten	2.4mm diameter, 2% thoriated tungsten
Arc length	approximately 1.5mm	approximately 1.5mm	approximately 1.5mm
Overlap	3±2s	3±2s	3±2s
Downslope	6±1s	6±1s	6±1s
Travel Speed	2.23 mm s^{-1}	3.67 mm s^{-1}	1.58 mm s^{-1}
Heat Input	371 J mm^{-1}	226 J mm^{-1}	523 J mm^{-1}

3.4. Post-Weld Sample Dissection

Following the welding of the samples, as previously detailed, the majority of the BDMS was sliced from the weld, tube and cladding by use of a high speed, low feed rate on an automated METASERV C1600 Cut-Off Machine with flood coolant. The remainder of the BDMS was removed by dissolving in a 25% Nitric Acid solution for between fifteen minutes and one hour depending on the amount of residual

BDMS material on the sample after cutting on the METASERV machine. The samples were then carefully radially sectioned on a Struers DISCATOM cut-off machine, using low feed rate with flood coolant, into eight sections per sample.

3.5. Accelerated Ageing of Alloy 690 Samples

In order to investigate the possible long term affects of the weld thermal cycle on PWR SG welds twenty of the alloy 690 with alloy 82 cladding samples welded to Westinghouse PWR specifications were given a low temperature thermal treatment for accelerated ageing purposes. The ageing times and temperatures used were based upon the previously mentioned work undertaken by Povich [65]. The thermal ageing methodology was as follows:

◊   The welded samples were placed in silica glass tubes under a partial pressure of argon (approximately 100mm Hg) in the same manner as previously described in section 3.1.3.1, on experimental alloys manufacture.

◊   The sealed samples were placed in a furnace and held at a temperature of 400°C for 200 hours.

◊   The samples were then removed from the furnace, the silica glass encasements were broken open and the specimens were allowed to cool in air.

This treatment was used by Povich to simulate the same microstructural changes that would occur in type 304 stainless steel during long time service at reactor operating temperatures. The temperatures and times chosen are believed to simulate approximately twenty years of service life according to the Povich criteria and the same method was used successfully by Briant and Hall [63] on Ni-Cr-Fe weld

45

consumable alloys 82 and 182 in both unwelded form and when welded to alloy 600. The possible issues associated with such forms of accelerated ageing were discussed during the literature review.

3.6. Characterisation of Welded Specimens

A variety of tests and observations were undertaken on the segments of laboratory welded tube samples. Comparisons were made with archive material from the Sizewell `B' PWR project [87].

3.6.1. Optical Metallography

Etching is a vital part of the analytical process - it was therefore important to overcome any possible etching problems early on. Segments of laboratory welded tube samples and archive material were mounted in bakelite, polished to a 1μm finish and then etched. The etchant used was, with the exception of the alloy 800 samples, 5% Nital which was incorporated as an electrolytic etching medium. The Nital solution revealed the grain boundaries and weld microstructures in the tube fusion zone (FZ), heat affected zone (HAZ) and the as received/prepared matrix tube (i.e. unaffected by the weld thermal cycle). The welded alloy 800 samples did not respond favourably to the 5% Nital etch as either a swab or an electrolytic reagent. The most reliable etchant tested was found to be 10% ammonium persulfate in water used electrolytically for approximately thirty seconds, this was subsequently used as the etchant for the alloy 800 samples.

A series of optical micrographs were taken whilst characterising the microstructure of the samples. Measurements were taken of the width of the HAZ of the samples.

Measurements of grain size were made using the mean linear intercept method and are quoted in the results, section 4.2.1, to within 95% confidence limits.

Microhardness readings were taken across the weld and HAZ into the matrix (i.e. FZ, HAZ and matrix) of the tubes. The measurements were made using a Tukon Micro-Hardness Testing Machine with a Vickers type 360° indenter. Ten readings were taken in each area and a mean value recorded.

3.6.2. Electron Microscopy

Scanning Electron Microscopy and Transmission Electron Microscopy was used to further analyse the welded specimens. Visual images were photographed and, where appropriate, Energy dispersive X-Ray Analysis was undertaken. A number of specific sample preparation techniques were used and these are detailed below.

3.6.2.1. Scanning Electron Microscopy

The Scanning Electron Microscope (SEM) was employed to examine the microstructure and composition of the various welded samples. The particular SEM used was a Jeol 840A with EDX (Energy Dispersersive X-Ray) analyser attachment. The samples were mounted in conductive bakelite and lightly etched as described in the section for optical metallography. Originally, the alloy 690 samples were etched in a 2% Bromine/Methanol solution as recommended by Lowenstein *et al* for SEM work on alloy 690 [88]. However, the bromine/methanol etch, whilst giving good results visually, was found to be unsuitable for use with quantitative analysis since the etch was severe and left an uneven surface. Bromine is also toxic and consequently had to be handled in a fume cupboard. Furthermore, the solution needed to be used fresh (i.e. made immediately prior to use) and had to be disposed

of with care since it is considered an environmental pollutant. For these reasons it was decided to revert to the electrolytic use of a 5% Nital etchant on alloy 690 and alloy 600 during sample preparation for SEM microscopy. The 10% ammonium persulfate solution was used to etch the alloy 800 samples throughout.

The EDX system was first used to map Ni and Cr concentrations across the FZ, HAZ and Matrix of alloy 690 samples welded to PWR specifications with I82 cladding. Then quantitative analysis was undertaken in the three zones - FZ HAZ and Matrix. Spot analysis in two areas, at the centre of a grain and across a grain boundary region was recorded four times in each of the three zones for each welded sample. The results were normalised by the EDX computer controller and then mean compositions were calculated. The limitation of the SEM/EDX for this work was the diameter of the beam which, if analysis of the grain boundary was required, was too wide. As a result of this, on grain boundary spot analysis by SEM, only data on the composition of the materials across the grain boundary region could be recorded.

3.6.2.2. Transmission Electron Microscopy

A Phillips CM20 Transmission Electron Microscope (TEM) with Scanning TEM (STEM) and EDX attachments was employed for examination of any precipitates present in the various welded samples. Thin foils were produced in the conventional manner. 3mm diameter circular coupons were taken from the welded samples by use of spark erosion machining. The samples were fixed to a custom-made jig in such a manner that the fusion line of the weld was positioned across the centre of the coupons after machining. These were then progressively thinned by hand polishing to approximately $80\mu m$ thickness.

Originally the thinned samples were placed in a Struers electropolishing cell to be electropolished and dished using a 6% perchloric acid solution in glacial acetic acid at a temperature of -50°C at a current of 1.75mA. This method proved unsatisfactory since the electrolyte did not always perforate the thin foil in its centre (i.e. along the fusion line); this was necessary since investigation of the inter and intra granular microstructure in the FZ and HAZ was the primary requirement of the TEM investigations. A number of the welded alloy 600 and 690 samples were sent to AEA Technology, Materials Performance Department, Structural Integrity Division, Harwell, for collaboration in high resolution transmission electron microscopy using a Phillips EM430 300KeV TEM unit. During the thin foil sample preparation at Harwell using electropolishing as a perforating mechanism, similar problems were found to occur [89] and whilst the methodology was persevered with it was acknowledged to be both time consuming and only moderately successful [90].

For the programme of work at Sheffield Hallam University a different technique was therefore developed for dishing and controlled geometrical perforation of the thin foil specimens. Following the spark erosion of the 3mm foils from the welded laboratory samples they were thinned by hand polishing to approximately 80μm thickness. During this original thinning process the samples were occasionally lightly electrolytically etched in 5% Nital solution to confirm that the weld fusion line was still positioned across the centre of the samples. The samples were then polished to 1μm finish with diamond paste and a soft nap. Each foil was then in turn mounted on a Gatan Model 656 dimple grinder and ground with diamond paste in suspension to a minimum dimple thickness of 5-15μm in the centre of the samples (i.e. on the weld fusion line). Whilst still on the dimple grinder, the dimple was then final polished with alumina suspension polish to approximately 0.05μm surface finish.

The samples were then placed in a Gatan Model 691 Precision Ion Polishing System and ion beam milled, to perforate the dimple, using the following machine parameter settings:

Table Rpm: 5
HT/KeV: 5
Current, left gun (μA): 13
Current, Right gun (μA): 13
Gas: Argon

An autodetection unit was fitted and used for detecting sample perforation. A typical time taken for the ion beam milling to perforate was ½hr to 1½hrs depending upon the original dimple thickness. Specimens produced by this method were consistently perforated across the weld fusion line in all cases. During the TEM studies this allowed guaranteed views of the FZ and HAZ.

There were a number of advantages with this sample preparation method over that used at AEA Harwell laboratories:

◊   100% success rate in perforating thin foils along the weld fusion line, with associated assured area of selection for TEM investigations.

◊   The method does not require the use of perchloric acid solution which is a hazardous material, toxic, potentially explosive, needing to be handled with care and kept at low temperature ($\approx$-50°C) for safe utilisation.

◊   Comparatively quick sample preparation times - from start of electro-discharge machining to final perforation of thin foil taking typically between four and six hours.

3.7. Corrosion Tests - Modified Huey Testing

To investigate any relative degree of grain boundary 'sensitisation' (caused by Cr depletion) in the base metal, heat affected zone and weld metal a Modified Huey test was performed on segments of laboratory welded tube samples. The test consisted of 48 hour exposure to boiling 60% nitric acid. Whilst weight loss measurements were taken, these were not used for evaluation. Metallographic cross-sections of the samples were taken, polished and etched following the testing and these used as an indication of severity of any attack. The Modified Huey Testing was undertaken for comparative purposes only and was in no way designed to simulate PWR in-service environments.

3.8. Constant Extension Rate Testing

To evaluate the effects of the weld thermal cycle on the high temperature properties and failure modes of alloy 690 a series of Constant Extension Rate Tests (CERT) were devised. These were conducted on an Instron 4200 Series testing machine, with micro-computer controller, in an autoclave at an internal temperature of 320°C, at a pressure of 1½bar and with argon environment. The extension rate used was $7x10^{-5}s^{-1}$, this rate was chosen since it was the slowest rate available on the Instron testing machine used. Angeliu and Was [91] undertook testing of Ni-Cr-Fe alloys in similar environments (360°C in argon) when investigating the influence of C and Cr on creep and IG cracking, thus providing detailed results for comparison. Two strain rates were used by Angeliu and Was, $1x10^{-7}s^{-1}$ and $3x10^{-7}s^{-1}$ respectively.

3.8.1. CERT Sample Preparation

A technique was developed for the manufacture of CERT samples from the alloy 690 SG tubing materials. Two 50mm long samples of Alloy 690 SG tube from the Sizewell `B' cast were obtained. One of the samples was sliced in two on a Struers DISCATOM cut-off machine, using low feed rate with flood coolant. Both pieces of these bisected samples were placed on a dedicated mandrel which held together the two halves whilst they were autogenously welded by automated orbital GTAW with parameters set to simulate welding to PWR specifications. The prepared tubing samples (both welded and unwelded) were then in turn placed on a Beaver NC5 numerically controlled milling machine tool.

A bespoke CNC machining program was written to enable test specimens to be cut directly from the tube walls, in the case of the welded samples this included the fusion line in the centre of the gauge length of the final milled specimens. The CNC program is listed in the appendix, figure 8. The program was downloaded to the milling machine processor via a serial connection and the samples cut out of the tube(s). By rotating the tube sections through 120° between machining cycles it was possible to cut three specimens from each piece of tube. These test specimens were then placed on a custom-built fixture and a previously manufactured austenitic stainless steel boss clamped up to each end. Each boss was internally threaded in order to screw onto the load bars operating with the autoclave utilised for this testing. The jig, bosses and samples were then placed in the vacuum chamber of a dedicated electron beam welding (EBW) unit and the chamber evacuated. The specimens were EB welded to the bosses using the following settings:

Weld Parameters - EB Welding CERT Samples to Holders

◊ Voltage: 90Kv

◊ Beam Current: 11mA

◊ Focus Current: 945A

◊ Circle Generation Current: 0.1A

◊ Surface Speed: 40 inches per minute (IPM)

The use of EBW as the joining method gave a very small HAZ adjacent to the weld. Since this zone was in the wide 'shoulder' of the machined specimens and away from the gauge length sections, it was assured that the test results were not altered as a consequence of sample welding during assembly. A picture of one of the CERT samples, before and after testing, is shown in the appendix, figure 51. The samples were then tested by being mounted on the load bars, placed in the centre of the autoclave, brought to temperature (320°C) in the desired environment (argon) and tested to fracture. The relevant test data was recorded on microcomputer and SEM microscopy was undertaken on the sample fracture surfaces.

This chapter has outlined the procedures and materials used in this research programme. The next chapter will incorporate the results from the experimentation.

4. Experimental Results

4.1. Temperature Profiles During Welding

The readings taken from the thermocouples attached to the samples during the three weld thermal cycles used are shown in figures 9-12. The temperature data is presented in figures 9-11 in such a way as to show the temperature gradients from the maximum temperature recorded at each thermocouple (T_{max}) followed by a 2.4s profile of the temperature decay, the first thermocouple being placed 0.1mm from the fusion line and each following thermocouple being progressively a further 0.1mm away. Figure 12 shows the comparative maximum temperatures recorded during each weld thermal cycle against distance from the weld fusion line.

For all three weld thermal cycles used the maximum temperature difference between thermocouples (i.e. progressively 0.1mm down the tube from the fusion line) was within the range 60°C - 100°C. Within only one second the temperatures begin to converge slightly, towards eventual steady-state uniform ambient. There was no discernible difference in the temperature profiles between different tubing materials though they are known to have differing coefficients of thermal conductivity. Since the bulk of the samples for welding consisted of the dbms bar simulating the tubesheet for heat-sink purposes it seems reasonable to assume that this material had the dominant effect for heat transfer purposes during the weld thermal cycle and thus masked any slight differences in SG tubing heat transfer characteristics. It should be noted that this was confirmed by SG fabricators who stated that the weld parameters used would not be altered when incorporating any of the three materials under investigation in PWR design [92].

4.2. Optical Metallography

Representative optical micrographs of the samples are shown in figures 13 to 26. Figures 13 and 14 indicate that the laboratory welded specimens of alloy 690 (PWR specified weld parameters) had a comparable weld microstructure to the archive material supplied from the Sizewell `B' project. This again indicated that the experimental laboratory welding techniques used adequately simulated actual SG fabrication weld thermal cycles. Figures 15 to 26 show a series of micrographs of the as received materials and the experimental melts, also shown are their microstructures following the application of the weld thermal cycles. The accelerated aged alloy 690 samples were visually identical to their original welded condition, and the alloy 690 samples welded to alloy 52 cladding are also identical to the PWR welds, so neither are included as optical micrographs; metallurgical and compositional differences in those samples are shown and discussed later in section 5. The micrographs show as a result of the weld thermal cycle that cellular dendritic grain formation with columnar grains branching out from the cellular dendritic structure in the weld fusion zone in all cases. Also evident is the grain growth in the weld HAZ. This grain growth is non-homogeneous in nature thereby producing a range of grain sizes within the HAZ of the materials investigated.

4.2.1. Heat Affected Zone Width

Measurements of the width of the HAZ were taken at five points along each sample and a mean reading recorded. The results are shown in table 4. Whilst the mean values are representative of the HAZ widths of the samples under investigation, there was a variation of approximately ±10% from these figures. It was also noticeable that

the HA zones were largest at the edge of the tube sections and smallest at the centre in all cases, including that of the archive weld material from the Sizewell `B' project.

4.2.2. Grain Sizing

As previously stated, and shown in the micrographs 15 to 26, the grain growth is non-homogeneous within the HAZ of the welded samples. Therefore the measurements of grain size are presented as a range for the HAZ regions and as a definitive size for the matrix of the samples. The results are shown in table 5. Measurements of grain size were made using the mean linear intercept method and are quoted to within 95% confidence limits. The larger grains were almost exclusively to be found towards the edges of the tube.

4.2.3. Microhardness Measurements

Microhardness readings were taken across the weld and weld affected areas into the matrix (i.e. FZ, HAZ and matrix) of the tubes as detailed previously. The results (shown in table 6) are an average of ten readings in each region and are quoted as Vickers microhardness numbers. The results in each case were fairly consistent, with minimal scatter and correspondingly low standard deviation values. There are indications that the weld thermal cycle on the materials investigated has affected the microhardness of the fusion zone, fusion line and the HAZ. It can be seen that the experimental melts had higher hardness values in all areas. This corresponds to a smaller average grain size.

4.2.3.1. Heat Input and Heat Affected Zone Width

Figure 27 and table 7 show from the laboratory investigations the effect of heat input (assumed 100% transfer of heat energy during welding) on the width of the HAZ in the alloy 690 samples and the associated data respectively. It is noticeable that the relationship is almost linear in nature and therefore can be written in mathematical form as:

$Y = \alpha X + \beta$ where:

Y = width of heat affected zone

X = heat energy input in Jmm^{-1}

α & β are constants representing gradient of the slope the intercept of the Y-axis, respectively.

The gradient of the graph identifies the rate of change of the grain size with respect to heat input, whilst the Y-axis intercept is the original grain size. Extrapolation of the experimental data and regression analysis give the following values to the constants:

$\alpha = 0.1$

$\beta = 39$

which, when substituted into the formula, yields the equation:

$Y = 0.1X + 39$

Two points need to be made regarding the validity of this derived equation. If taken out of 'weldable range' (i.e. calculated for heat energy inputs which would not result in a physical weld) then the resulting HAZ width calculation would be meaningless. For example, at $0Jmm^{-1}$ heat energy input the formula would predict a 'HAZ' width of $39\mu m$. However, since this is approximately the grain size of the original tubing material, it somewhat supports the validity of the derived formula. The heat energy inputs for laboratory weld thermal cycles used were taken as high and as low as possible whilst still guaranteeing weld integrity. Since the laboratory welds

compared favourably to archive material from SG welding of the Sizewell `B' PWR it is likely that similar limits would apply in actual SG fabrication.

It would therefore be more accurate to state the derived equation as follows:

$$Y = 0.1X + 39 \text{ (for } X \geq 226 \text{ \& } \leq 523) \text{ where:}$$

Y = width of heat affected zone in μm

X = heat energy input in Jmm^{-1} (100% efficiency assumed)

The simplified formula derived includes the theoretical maximum heat energy input rate value, X, which is calculated as shown previously in the section on weld parameters used. The actual efficiency, calculated from the experimental temperature readings, is to be found in the discussion section of the thesis, section 5.

4.3. Scanning Electron Microscopy

The Ni and Cr maps from EDX analysis across the fusion zone and HAZ of the alloy 690 specimens welded to PWR specifications with alloy 82 cladding (figure 28) show that there is an increasing Cr content across the area, from fusion zone towards the matrix 690, with a corresponding decreasing Ni content. This is consistent with the differing percentages of Ni and Cr in the alloys 690 and 82, as shown in tables 1 and 2. Figures 29 to 31 identify typical weld microstructures. Figure 29 gives a low magnification image of a welded area and clearly shows the cellular and columnar grain growth in the edge of the fusion zone, whilst figures 30 and 31 show this microstructure in more detail.

4.3.1. SEM Quantitative Analysis

The results of the quantitative analysis on the areas previously detailed in the experimental method are shown in tables 8 to 18. Quantitative measurements were made of the following constitutional elements:

Aluminium (Al)

Silicon (Si)

Niobium (Nb)

Chromium (Cr)

Manganese (Mn)

Iron (Fe)

Nickel (Ni)

Titanium (Ti).

The lighter elements in the carbon (C) range were not measured.

The alloy 690 samples welded with alloy 82 cladding (tables 8 to 13) all show clearly the alloy 690 Cr dilution in the fusion zone which was highlighted earlier on the Ni/Cr maps (figure 28). The quantitative analysis figures are normalised percentages and so the measurements are subject to interpretation since they are slightly higher than the actual concentrations. Within the matrix of the samples there is good correlation between the SEM analytical readings and the compositional measurements given in tables 1 to 3, also the SEM quantitative analysis was undertaken with reference to a real-time cobalt standard, as opposed to virtual standards, for increased accuracy.

There is seen to be large imbalances in the composition of the fusion zones of the alloy 800 samples welded with alloy 82 when compared to the alloy 800 matrix. Whilst alloy 800 is often welded with such high nickel filler metals as alloy 82, other materials are now available such as alloy 556, which was investigated by Ernst *et al* [93], and was found to be compatible with the alloy 800 type material range and gave sound quality welded joints. The welded areas of the alloy 600 samples, with alloy 82 cladding, had fairly consistent chemical composition with regard to the major elemental concentrations. This would have been expected due to the similarity of the two materials and the fact that alloy 82 was primarily designed for use with alloy 600. Very little compositional variation was found between intragranular and grain boundary regions, for any given zone, in any of the samples examined.

The accelerated ageing of the alloy 690/82 specimens had seemingly little effect on the composition of the zones investigated. In all cases, apart from those of the experimental melts, the high levels of Nb in the fusion areas, when compared to the matrix materials, are seen to come from the filler metal cladding material(s) used. All the I690 specimens and the I600 specimen were shown to have a high dilution of the Fe in their fusion zones when welded with I82 cladding, again consistent with a blend of I82 and I690 or I600 in the FZ. Stubbe *et al* [94] undertook investigations which showed that a low percentage of Fe coupled with high Ni concentrations could be detrimental to the in-service behaviour of the SG tubes and this fact will be returned to during further discussion, section 5. The alloy 690 samples welded with alloy 52 cladding show a more balanced composition through the various areas analysed.

4.4. Transmission Electron Microscopy

The TEM investigations on the materials revealed a number of interesting results. The as-received materials in the thermally treated condition were known to contain semi-continuous chains of grain boundary carbides. This was also the case with the experimental melts following thermal treatment. STEM scans of these grain boundary carbides showed them to be of a Cr rich nature. A scan of one of these carbides from an alloy 690 sample is shown in figure 32. Micrographs of the same carbides are to be seen in figures 33 and 34, in bright field and dark field respectively. The particles were identified as being of $Cr_{23}C_6$ form. A small number of Ti rich intragranular TiCN particles were also identified as being present, except in the experimental melts. The experimental melts, where Nb had been substituted for Ti, was found to contain a similar distribution of intragranular particles but in these cases they were of NbCN form. The fusion zone had previously been shown (figures 29-31) to be of a cellular dendritic nature. The TEM investigations found no evidence of carbide decoration within this zone.

Following the welding process there is a marked difference in the microstructure within the HAZ of all the samples. Irrespective of the alloy type, cladding material used and/or weld heat input during the thermal cycle there was an absence of precipitates at the grain boundaries, except at the outermost edge of the HAZ where it bordered upon the unaffected matrix; at this section there were a small number of intergranular carbides present. The HAZ intragranular regions occasionally contained a small number of Cr rich precipitates but no more heavily distributed than before welding, this indicates the possibility that all the HAZ Cr rich grain boundary precipitates had been taken into solution except on the very edge of the HAZ/matrix interface where only partial solution of precipitates had taken place. This same precipitate free HAZ microstructure was also found during the collaborative TEM work undertaken at Harwell [89] and thus confirms those studies. Figure 35 shows a

typical precipitate free HAZ grain boundary. The actual sample shown is alloy 690 welded to PWR specifications.

A small number of TiCN particles were still found to be present intragranularly after welding in the HAZ of most samples (in the case of the experimental melts the NbCN particles were still present) and thus it is hypothesised that these particles (Ti or Nb rich) and their distribution patterns within the HAZ had been largely unaffected by any of the weld thermal cycles employed. Figure 36 shows a Nb rich particle in the HAZ of welded experimental melt A, whilst figures 37 and 38 show an intragranular TiCN particle in the HAZ of alloy 690 welded to PWR specifications and its corresponding spectrum, respectively. Figures 39 to 44 show representative spectra taken during STEM analysis.

In order to ascertain the amount of intergranular carbide precipitation within the HAZ, as noted by microscopy, volume fraction measurements were taken. Details are given next, in section 4.5.

4.5. Volume Fraction Precipitate across the HAZ

Whilst by the microscopic examination it could be noted that the HAZ had very few carbides present, it was deemed expedient to quantify this low distribution. In order to achieve this, a number of micrographs were converted into digital images (Tagged Image File {TIF} format). These were then analysed using the Aquitas Image Analysis software to obtain volume fraction precipitate figures. Two regions of the HAZ were analysed, firstly from the fusion line to the mean centre of the HAZ and, secondly, from the mean centre of the HAZ up to the HAZ/Matrix interface. The results are to be seen in the appendix, table 22.

4.6. Corrosion Tests - Modified Huey Results

By weighing the samples before and after testing weight loss measurements were gained but these were not used for evaluation since there was no way of quantifying which zone(s) (fusion, heat affected or matrix) had been subjected to weight change(s), if any, and in what proportions. Metallographic cross-sections of the samples had been taken, polished and etched following the testing and these used as an indication of severity of attack using the following ratings:

◊   NA = No Attack → unaffected by the test.

◊   LA = Light Attack → slightly affected by the test.

◊   SA = Severe Attack → severely affected by the test.

The results are recorded in table 19. Clearly identified is the fact that none of the alloy 690 samples were attacked during the test, irrespective of weld parameters or ageing methods used. Figure 45 shows a representative micrograph of an alloy 690 sample after the test. This was also the result found for the experimental melts, with no evidence of inter or intragranular corrosive attack. The alloy 600 samples had some light attack in localised areas, as can be seen in figure 46. The alloy 800 samples were seen to be the most detrimentally attacked of the specimens tested as is shown in figure 47, where grain drop-out had been found to occur.

4.7. Constant Extension Rate Test Results

The welded and unwelded samples had both been tested to fracture in the argon environment at elevated temperature. Representative SEM micrographs of the

fracture surfaces are seen in figures 48 and 49 respectively. These indicate ductile fractures in both cases. The yield strengths and ultimate tensile strengths of the materials experimentally gained under the test conditions (i.e. constant extension at 320°C in Argon at slight overpressure) are listed in table 20. The data indicates a slight lowering of both figures when in the welded condition in comparison to unwelded. The results of this test at elevated temperature also show a slight lowering of these material properties in comparison to the manufacturers published data on the physical properties of alloy 690 [95] and the findings of Smith [13] when testing as-received archive alloy 690 tubing material from the Sizewell B project.

5. Discussion

The experimental results have highlighted several changes to the alloys under investigation, following the application of a weld thermal cycle. A number of the microstructural changes, such as grain growth, were to be expected from classical welding theory but other effects were not predicted. Striking compositional changes were noted within the welded regions of the materials tested; this was especially so in the fusion zone when the alloy 82 weld consumable was used in conjunction with the alloy 690 tubing. These factors may well change the corrosion resistance and also the mechanical response of the materials, when subject to PWR in-service environments.

Whilst it is acknowledged that the welded regions of heat exchanger tubes are small in comparison to the whole of the SG structure(s) it is critical that they survive for the lifetime of the matrix (non weld affected) section of the tubes. Looking at the results of this research investigation and the associated literature review shows a number of important areas for debate. This discussion will view the results and in doing so highlight these key issues.

5.1. Weld Heat Inputs

The thermal energy inputs used during welding were based upon an original value taken from the specified weld parameters for Westinghouse Model F SG fabrication [86], i.e. those used in the manufacture of the Sizewell B PWR. The increases and decreases in heat input subsequently investigated were at levels to which the laboratory equipment would weld a structurally integral joint. The range chosen was

thus, in heat input rate terms, from 226 J mm^{-1} to 523 J mm^{-1}, assuming 100% arc efficiency.

5.1.1. Welding Efficiency

Since the welding process was not 100% efficient in heat energy transfer terms the actual efficiency of the welding technique used during the laboratory manufacture of welds needed to be found. The GTAW process is not a particularly efficient process, with regard to heat transfer, since a great deal of the energy is dissipated between the electrode and the workpiece. Published data gives a range of typical efficiency for this weld method of between 22% and 48% [96].

To calculate an efficiency factor from the experimental data it was assumed that the weld was deposited on a plate with a thickness of 25mm, this being the amount of cladding used plus an allowance to simulate the tubeplate. Since the experimental data had yielded the peak temperatures reached at varying distances away from the weld fusion line the Peak Temperature Equation (PTE) [97] was used as a method of gaining an efficiency factor. The PTE predicts that in the base metal adjacent to the weld:

$$\frac{1}{T_p - T_0} = \frac{4.1\rho CtY}{H_{net}} + \frac{1}{T_m - T_0}$$

where:

T_p = the peak or maximum temperature (°C), at a distance, Y (mm), from the weld fusion boundary.

T_0 = Initial Uniform Temperature of Weld Zone.

T_m = Melting temperature (°C), (specifically, liquidus temperature of the metal being welded).

H_{net} = net energy input = $\dfrac{\eta EI}{v}$;

66

E = Volts;

I = Amps;

V = velocity of heat source, (mm.min^{-1});

η = efficiency

ρ = density of material (g mm^{-1})

C = specific heat of the solid metal (J g^{-1}.$^\circ$C)

ρC = volumetric specific heat (J mm^{-3}. $^\circ$C)

t = thickness of 'plate' (mm)

The experimental efficiency values were calculated for the Alloy 690 specimens with the three heat inputs used and at the positions of the six thermocouples. A mean value of η was then taken for each of the weld operations. The results are listed below:

thermocouple distance from fusion line (mm)	PWR Parameters % efficiency	Increased Heat % efficiency	Decreased Heat % efficiency
0.1	21.8	27.3	24.6
0.2	35.0	37.3	37.3
0.3	44.4	46.3	38.8
0.4	43.9	46.4	43.5
0.5	38.4	45.6	42.9
0.6	36.6	40.2	39.6
average efficiency :-	36.68%	40.52%	37.78%

The measured experimental efficiencies of the GTAW process are, thus, within the published data range. In all three cases, the experimental values for efficiency calculated from the first thermocouple readings (i.e. 0.1mm from the fusion line) were lower than other results. The difficulty in positioning the thermocouple so close to the fusion line would account for low experimental values, as a lowered (T_p-T_0) value would give such results. Also, there will undoubtedly have been losses associated with the thermocouples themselves resulting in lower values of T_p.

5.2. HAZ Grain Size

As a result of the experimentation it was seen that altering the thermal energy inputs of the weld thermal cycles had no effect on the range of grain size within the heat affected zone of the specimens, though the actual width of the HAZ did change as will be discussed later. There was a higher percentage increase in the grain size of the experimental melts when compared to both the archive Sizewell B welds and the laboratory welds from commercial tubing. Taking an average grain size in the HAZ, from the range shown in table 5, gives an increase of 183% in grain size within the HAZ of the experimental melts; the alloy 600 specimens come closest with a 147% increase. These materials correspond to the materials with the smallest initial grain sizes. The other materials showed a grain size increase in the HAZ of approximately 50%.

The weld parameters used for the experimental melt tubing were identical to PWR SG fabrication and there was a heat sink approaching infinity in terms of heat conduction from the HAZ (i.e. the bdms bar) producing a temperature profile of a similar nature to all other alloys when welded to PWR weld specifications. The fact that the alloy 600 samples showed a similarly high amount of grain growth shows that materials with small initial grain sizes exhibit higher grain growth rates than those with initially larger grains, when subjected to an identical weld thermal cycle. This phenomenon is explained in the grain boundary liquation discussed later.

Another factor affecting the grain growth will have been processing route, the commercial materials having been pilgered whilst the two experimentally manufactured materials were bored and turned prior to STT. The pilgering process will have produced work hardening in the surface of the commercial materials. A

percentage of this work hardening will have remained following the STT it will affect grain boundary mobility. Discussion with other researchers [11] confirmed this hypothesis and also revealed that alloy 800 tubing for nuclear applications is normally deliberately manufactured with residual work hardening for this purpose.

5.2.1. HAZ Grain Growth Mechanism

Grain growth is a thermally activated process and a threshold temperature exists in all metals above which grain boundary migration will occur, the grain boundaries merging to form the larger grains noted in the HAZ of all the welded samples. Work by Lippold *et al* [98] showed that in single phase-materials the locus of this temperature usually represents the boundary of the HAZ, with grain boundary migration increasing as a function of proximity to the fusion line. Lippold *et al* also found HAZ grain boundary liquation occurring during the welding of austenitic stainless steels and noted that when grain boundary precipitates were present the likelihood of interaction between the grain boundary and the particle was high.

Evidence of grain growth through grain boundary liquation was found in the author's research and can be seen in the optical micrographs of the welded samples, in figures 14 to 26. Grain growth in the presence of grain boundary liquation in the HAZ is highlighted by the sudden disappearance of some grain boundaries in the HAZ where sections appear to be missing. All of the welded samples, regardless of heat input during the weld thermal cycle, exhibited traces of liquation at the grain boundaries. The effect of grain boundary liquation on the role of grain growth is discussed in detail in the seminal work of Burke *et al* [99], where it is concluded that the driving force for grain growth is, indeed, the surface energy of the grain boundaries.

The mean linear intercept method of grain sizing was used which assumes a 3-dimensional grain shape. This accounts for differences in cross-sectional area due to the actual plane of the sample surface. The relatively small width of the HAZ in the samples together with a non-uniform and uneven grain growth made definitive grain sizing difficult. The mean linear intercept method was still not sufficient to define a standard grain size in any of the specimens following welding and thus a range of experimental measurements of grain size within the HAZ were recorded.

5.2.2. Grain Growth and HAZ Strength

In materials such as the fully austenitic alloys under investigation, the primary grain size will have a direct affect on the strength. The grain size dependence of the yield stress (σ_y) is described by the Hall-Petch relationship:

$$\sigma_y = \sigma_i + k \, d^{-\frac{1}{2}}$$

where σ_i is the friction stress (representing the overall resistance of the crystal lattice to dislocation movement), k is the locking parameter (which measures the relative hardening contribution of the grain boundaries), and d is the average grain diameter. Since the grain sizes across the HAZ of the experimental measurements varied substantially, as commented upon previously, the Hall Petch equation has not been used directly. However, it is significant in that it predicts a lowering of the yield strength in the HAZ adjacent to the fusion line after welding; this will reduce the overall load-bearing capacity of the joint.

5.3. Nb Substitution for Ti

It is feasible that the Nb substitution for Ti in the experimental melts had some effect on the amount of grain growth in the HAZ. The temperatures in the HAZ during the weld thermal cycle were insufficient for liquation of any Nb or Ti rich carbides, such particles having been formed during the initial alloy melt. Studies performed by Radhakrishnan *et al* [100] on the Ni-base superalloy 718 suggested that grain boundary liquation reactions involving Nb rich carbides and the kinetics of these reactions in such an alloy are strongly dependent upon both the composition of the surrounding matrix and the weld thermal cycle. Yamauchi *et al* [81] did not comment on grain growth changes in the HAZ following Nb additions to alloy 600 type experimental melts. During the current experimentation the same weld thermal cycle was applied to the experimental melts as was applied to the other samples. The percentage grain growth in the HAZ of the experimental melts was larger. Thus the findings of the author are in general agreement with those of Radhakrishnan confirming that grain boundary liquation will occur as the transport mechanism for grain growth, though for a different family of Ni-Cr rich alloys.

As previously stated, the higher percentage grain growth occurred in the weld HAZ of the experimental melts than in the welds of the commercially produced materials will have been due to the effects of processing route for manufacture. The experimental tubes had been turned and bored as opposed to the as-received STT tubing which had been pilgered.

The experimentally produced melts were unaffected by the medium used for the Modified Huey Testing. The commercial alloy 690 samples were also unaffected by this test so it can be stated that the experimental material with Nb substitution for Ti was equal in corrosion resistance to this form of testing over the time period used

(i.e. 48 hours). The tests undertaken by Yamauchi *et al* [81] on alloy 600 type materials had shown an improved IGA resistance in simulated PWR primary side environments when Nb was included instead of Ti.

5.4. Grain Boundary Precipitate Dissolution

The findings of the research with regard to carbide distribution show little evidence of Cr rich carbides in the HAZ of the welded samples. Before welding the STT undergone by the tubes has promoted the formation of semi-continuous chains of grain boundary carbides which have been noted and identified in the associated optical, SEM and TEM investigations. The same absence of carbides, both inter and intra-granular, in the HAZ was noted by AEA Technology in their collaborative TEM studies [89]. Thus the HAZ formed as a result of the weld thermal cycle must have been subjected to heat energy input sufficient for dissolution of the Cr carbides.

Bowes *et al* [101] conducted studies of the HAZ thermal cycle affects in alloy 718 using Gleeble simulation. In those investigations it was stated that the previously discussed grain growth had been identified and it was also noted that this area adjacent to the weld exhibited grain boundary precipitate dissolution. It was argued that the area of transition from precipitate-free to precipitated grain boundaries marked the limit of the weld HAZ. Whilst the precipitates found in the alloy 718 are of a Nb rich nature, as opposed to the Cr rich precipitates in the Ni-Cr-Fe alloys 690, 600 and 800, the same conclusion as to identification of the HAZ by its grain boundary precipitate free nature is drawn from both the work of the author and stated in the report written from the collaborative studies with AEA Technology [89]. The proviso to this hypothesis is the assumption that grain boundary precipitates exist in the materials prior to welding, but in the case of all the alloys investigated this was so. The volume fraction figures (table 22) produce further supporting evidence for

72

grain boundary dissolution within the HAZ. The areas from the fusion line to the HAZ mean centre are virtually precipitate free, whilst a small number of carbides begin to appear as the HAZ limits are approached.

The shape, size and distribution of the Ti(CN) particles in the HAZ is unaffected by the weld thermal cycle. In the case of the experimental melts, the Nb(CN) precipitates are similarly unaffected in the HAZ. The grain boundary Cr rich carbide precipitation in STT NiCr alloys has been shown to be critical in corrosion control [13]. The delicate balance of precipitate distribution and alloy microstructure introduced by the STT is significantly altered by the heat of the welding process.

Commercially, a great deal of time, effort and expense has been taken during the STT in forming the grain boundary carbides as a preferred microstructure for PWR SG applications and operating environments, whilst allowing for the back diffusion of Cr to the Cr denuded areas adjacent to the grain boundaries. Therefore, the precipitate free microstructure resulting from welding is both undesirable and in conflict with commercial tubing manufacturers optimised microstructure. The dissolution of these carbides in the HAZ as an effect of the weld thermal cycle must be detrimental to the long term life expectancy of the materials since previous studies [5], [13], [34] have indicated that the grain boundary Cr rich precipitates act to pin the grain boundaries and thereby increase resistance to intergranular attack in simulated PWR primary side environments.

5.5. Heat Affected Zone Microhardness

It is evident from the microhardness results (table 6) that the HAZ has a lower microhardness than the fusion zone. Looking more closely at the comparative microhardness between the HAZ and unaffected matrix it is seen that the various

alloy 690 specimens showed a 7%-8% lowering in microhardness, except in the case of the samples subjected to two weld thermal cycles where the microhardness was 10% lowered. The alloy 800 samples were shown to exhibit a similar, lower, microhardness in the HAZ of 8%.

There is a difference in values of the microhardness results in the alloy 600 material and the experimental melts, though the trends are the same. In all areas tested these materials have a higher microhardness value than that of the other materials. This corresponds to the smaller original grain size. The percentage lowering of microhardness in the HAZ of these three materials as a result of welding is higher, at 13%, and relates directly to the higher percentage increase in grain size within the HAZ following the application of the weld thermal cycle. Bowes *et al* [101] also undertook microhardness measurements in the HAZ of the 718 type alloys investigated, following the application of a Gleeble simulation weld thermal cycle. The findings corroborate those of the author, in that the microhardness in the HAZ region is lower than in the matrix STT tubing material.

5.6. Changes in Composition after Welding

There are compositional changes within the fusion and heat affected zones of the materials (tables 8 to 18), in some cases the resulting chemical balance of elements is of such proportions as to warrant future investigation. Particular attention is drawn to the combination of alloy 690 tube with alloy 82 weld consumable cladding (tables 8 to 13). Within the fusion zone of the welds the Ni/Cr ratio has proportions approaching stochiometric (i.e. 2/1 ratio) for the formation of secondary phase Ni_2Cr which would strain the previously fully austenitic crystal lattice. The potential significance in an operating PWR of such a transformation was indicated by the research of Stubbe *et al* [94], as increased brittleness of the materials. The matrix

74

alloy 690 tubing has a Ni/Cr ratio composition close to stochiometric but accompanied by Fe levels of around 8%. The investigations of Stubbe et al [94] showed the possibility of this short range order/long range order (SRO/LRO) in alloy 690 type materials. One of the conclusions drawn from the research was that an Fe level in the region of 5% or below was necessary for onset of SRO/LRO.

Both the fusion zones of the alloy 690/82 welds manufactured by the author to simulate PWR SG welds and of the archive 690/82 welds exhibited Fe levels close to this threshold limit proposed by Stubbe. There are a considerable number of operating PWR SGs world wide manufactured with the alloy 690 tube and alloy 82 weld material combinations, including the British PWR - Sizewell B. The author was unable to put a precise figure on the numbers despite extensive searching and discussion [102]; the difficulties being the commercial sensitivity of the manufacturers of PWR SGs coupled with the fact that there have been a large number of replacement SGs fitted with this combination of materials. It can be stated that the vast majority of new PWR plants built to Westinghouse design between 1989 and 1993 and most similar replacement SG programmes over that period, will have incorporated alloy 690 tubing and alloy 82 weld consumable cladding; since 1993 the alloy 52 weld consumable has become the preferred standard for use as cladding in this application. The incubation time for onset of this hypothetical in-service degradation by phase transformation is long and it is uncertain if the operating temperatures and pressures of primary side PWR plant is sufficient for the onset of the phenomenon. It is a possible degradation mechanism and operating PWR plants which may be susceptible should be appropriately monitored.

When alloy 690 tubing was welded incorporating the alloy 52 weld consumable as the cladding material, the chemical composition within the resulting fusion zone and HAZ was similar to that of the unaffected tube (table 18). This is in stark contrast to the composition found following welding with alloy 82 and can be seen from table

18. The alloy 52 had been developed for use with alloy 690. Reports and investigations [66], [69] concluded that the increased Cr content of alloy 52 (table 2), [68] improved the resistance to SCC in the PWR pure water environment. Also noticeable from tables 8 to 13 is the fact that the %Fe content remained within a tight range of 10%-9.24%, thus giving a safety factor of approximately 100% over the critical 5% minimum Fe limit suggested by Stubbe *et al* [94] for any possibility of phase changes in such materials. The results show that the use of alloy 52 as the weld consumable/cladding material with alloy 690 tubing gives a weld and welded zone which is likely to remain stable over time, however, since no research to date has revealed the reasons why the Fe level above 5% stabilises these Ni/Cr alloys, the possibility of secondary phase transformation still exists.

5.7. Modified Huey Testing

The presence of 'sensitisation' can be ascertained using the Modified Huey Test. For the purposes of this research it was used for comparative testing purposes only and in no way meant to simulate operating environment(s). The results (table 19, figure 45) showed little or no attack of any alloy 690 samples over the welded, heat affected areas, or in the matrix tubing material. The material which had been accelerated aged to simulate twenty years service life was similarly unaffected by the testing. Results from previous detailed work by Smith [13] on this alloy have shown that the Cr content in areas adjacent to the grain boundary Cr carbide did not fall below 22% Cr when looking at as-received, STT condition alloy 690 material. The lowest grain boundary region Cr value found with experimentally welded alloy 690 in this research was 21.6% (table 12) in the fusion zone following a weld thermal cycle with increased heat input. A slightly higher Cr value of 21.9% was found intragranularly in the same sample. Thus attack by environments encountered when using the Modified Huey Test would not have been expected since previous research had proposed far lower minimum weight percent grain boundary region Cr levels for

corrosion resistance [55], [53], [16], [58]. It should be noted, however, that the figures quoted in the results have been acquired from SEM whilst the comparative published literature quoted exclusively used STEM. With the larger width beam of SEM, only an average reading across the grain boundary region is possible. Therefore, the results are open to interpretation.

The samples of welded alloy 600 were subject to light intergranular attack in the HAZ and matrix (table 19, figure 46). Results from previous work have shown that the Cr content, in areas adjacent to the grain boundary Cr rich carbides, may fall to as low as 7.7% in alloy 600 [53] thus rendering the alloy susceptible to corrosive attack in the test environment. The results found from the research by the author on alloy 600 (table 14) found levels of Cr in the range 16%-19%, a higher level than any previous research had proposed as a threshold for attack [55], [53], [16], [58].

Test specimens of welded alloy 800 were lightly intergranularly attacked in the fusion zone and severely intergranularly attacked in all other areas, as can be seen from table 19 and representative micrograph figure 47. It was noted that no corrosion occurred in the zones of the alloy 690 and alloy 690 type experimental melts, with only light intergranular attack on the alloy 600 welded specimens tested. Based upon the findings of previous research [55], [53], [16], [58] the chemical compositional results (tables 8 to 18) show the Cr content of the alloy 690 samples and experimental melts is not of a low enough percentage for attack during Modified Huey Testing to occur in any region. The Cr levels of the HAZ in the alloy 600 specimens was also high enough to preclude attack but light attack was visible.

As previously stated, the tests undertaken by Yamauchi et al [81] on alloy 600 type materials had shown an improved IGA resistance in simulated primary side environments when Nb was included instead of Ti. The studies by Yamauchi were

conducted on experimental melts using weight percentages of Nb in the region of 2.5%, an amount of Nb at which it is major alloying addition. Yamauchi et el concluded that suppressing the precipitation of Cr carbides by the stabilisation of the carbon as NbC lowered the grain boundary 'sensitisation' and so improved the corrosion resistance of the material. The results of the investigations for this thesis do not contradict the conclusions of Yamauchi *et al* in that they show Nb substitution for Ti in alloy 690 type material gives a high resistance to attack in the modified Huey test environment used.

Since the Modified Huey Test is primarily intended to show 'sensitisation', and, as in the HAZ of all the samples the majority of the Cr rich carbides had returned to solution, there should have been no 'sensitisation' and no attack. This should also have been the case for the alloy 800 samples where severe attack was recorded. This anomaly highlights the fact that no account is taken of processing and previous thermal history of the materials in the compilation of the minimum Cr levels. The pilgering process may well affect the 'sensitisation' resistance of the alloys in the absence of grain boundary Cr rich carbides. Also, the materials tested in the previous research investigations [55], [53], [16], [58] had been thermally treated in such a manner as to ensure an amount of 'sensitisation' in the grain boundary region. Further, the medium used in the test, boiling 60% nitric acid, was of a higher concentration than normally used. This percentage was chosen in order to increase the possibility of some form of attack on the alloy 690 specimens during the test and the hypothesis of the author is that this high acid concentration is the reason why light attack was seen on the alloy 600 specimens and why the alloy 800 specimens were severely affected.

To summarise, comparing the results from the Modified Huey Tests on the range of materials investigated, the alloy 690 samples all performed excellently with no signs of corrosive attack. This was also the case for the experimental alloy 690 type alloys

with Nb substitution for Ti. The alloy 600 samples showed only light attack within the HAZ. The alloy 800 samples were attacked in all areas, severely so in the HAZ and matrix.

5.8. Constant Extension Rate Testing

The welded and unwelded specimens had similar fracture surfaces following the testing in pure argon at 320°C indicating ductile failures. Angeliu and Was [91] postulated that the intergranular cracking susceptibility of Ni/Cr based alloys was inherently linked to their creep behaviour and undertook CERT testing in argon environments at 360°C. The difficulties with making direct comparisons to the work of Angeliu and Was are two-fold. Firstly, high purity experimental melts were used by Was as opposed to commercial materials and secondly the equipment used was capable of slower CERT rate and the testing rates were typically around 100 times slower than those used in the research by the author. These tests had been run at a higher rate than would have been preferred. This was due to the physical limitations of the machine used. What is clear, however, is that Angeliu and Was also found the fracture surfaces of their samples to exhibit ductile failure characteristics. Creep deformation was not identified in the studies by the author but the higher CERT rates used would have precluded any signs of such failure mechanisms.

5.9. Concluding Discussion

To date, the tube to tubeplate welded region of PWR SGs has not been considered an area of primary concern although it has been acknowledged that the weld thermal cycle has a detrimental affect on the materials [11]. The continued search for improved materials and materials reliability has led to the increased use of alloy 690 as a tubing material. The material has been used in service since the late 1980's in both new SG plant construction (as was the case for Sizewell B) and in replacement

SGs; to date, the service record of the material has been excellent but this period is only a small amount of the hopeful life of a new PWR plant. With this increased reliability of the heat exchanger tubes the results from the research by the author indicate that the welded region is now a possible area for onset of degradation and failure. Whilst the SG fabricators argue that the weld is non-critical since the tubes are fully hydraulically expanded into the tubesheet, the welds have recently been known to leak under reverse pressure hydro tests on French PWR systems [103].

This research has indicated that the precipitate distribution is adversely affected by the welding process during SG fabrication, with the majority of the Cr rich grain boundary precipitates taken into solution in the HAZ. There has also been a highlighting of the detrimental composition changes, particularly in the weld fusion zone, following the weld thermal cycle. Alloy 52 is now the preferred weld consumable for use as the tubeplate cladding material with alloy 690 tubing and its adoption and continued use is welcomed as it has a chemical composition closely matching alloy 690. However, a considerable number of PWRs are in operation with the alloy 82 weld consumable cladding to alloy 690 heat exchanger tube combination of materials in their SGs. Results from this research indicate a possible problem of phase transformation over time within the fusion zone of these materials due to the Ni/Cr ratios and low Fe content after welding.

Other degradation processes affect the materials when the Fe content is lowered and any Pb contamination, which can lead to catastrophic failure [11], [104], [105] is compounded in such cases. It has further been shown that the grain growth in the HAZ of the materials due to the effects of the weld thermal cycle gives a non-uniform grain size in this zone. In the alloy 690 samples the resulting range of grain sizes are larger than recommended in PWR SG manufacture [4].

A number of conclusions can be drawn from this research programme. These are detailed in the next section.

6. Conclusions

A method of metallographic sample preparation for TEM thin foil specimens which ensures foil perforation in a specific region (e.g. HAZ) has been developed and documented. The technique has a number of distinct advantages over other methods, these being:

◊ Reproducibility.

◊ Assured perforation in centre of foil.

◊ Reliable and highly efficient.

◊ Dispenses with the use of hazardous materials such as perchloric acid.

◊ Relatively fast sample preparation time.

Samples of alloy 690 SG tube autogenously welded to alloy 82 weld consumable cladding have been manufactured and these specimens compare favourably with archive material from the Sizewell B PWR SG programme. The method of weld sample preparation has been documented and is repeatable with a high degree of accuracy.

Weld thermal cycles using increased and decreased heat inputs have been used to define the upper and lower limits allowed whilst ensuring a structurally integral welded joint. These welds have been characterised and any changes in the welds from the use of these cycles noted.

Welded samples of alloy 690 SG tubing to alloy 52 weld consumable cladding have been produced using recommended PWR weld parameters. These samples have been

compared with the experimental and archive alloy 690/alloy 82 combinations and the results recorded. The combination of alloy 690 tube with alloy 52 cladding has been identified as a viable match of materials.

The weld thermal cycle has been shown to alter the specially thermally treated (STT) microstructure of alloys 600 and 690 and the processed alloy 800.

During welding, the thermal cycle experienced by the HAZ resulted in dissolution of the base metal Cr rich precipitates within the HAZ region. This was the case for all the materials investigated and irrespective of the experimental weld thermal cycle used. Since the original STT microstructure of semi-continuous chains of grain boundary Cr rich precipitates is acknowledged as beneficial, it must be expected that this dissolution adversely affects the environmental degradation resistance and associated life expectancy of the materials.

The microhardness of the HAZ resulting from welding is lower than that of the original SG tubing material. When using weld parameters and materials specified for the Sizewell B PWR this reduction in microhardness was 6%-7%. For samples subjected to two weld thermal cycles, used to simulate the effects of weld repair, this reduction increased to 10%.

Ti rich precipitates, and in the case of the experimental melts Nb rich precipitates, were identified in the fusion zone, HAZ and matrix of the materials and welds tested.

The width of the relatively precipitate free region adjacent to the fusion zone of the welded samples indicated the size of the weld HAZ, the transition from precipitate free to precipitate decorated grain boundaries being the true limit of the HAZ.

The precipitate dissolution with its associated grain boundary liquation gives rise to a loss of strength and to heterogeneous grain growth in the HAZ. In the case of the alloy 690 specimens and the archive welds from the Sizewell B project the resulting range of grain sizes in the HAZ is larger than the ASTM6 or smaller recommended by the French manufacturers, Vallourec, for nuclear PWR SG applications [4].

The benefits to be gained from the substitution of Nb for Ti in alloy 690 type materials was inconclusive. The experimental materials performed well and investigations of the microstructure of the materials indicated a suitability for use. More work is needed on long term testing using in-service environments before the initial positive results can be substantiated.

The microhardness of the weld affected areas (fusion zone and heat affected zone) is lower than that of the matrix in all cases. The reduction is not of proportions to cause concern, nor any increased probability of tube failure due to this hardness change.

Welded alloy 690 to alloy 82 cladding was immune to IGA in the Modified Huey Test under the conditions used, irrespective of the weld thermal cycle employed. Welded alloy 690 to alloy 52 was also immune to attack in these environments. Accelerated ageing of the welds did not affect the high resistance of the alloy 690 welds to attack under the Modified Huey Test conditions used.

The HAZ of autogenously welded alloy 600 was lightly attacked intergranularly when exposed to the Modified Huey Test. The fusion zone consisting of an alloy of alloy 600 and alloy 82, and the alloy 600 matrix were both unaffected.

Autogenously welded alloy 800 samples were intergranularly attacked in the fusion zone, HAZ and matrix when exposed to the Modified Huey Test. Within the HAZ and matrix the attack was severe and resulted in grain drop-out on the tube sample edges.

An analysis of the weld fusion zone of the alloy 690 specimens incorporating alloy 82 weld consumable as the cladding material has revealed that the chemical composition is approaching that required for short range order and/or long range order (SRO/LRO) to occur.

Incorporation of the alloy 52 weld consumable as the cladding material for use with alloy 690 tubing in the experimental welds resulted in a microstructural and chemical composition suitable for PWR steam generator applications.

Constant Extension Rate Testing (CERT) in argon at 320°C indicated ductile fracture modes in both welded and unwelded specimens of alloy 690 manufactured from commercial archive tubing from the Sizewell B PWR SG project.

During CERT experimentation the 0.2% yield strength (YS) and the ultimate tensile strength (UTS) of the unwelded samples was lowered at this elevated temperature, similar in magnitude to PWR primary side operating temperature. With the welded samples YS and UTS were lowered further.

During CERT experimentation, fracture of the welded samples occurred across the HAZ in all cases.

7. Recommendations for Future Work

7.1. Long and Short Range Ordering

The weld fusion zones of the alloy 690 specimens incorporating alloy 82 weld consumable as the cladding material have a potentially deleterious chemical composition. The Ni and Cr concentrations coupled with the low amounts of Fe recorded indicate the possibility of long range/short range order changes at high temperature. To investigate this potential phenomena it is recommended that experimental melts be produced which approximate to the weld fusion zone compositions described. Characterisation of these experimental melts should be carried out in terms of physical properties and microstructural examination.

The materials should be heat-treated over a range of temperatures and times and a critical temperature for the onset of short range/long range ordering within the specimens be identified. Transmission electron microscopy (TEM) examinations should be carried out to ascertain the onset of ordering in terms of time and temperatures. An examination of how alloy composition variations affects the short/long range ordering should also be undertaken. Presently there is insufficient data to predict the likelihood of SRO or LRO in alloy 690 under operating conditions. The work recommended would more clearly identify the effect that time/temperature and critical Fe content has for the onset of ordering.

7.2. Nb substitution for Ti

The possible benefits of such a substitution needs further clarification. A series of experimental melts with alloy 690 type composition with the substitution of Nb for Ti should be produced and then manufactured into tubing material by means of the pilgering process. Samples of these tubes should be treated to a series of STT times and temperatures and the resulting microstructures examined with particular attention to the shape size and distribution of the Nb rich precipitates formed.

A number of these samples should be welded using PWR weld parameters, whilst other samples should be kept in STT conditions. The welded samples should then be microstructurally examined and similarities with work from this thesis noted. Long term corrosion studies should be undertaken (minimum 5,000 hours) in controlled, simulated PWR primary side environments. More detailed conclusions can then be drawn and the results compared.

References

1.   R L Sylvester, J P Fogarty, J L Thomson. 'Sizewell 'B' Steam Generator design builds upon the Westinghouse Model F to meet United Kingdom Safety Case.' Sizewell 'B' - The First of the UK PWR Power Stations, Ramada Renaissance Hotel, Manchester. 13-14 September 1989. Conf. Proc., p143-154.

2.   P Skeldon, P M Scott, P Hurst. 'Environmentally Assisted Cracking of Alloy X-750 in Simulated PWR Coolant.' Corrosion 1992. Vol. 48, p553-569.

3.   W Marshall. 'An assessment of the integrity of PWR pressure vessels - second report by a study group'. UKAEA, London, March 1992.

4.   D Vuillaume. 'PWR steam generator tubes in Alloy 690 - Key manufacturing steps and their influence.' Vallourec Industries, France. Technical Report No. 2088 1st edition - January 1987.

5.   H Domain, R H Emanuelson, L W Sarver, G J Theus, L Katz. 'Effect of Microstructure on Stress Corrosion Cracking of Alloy 600 in High Purity Water.' Corrosion 1977. Vol. 33, p26.

6.   A M Lancha, D Gómez-Briceño, M García, E López Toribio. 'AES and SEM/EDS Analysis of Deposits in Pulled Steam Generator Tubes.' Sixth International Symposium on Environmental Degradation of Materials in Nuclear Power Systems - Water Reactors - Bahia Resort Hotel, San Diego, CA, USA 1-5 August 1993. p845-853. Conf. Proc.

7.   'Research Office Reconsiders Stance on New Steam Generator Criteria ' - Nucleonics Week. 3 December 1992. Vol. 33, No 49, p5.

8.   'RG&E to Replace Steam Generators, a Hopeful Sign Amidst Shutdowns.' - Nucleonics Week. 31 December 1992. Vol. 33, No 52, p1.

9. 'PGE to Shut Down Trojan Rather Than Spend More on Steam Generators.' - Nucleonics Week. 7 January 1993. Vol. 34, No 1, p1.

10. I L W Wilson, F W Pement, R G Aspden, R T Begley. 'Caustic Stress-Corrosion Behavior of Fe-Ni-Cr Nuclear Steam Generator Tubing Alloys.' Nuclear Technology, October 1976. Vol. 31, p70.

11. Private Communication with L Nelson, R Pathania, A McIlree, Electric Power Research Institute (EPRI), Palo Alto, CA, United States of America. - August 1993.

12. G P Airey, A R Vaia, R G Aspden. 'A Stress Corrosion Cracking Evaluation of Inconel 690 for Steam Generator Tubing Applications.' Nuclear Technology, November 1981. Vol. 55, p436.

13. A J Smith. 'The Microstructure and Precipitation Effects in Inconel Alloy 690.' PhD Thesis, Sheffield City Polytechnic, 1990.

14. R Tuttle. 'The Effect of the Weld Thermal Cycle on the Corrosion Resistance of Alloy 690.' Junior Euromat '92 - Lausanne, Switzerland 24-28 August 1992. Conf.Proc., p134-135.

15. K Stiller. 'Intergranular precipitation in Ni-Cr-Fe alloys.' Surface Science. Edition 266 (1992). p402-408.

16. Ernest L Hall and Clyde L Briant. 'The Microstructural Response of Mill-Annealed and Solution-Annealed INCONEL 600 to Heat Treatment.' Metallurgical Transactions A, July 1985. Vol. 16A, p1225-1236.

17. M H Lewis, B Hattersley. 'Precipitation of $M_{23}C_6$ in Austenitic Steels.' Acta Metallurgica, November 1965. Vol. 13, p1159-1168.

18. T M Angeliu, G S Was. 'Behavior of Grain Boundary Chemistry and Precipitates upon Thermal Treatment of Controlled Purity Alloy 690.' Metallurgical Transactions A, August 1990. Vol. 21A, p2097-2107.

19. Private Communication with Dr B Hattersley, Sheffield Hallam University - April 1993.

20. W F Smith. 'Structure and Properties of Engineering Alloys.' 2nd Edition, 1993. McGraw Hill Publications. Chapter 7, (Stainless Steels).

21. J M Sarver, J R Crum, W L Mankins. 'Carbide Precipitation and SCC Behavior of Inconel Alloy 690.' Corrosion, May 1988. Vol. 44, No 5, p288-289.

22. R A Page, A McMinn. 'Relative Stress Corrosion Susceptibilities of Alloys 690 and 600 in Simulated Boiling Water Reactor Environments.' Metallurgical Transactions A, May 1986. Vol. 17A, p877-887.

23. Sizewell 'B' Public Inquiry Report No. LPA/P/4. 'Structural Integrity of the Primary Circuit - (figures and tables).' Publ. Suffolk County Council & Suffolk Coastal District Council, April 1983.

24. C Gimond. 'Corrosion Performance of Alloy 690.' Proceedings, EPRI Workshop on Thermally Treated Alloy 690 for Nuclear Steam Generators, Pittsburgh, June 1985.

25. 'Vessel Head Penetration Cracks Found in Second Generation PWRs.' Nucleonics Week - 17 December 1992. Vol. 33, No 51, p1.

26. 'EDF Learns Tough Lessons From Cracked Vessel Head Penetrations.' Nucleonics Week - 17 December 1992. Vol. 33, No 51, p16.

27. 'Emphasis on Steam Generator Replacement Shifts to US.' ATOM May/June 1992. No 422, p8.

28. J C Smith, M D Lees. 'Design of the Replacement Steam Generators for Millstone II.' Joint ASME/IEE Power Generation Conference, Dallas, Texas, October 24-26 1989. Conf. Proc., p1-7.

29. 'Steam Generator Replacements are on Schedule at North Anna.' Nucleonics Week - 28 January 1993. Vol. 34, No 4, p8.

30. P Gane. 'Microstructure and Precipitation Effects in Inconel Alloy 600.' PhD Thesis, Sheffield Hallam University, April 1992

31. G S Was. 'Grain-Boundary Chemistry and Intergranular Fracture in Austenitic Nickel-Base Alloys - A Review.' Corrosion, April 1990. Vol. 46, No 4, p319-330.

32. 'Steam Generator Woes Play Role in Extended Bruce-3 Shutdown.' - Nucleonics Week. 14 January 1993. Vol. 34, No 2, p3.

33. S Smialowska, G Cragnolino, D Macdonald. 'Surface and Grain Boundary Segregation, Stress Corrosion Cracking, and Corrosion Fatigue on Inconel 600.' Electric Power Research Institute (EPRI) Interim Report No. NP-3949M. March 1985.

34. D R Johns, F R Beckitt. 'Factors Influencing the Thermal Stabilisation of Alloy 600 tubing Against Intergranular Corrosion.' Corrosion Science, 1990. Vol. 30, No 2/3, p223-237.

35. P M Scott. 'A Review of Environmental-Sensitive Fracture in Water Reactor Materials.' Corrosion Science, 1985. Vol. 25, No 8/9, p583-606.

36. A W Klein, R J Jacko, C E Sessions, A R Vaia. 'Performance of Thermally Treated Inconel 600 and Inconel 690 Steam Generator Tubing Alloys.' NEA/CSNI-UNIPEDE specialist meeting on Steam Generators - Stockholm, Sweden 1-5 October 1984. Conf. Proc., CSNI Report No.91 Vol. II, p434-444.

37. G Economy, R Jacko, F W Pement. 'IGSCC Behavior of Alloy 600 Steam Generator Tubing in Water or Steam Tests Above 360 C.' Corrosion, December 1987. Vol. 43, No n12, p727-734.

38. J Champredonde, D Buisine, F Cattant, C Pichon, A Gelpi, C Benhamou, M Vaindirlis. 'Stress Corrosion Cracking of Vessel Head Penetrations in French PWRs.' Sixth International Symposium on Environmental Degradation of Materials in Nuclear Power Systems - Water Reactors - Bahia Resort Hotel, San Diego, CA, USA 1-5 August 1993. p845-853. Conf. Proc.

39. C Faidy, C Pichon, S Bhandari, J Vagner. 'Stress Corrosion Cracking in French PWR CRDM Penetrations.' SISSI 94 - International Seminar on Structural Integrity. Saday, France 28-29 April 1994. Conf. Proc.

40. 'French Eye Standards For Repairing Vessel Head Penetration Cracks.' Nucleonics Week - 28 January 1993. Vol. 34, No 4, p9.

41. 'First cracks found above the vessel head.' ATOM March/April 1994. No 433, p10.

42. A Mignone, M F Maday, A Borello, M Vittori. 'Effect of Chemical Composition, Thermal Treatment and Caustic Concentration on the SCC Behavior of Alloy 800.' Corrosion, January 1990. Vol. 46, No 1, p57-65.

43. J Stubbe, F Wolters, K De Ranter, Ph Somville. 'Why Inconel 800 was selected as the tube material for the new Steam Generators of Doel 3.' International Colloquium on Contribution of Materials Investigation to the Resolution of Problems in PWR Plants - Fontevraud, France 10-14 Sept. 1990. Conf. Proc., p398-407.

44. J O Nilsson. 'Influence of dislocation precipitation interaction on low cycle fatigue resistance of Alloy 800 at 600°C.' Materials Science, July 1984. Vol. 18, p351-355.

45. G Airey, I Woolsey. 'Water Chemistry - Preventing erosion - corrosion at Sizewell 'B'.' Nuclear Engineering International, October 1989.

46. W B Jones, R M Allen. 'Mechanical Behavior of Alloy 800 at 838K.' Metallurgical Transactions A, April 1992. Vol. 13A, p637-648.

47. J A Lambert. 'The effect of cast-to-cast variations on the quality of thin section nickel containing alloy welded joints.' Welding & Fabrication, May 1990.

48.	A D Romig Jr., J C Lippold, M J Cieslak. 'An Analytical Electron Microscope Investigation of the Phase Transformations in a Simulated Heat-Affected Zone in Alloy 800.' Metallurgical Transactions A, January 1988. Vol. 19A, p35-50.

49.	G P Rothwell, J A Bernie, A K Tiller. 'A review of the corrosion behaviour of INCOLOY 800 in pressurized-water reactor steam generator environments.' National Physical Laboratory, Teddington, Middlesex. Report No. 0021 NPK.63/16/14 for Health & Safety Executive Nuclear Installations Inspectorate. 18 Feb. 1977.

50.	Departmental Brochure 1992/93, Department des Materiaux, Laboratoire de Metallurgie des Soudres, Ecole Polytechnique Federal de Lausanne, Lausanne, Switzerland. p5.

51.	R E Dolby, D J Widgery, 'Simulation of HAZ Microstructures.' The Welding Institute. April 1972.

52.	P L Andresen. 'Effects of Temperature on Crack Growth in Sensitized Type 304 Stainless Steel and Alloy 600.' Corrosion '92, 26 April - 1 May 1992, Nashville, Tennessee. Paper no 89 p89/1-89/8

53.	J J Kai, C H Tsai, G P Yu. 'The IGSCC, sensitization, and microstructure of Alloys 600 and 690.' Nuclear Engineering and Design, Vol. 144, 1993. p449-457.

54.	R C Scarberry, S C Pearman, J R Crum. 'Precipitation Reactions in Inconel Alloy 600 and Their Effect on Corrosion Behavior.' Corrosion, Vol. 32 No 10, October 1976. p401-406.

55.	G P Airey, A R Vaia, N Pessall, R G Aspden. 'Detecting Grain-Boundary Chromium Depletion in Inconel 600.' Journal of Metals, November 1981. p28-35.

56. G S Was, R M Kruger. 'A Thermodynamic and Kinetic Basis for Understanding Chromium Depletion in Ni-Cr-Fe Alloys.' Acta Metallurgica, Vol. 33 No 5, 1985. p841-854.

57. J M Sarver, J R Crum, W L Mankins. 'Carbide Precipitation and the Effect of Thermal Treatments on the SCC Behavior of Inconel 690.' 3rd International Symposium on Environmental Degradation of Materials in Nuclear Power Systems - Water Reactors. TMS, Kohler, WI. 1988.

58. C L Briant, E L Hall. 'Intergranular Corrosion of High Chromium Nickel-Base Alloys.' Corrosion, July 1987, Vol. 43, No 7, p437-440.

59. R M Kruger, G S Was. 'The Influence of Boron on the Grain Boundary Chemistry and Microstructure of Ni-16Cr-9Fe-0.003C.' Metallurgical Transactions A, October 1988. Vol. 19A, p2555-2566.

60. D Gomez Briceno, L Castana Marin, S Garcia Redondo. 'Influence of LiOH on PWSCC of Alloy 600.' International Atomic Energy Authority (IAEA) Specialists Meeting on Steam Generator Problems and Replacement - Madrid, Spain 13-16 December 1993. Conf. Proc.

61. P L Andresen. 'Observation and Prediction of the Effects of Water Chemistry and Mechanics on Environmentally Assisted Cracking of Inconels 182 Weld Metal and 600.' Corrosion, June 1988, Vol. 44, No 6, p376-385.

62. R A Page. 'Stress Corrosion Cracking of Alloys 600 and 690 and Nos. 82 and 182 Weld Metals in High Temperature Water.' Corrosion, October 1983. Vol. 39, No 10, p409-421.

63. C L Briant, E L Hall. 'The Microstructural Causes of Intergranular Corrosion of Alloys 82 and 182.' Corrosion, September 1987. Vol. 43, No 9, p539-548.

64. A McMinn, R A Page. 'Stress Corrosion Cracking of Inconel Alloys and Weldments in High-Temperature Water - The Effect of Sulfuric Acid Addition.' Corrosion, April 1988. Vol. 44, No 4, p239-247.

65. M J Povich. 'Low Temperature Sensitization of Type 304 Stainless Steel.' Corrosion, February 1978. Vol. 34, No 2, p60-65.

66. C L Briant, E L Hall. 'The Microstructure and Corrosion Resistance of Nickel-Based Filler Metals with High Chromium Contents.' The Welding Journal - Welding Research Supplement, February 1990, p60-67s.

67. R A Page, A McMinn. 'Stress Corrosion Cracking Resistance of Alloys 600 and 690 and Compatible Weld Metals in BWRs.' Electric Power Research Institute (EPRI) Report NP-5882S, Research Project 1566-1. July 1988.

68. INCONEL Filler Metal 52 and INCONEL Welding Electrode 152 Data Sheet. Inco Alloys International Data Sheet Publication No IAI-106. 1992.

69. R Brosilow, S Kiser. 'Better fillers for nuclear welds.' Welding Design and Fabrication, Vol. 66, No 12, Dec 1993, p32-33.

70. Jean-Pierre Mercier. 'How EdF has coped with vessel head penetration cracking.' ATOM magazine, May/June 1992. Vol. 422 p26-27.

71. R Bandy, D Van Rooyen. 'Stress Corrosion Cracking of Inconel Alloy 600 in High Temperature Water - An Update.' Corrosion, August 1984, Vol. 40, No 8. p425-430.

72. 'Vessel Head Penetration Cracking in Nuclear Reactors.' Greenpeace International and Greenpeace Sweden, March 1993.

73. V S Beckett. 'Safety philosophy and implications on plant design of Sizewell 'B'.' Sizewell 'B' - The First of the UK PWR Power Stations, Ramada Renaissance Hotel, Manchester. 13-14 September 1989. Conf. Proc., p7-12.

74. D B Boettcher, S J Cereghino. 'Diversity: safety system design against common mode failure.' Sizewell 'B' - The First of the UK PWR Power Stations, Ramada Renaissance Hotel, Manchester. 13-14 September 1989. Conf. Proc., p13-20.

75. Rapport sur les coûts de référence de la production d'eletricité d'origine thermique. Ministère de l'Industrie Français, September 1986.

76. 'Nuclear Industry Deflects Greenpeace on Cracking Issue.' Nucleonics Week - 1 April 1993. Vol. 34 No 13, p1.

77. J Bacot, M Guinot, J Tassera. 'Opting for a 2-cut scenario at Dampierre 1.' Nuclear Engineering International, January 1990. p29-32.

78. Etienne Pierson, Jacqueline Stubbe. 'SCC Testing of Steam Generator Tubes Repaired by Welded Sleeves.' Sixth International Symposium on Environmental Degradation of Materials in Nuclear Power Systems - Water Reactors - Bahia Resort Hotel, San Diego, CA, USA 1-5 August 1993. p697-704. Conf. Proc.

79. B Michaut, F Steltzlen, B Sala, Ch Laire, J Stubbe 'Nickel Electroplating as a Remedy to Steam Generator Tubing PWSCC.' Sixth International Symposium on Environmental Degradation of Materials in Nuclear Power Systems - Water Reactors - Bahia Resort Hotel, San Diego, CA, USA 1-5 August 1993. p713-719. Conf. Proc.

80. Yoshimitsu Kajii. 'Kansai looks at laser sleeving.' Nuclear Engineering International, January 1990. p35-36.

81. K Yamauchi, T Katori, T Okazaki, Y Sakaguchi. 'Improvement of intergranular stress corrosion cracking resistance of Ni-Cr-Fe alloy 600 by means of stabilization parameter control.' Nuclear Engineering and Design, Vol. 129, 1991 p321-330.

82. S M Payne, P McIntyre. 'Influence of Grain Boundary Microstructure on the Susceptibility of Alloy 600 to Intergranular Attack and Stress Corrosion Cracking.' Corrosion, May 1988, Vol. 44, No 5, p314-319.

83. G Kohn, B Herrmann, A Stern, E Rabinovitz, S Addess. 'Failure of welded Inconel-600 pipe in the cooling systems of a nuclear reactor.' Second Israel Materials Engineering Conference, Beer-Sheva, Israel, 21-23 February 1984. p147-151. Conf. Proc.

84. R A Patterson, R B Nemec, R D Reiswig. 'Discontinuities Formed in Inconel GTA Welds.' The Welding Journal - Welding Research Supplement, January 1987. p19s-25s.

85. J C Lippold. 'An Investigation of Heat-Affected Zone Hot Cracking in Alloy 800.' The Welding Journal - Welding Research Supplement, January 1983. p1s-11s.

86. 'Autogenous Gas Tungsten Arc Welding (GTAW) for Joining 11/16" x .040" Inconel Tubing to Inconel Clad Tubesheets (Flush).' Westinghouse Electric Corporation Nuclear Component Division, Process Specification Sheet No. 82127 RQ.

87. Archive SG tube-to-tubesheet weld material supplied by Babcock Energy Ltd., Renfrew, Scotland.

88. D B Lowenstein, C E Shoemaker, J A Gorman. 'Etching Techniques and Carbon Analysis for Alloy 690.' Fourth International Symposium on Environmental Degradation of Materials in Nuclear Power Systems - Water Reactors, Jekyll Island, Georgia, USA 6 - 10 August 1989. p5.2-5.15. Conf. Proc.

89. J M Titchmarsh, G Cattle. 'Microstructural Examination of Inconel Steam Generator Tubing.' HSE Co-ordinated Nuclear Safety Research Programme. Final Report (Confidential Document) No. AEA-RS-4377. November 1993. p.3,5,7-8.

90. Private Communication with J Titchmarsh. Formerly of AEA Technology, Harwell, now at Sheffield Hallam University, Materials Research Institute. November 1993.

91. T M Angeliu, G S Was. 'Creep and Intergranular Cracking of Ni-Cr-Fe-C in 360°C Argon.' Metallurgical and Materials Transactions A, Vol. 25A, June 1994. p1169-1183.

92. Private Communication with Babcock Energy Ltd, Renfrew, Scotland. February 1992.

93. S C Ernst, G Y Lai. 'A New Fe-Ni-Co-Cr Filler Metal for Joining Alloy 800H.' Materials Performance, Vol. 28(a), August 1989. p58-61.

94. J Stubbe, E Pierson. 'Possible effects of short and long range order on the in-service behaviour of nickel alloys used for steam generator tubes.' Belgisch Laboratorium Van De Elektriciteitsindustrie (LABORELEC) Internal Report No. C-EP/JS/GDJ/ld. 18th December 1989.

95. 'Inconel alloy 690' - Data Sheet - Inco Alloys International Publication #T-49, 1980.

96. K Easterling. 'Introduction to the Physical Metallurgy of Welding - 2nd Edition'. Butterworth-Heinemann Ltd. 1992. ISBN 0 7506 0394 1.

97. C.M. Adams Jnr. 'Cooling Rates and Peak Temperatures in Fusion Welding.' The Welding Journal - Welding Research Supplement, 37(5), 1958. P210s-215s

98. J C Lippold, W A Baeslack III, I Varol. 'Heat-Affected Zone Liquation Cracking in Austenitic and Duplex Stainless Steels.' The Welding Journal - Welding Research Supplement, January 1992. p1s-14s.

99. J E Burke, D Turnbull. 'Recrystallisation and Grain Growth.' In Chalmers: Progress in Metal Physics, III, 1952. p220-292.

100. B Radhakrishnan, R G Thompson. 'Kinetics of Grain Growth in the Weld Heat-Affected Zone of Alloy 718.' Metallurgical Transactions A, Vol. 24A, December 1993. p2773-2785.

101. R J Bowes, E F Nippes. 'Heat-Affected Zone Thermal Cycles in Inconel 718.' The Welding Journal - Welding Research Supplement, December 1993. p523s-528s.

102. Private Communication with R Nicholson, H M Nuclear Installations Inspectorate. March 1995.

103. Private Communication with R Nicholson, H M Nuclear Installations Inspectorate. June 1994.

104. T Sakai, T Senjuh, K Aoki, T Shingemistu, Y Kishi. 'A Study on Corrosion Resistance of Alloy 600 and 690 in High Temperature Water Containing Lead.' Corrosion '92 Conference, Nashville, Tennessee, 26 April - 1st May 1992. Conf. Proc.

105. P J King, F Gonzalez, J Brown. 'Stress Corrosion Cracking Experience in Steam Generators at Bruce NGS.' Sixth International Symposium on Environmental Degradation of Materials in Nuclear Power Systems - Water Reactors - Bahia Resort Hotel, San Diego, CA, USA 1-5 August 1993. p233-243. Conf. Proc.
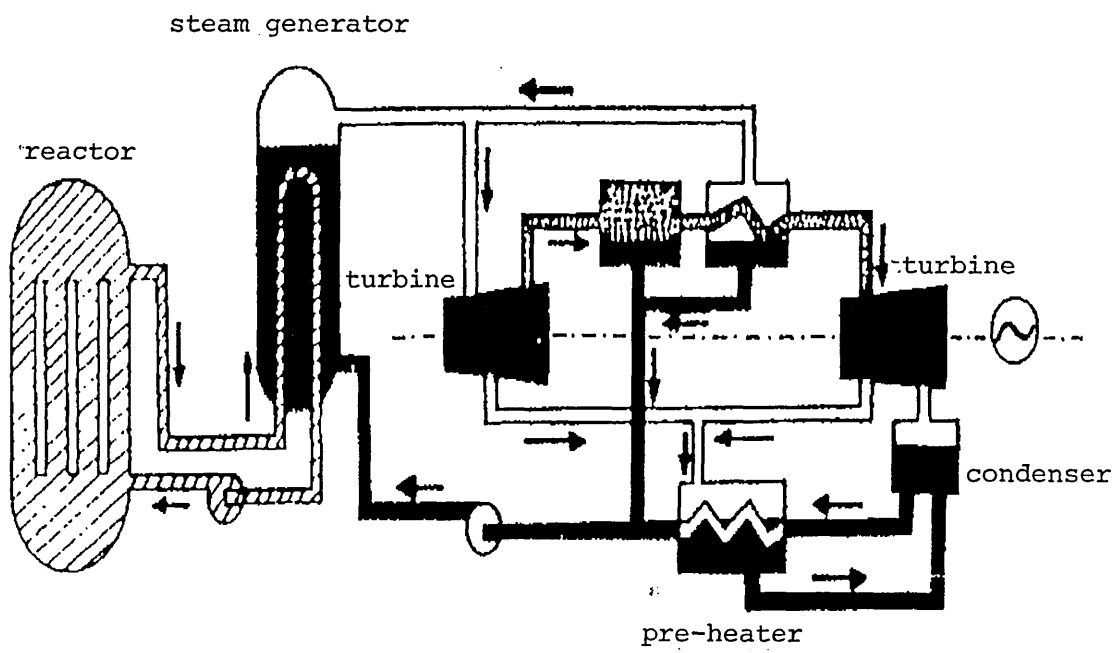
Figure 1. Schematic Diagram of a Pressurised Water Reactor System

Steam generator

Reactor coolant pump

Pressurizer

Nuclear reactor vessel
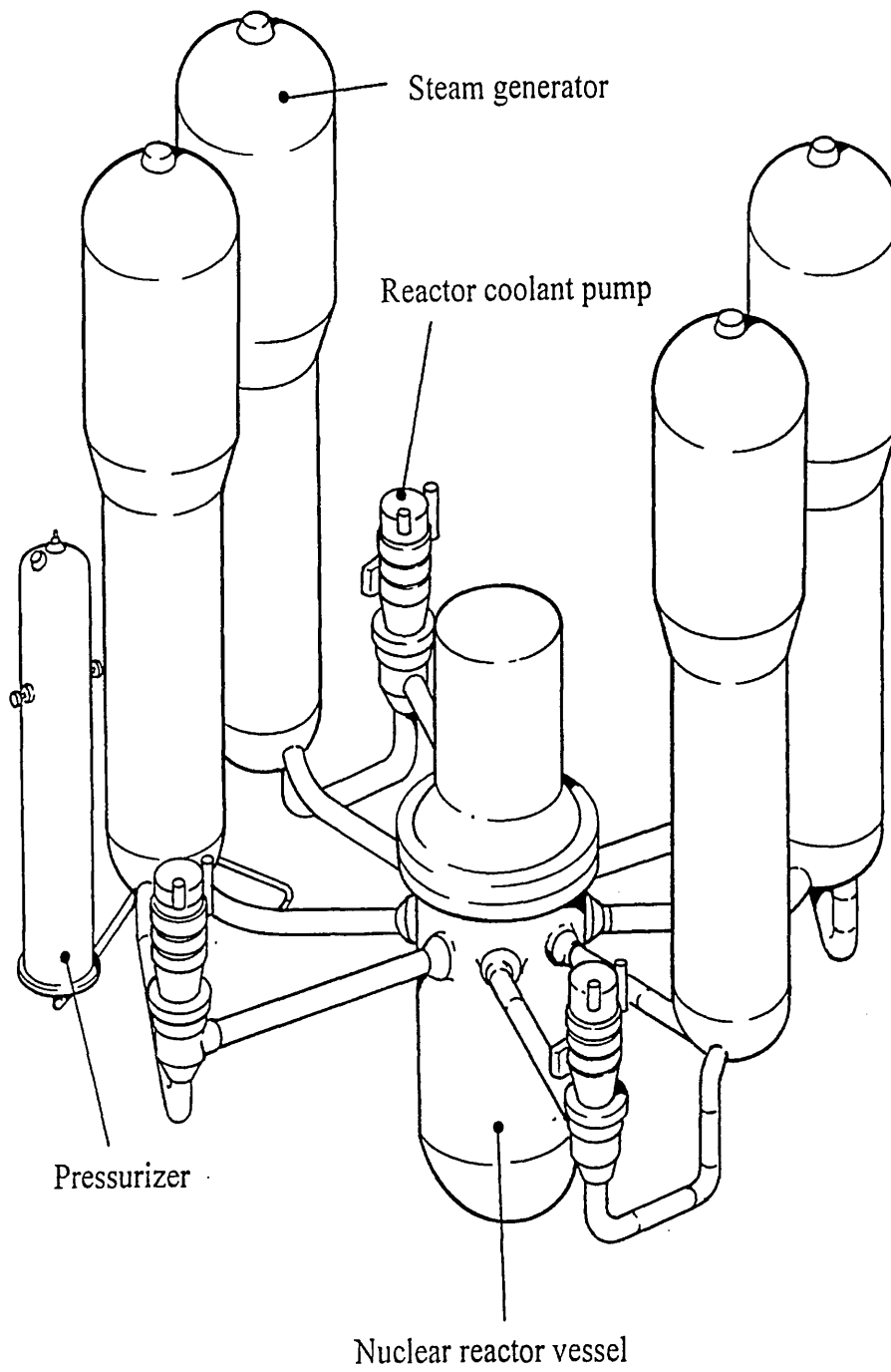
Figure 2. Sizewell B Nuclear Power Plant Steam Supply System
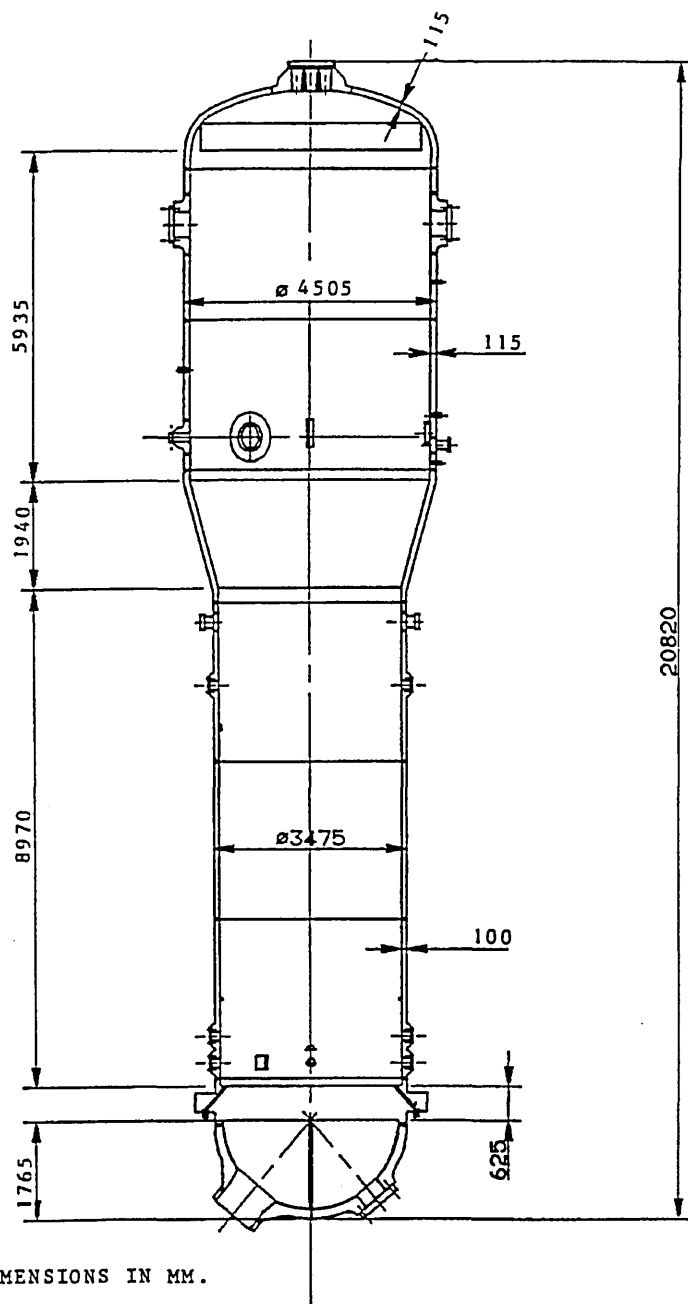
Figure 3. Westinghouse Model F Steam Generator Dimensions
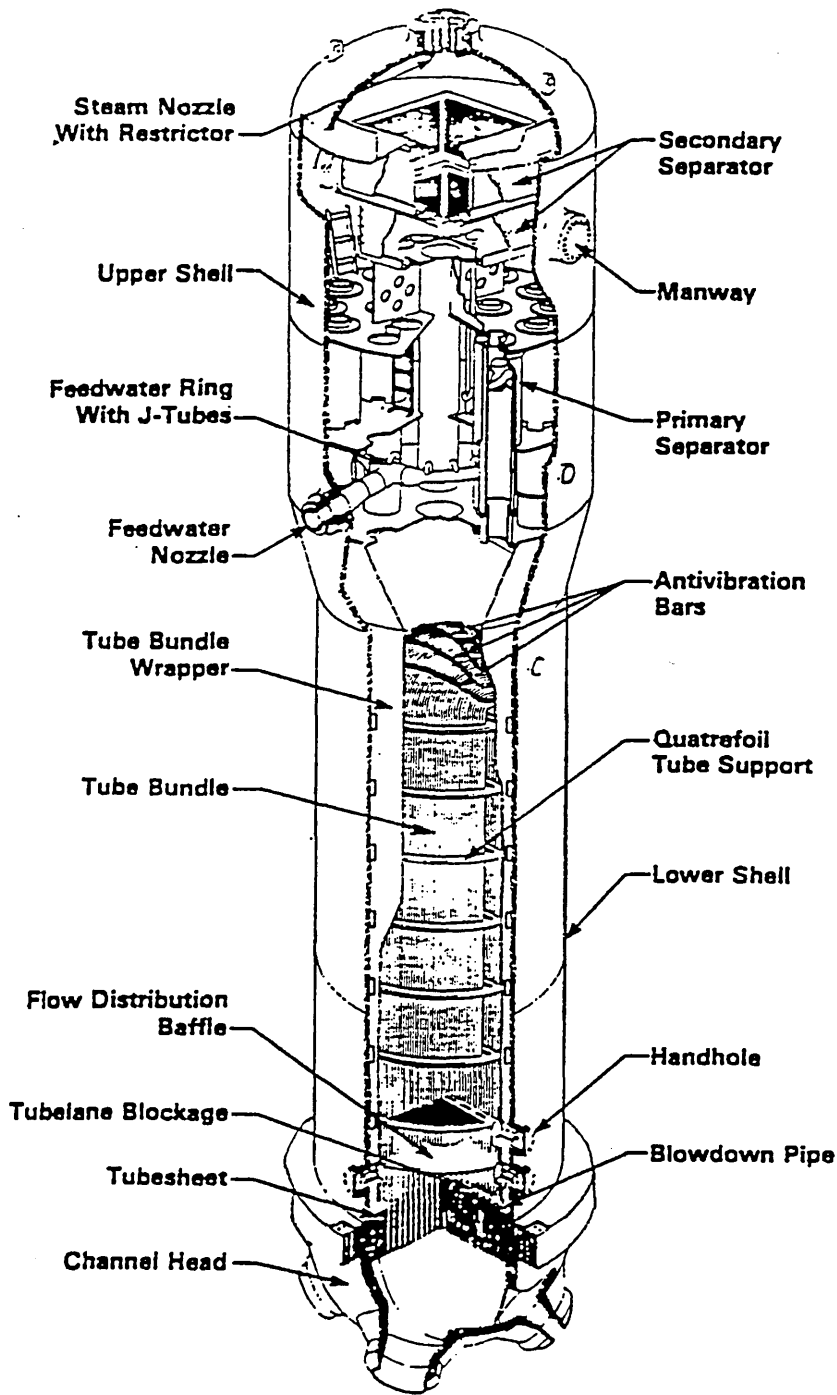
Figure 4. Sectioned View of Westinghouse Model F Steam Generator
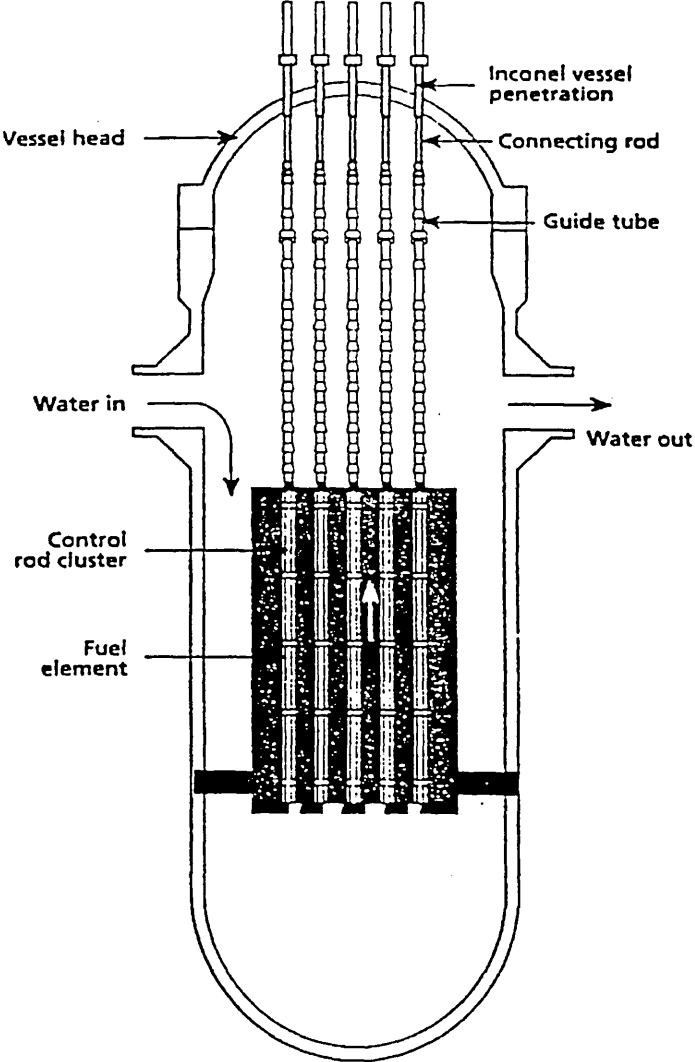
Figure 5. Sectioned View of PWR Reactor Pressure Vessel - showing reactor vessel head penetrations which allow the control rod drive mechanisms to pass through the reactor vessel head

Upper drive
mechanism

Thermal sleeve

Vessel head dome
carbon steel

Stainless steel cladding

Inconel 182 buttering

Inconel 182 weld

Inconel vessel penetration

Connecting rod

Conical guide
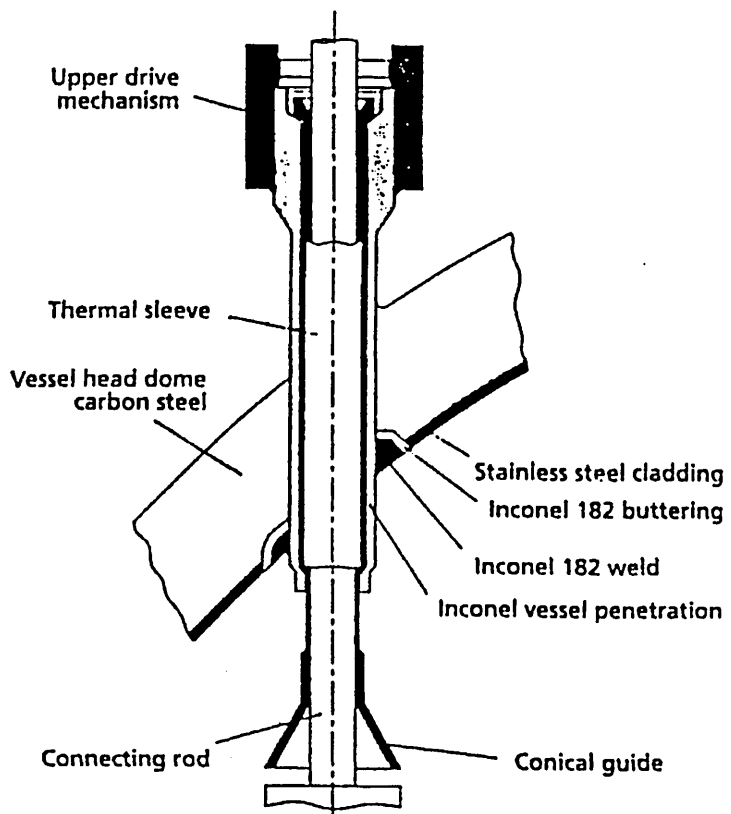
Figure 6. View of a single Reactor Vessel Head Penetration - showing cladding and weld areas where cracking has been found

Longitudinal cracks
radial azimuth

101mm

Counterbore 74mm
(nominal diameter 70mm)
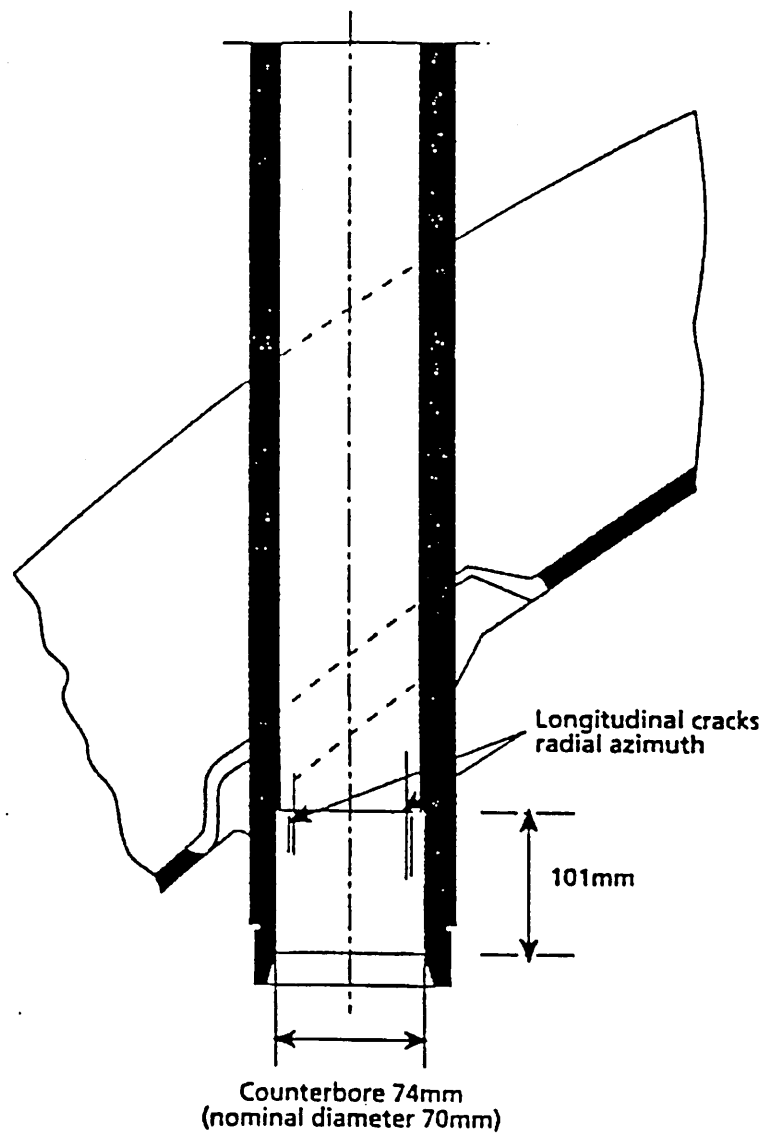
Figure 7. View of Reactor Vessel Head Penetration - indicating cracks which have been found are all longitudinal, from the inner diameter of the lower section of the adapter, under the weld, and propagating upwards towards the external part of the penetration.

7

Alloy	C	Cr	Ni	Fe	Ti	Si	Mn	P	S	Mo	Al	Co	Cu
690	0.018	30.05	59.10	9.55	0.39	0.39	0.41	0.100	0.002	0.01	0.30	<0.01	0.05
600	0.035	14.78	73.60	10.00	0.23	0.13	0.27	0.005	0.003	0.08	0.24	0.04	0.26
800	0.032	19.91	30.80	47.18	0.43	0.23	0.80	0.010	0.005	0.05	0.38	0.07	0.10

Table 1. Chemical composition of as-received steam generator tubing materials

Alloy	C	Cr	Ni	Fe	Ti	Si	Mn	P	S	Al	Co	Cu	Nb	Ta	B
182	0.03	20.78	70.60	2.56	0.35	0.11	2.95	0.003	0.005	0.099	<0.01	0.02	2.27	0.012	-
152	0.02	28.97	60.18	9.19	0.53	0.17	0.26	0.005	<0.01	0.640	0.02	<0.01	-	-	0.02

Table 2. Chemical composition of as-received weld consumable filler metals

Alloy	C	Cr	Ni	Fe	Si	Mn	P	S	Al	Co	Cu	Nb	N^2(ppm)
VMA	0.034	28.50	62	9.21	<0.10	<0.05	0	<0.003	0.06	<0.05	0	0.16	72
VMB	0.057	28.38	61.9	9.18	<0.10	<0.05	0	<0.003	0.07	<0.05	0	0.33	77

Table 3. Chemical composition of experimental alloy 690 type melts with Nb substitution for Ti.

8

NC program for manufacture of tensile specimens from material(s) in tubing form:

% (start of programme)

N1 G37 J3063 (canned cycle - wait to repeat)

N2 * TUBE TENSILE (comment)

N3 G71 G90 G00 X0 Y100 Z0 T0 M05 (absolute co-ordinates - rapid to datum)

N4 T1 (spindle on; coolant on - flood mode)

N5 X0 Y0 Z2 M03 S1075 (rapid lower to 2mm above tube - set spindle speed)

N6 X5 Y-9.5 (machining)

N7 GO1 Z-2.5 F30 M07 (machining)

N8 Y-16.5 (machining)

N9 X3 (machining)

N10 Y-28.5 (machining)

N11 X5 (machining)

N12 Y-35.5 (machining)

N13 G00 Z5 (rapid raise tool)

N14 X-5 (rapid move tool)

N15 G01 Z-2.5 (feed tool down)

N16 Y-28.5 (machining)

N17 X-3 (machining)

N18 Y-16.5 (machining)

N19 X-5 (machining)

N20 Y-9.5 (machining)

N21 G00 Z5 M8 (rapid raise tool)

N22 X0 Y100 Z0 T0 M05 (spindle off; coolant off; return to 100mm above datum)

N23 M30 C3063 (wait for restart button; repeat canned cycle)

% (end of programme)

Figure 8. CNC program for manufacture of CERT tensile samples
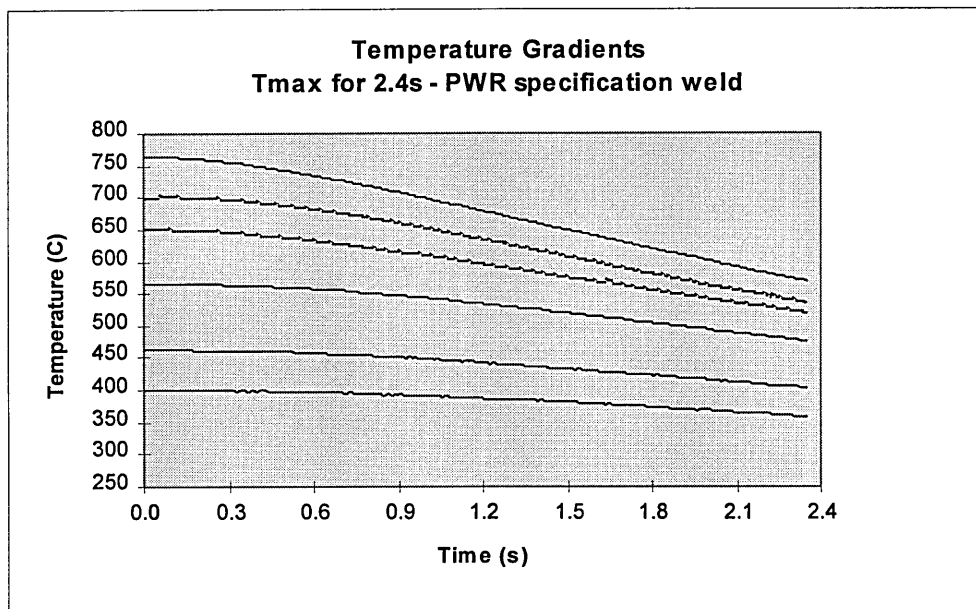
Figure 9. Graph of temperature profiles welding to PWR specifications
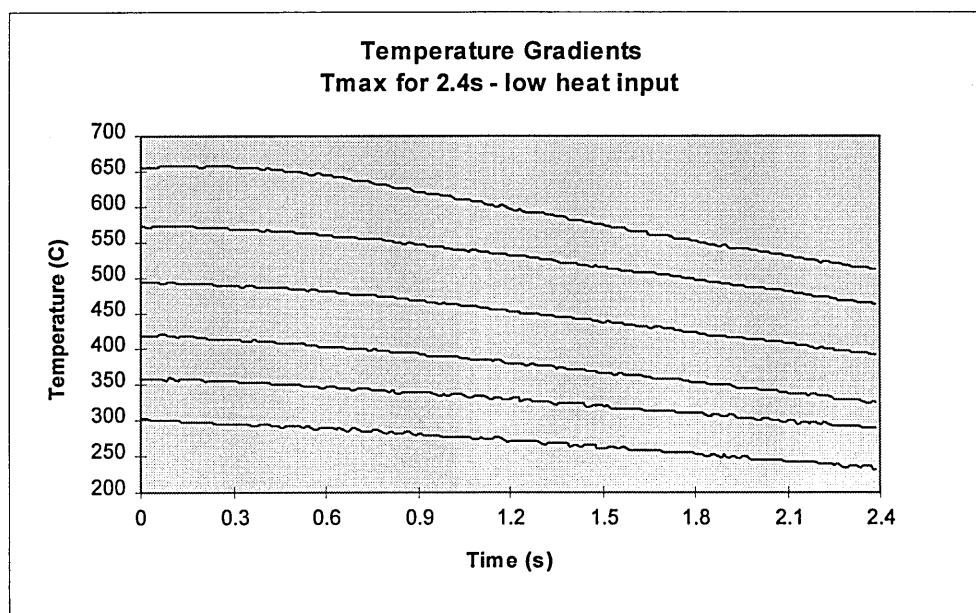
Figure 10. Graph of temperature profiles welding with lowered heat input
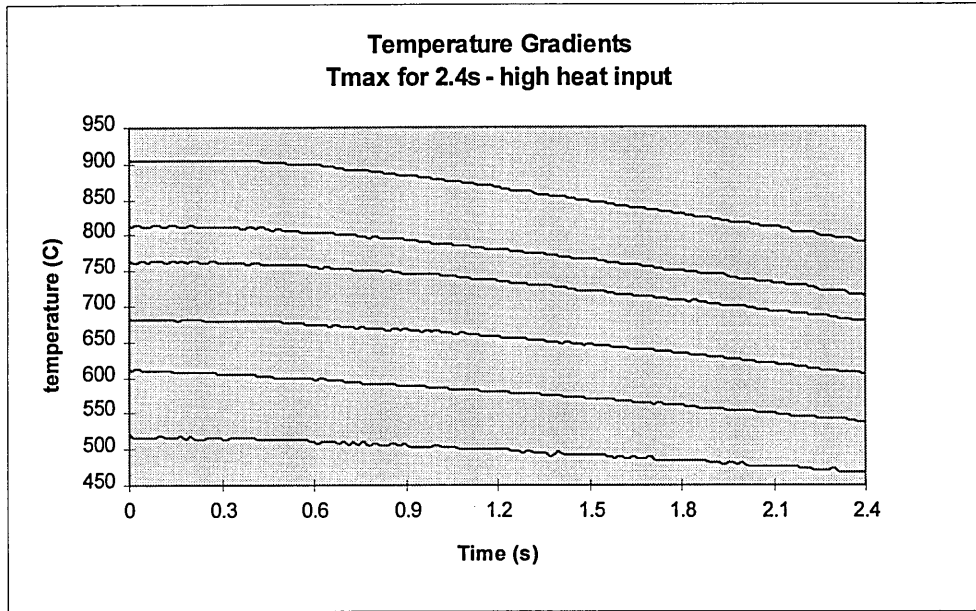
Figure 11. Graph of temperature profiles welding with increased heat input
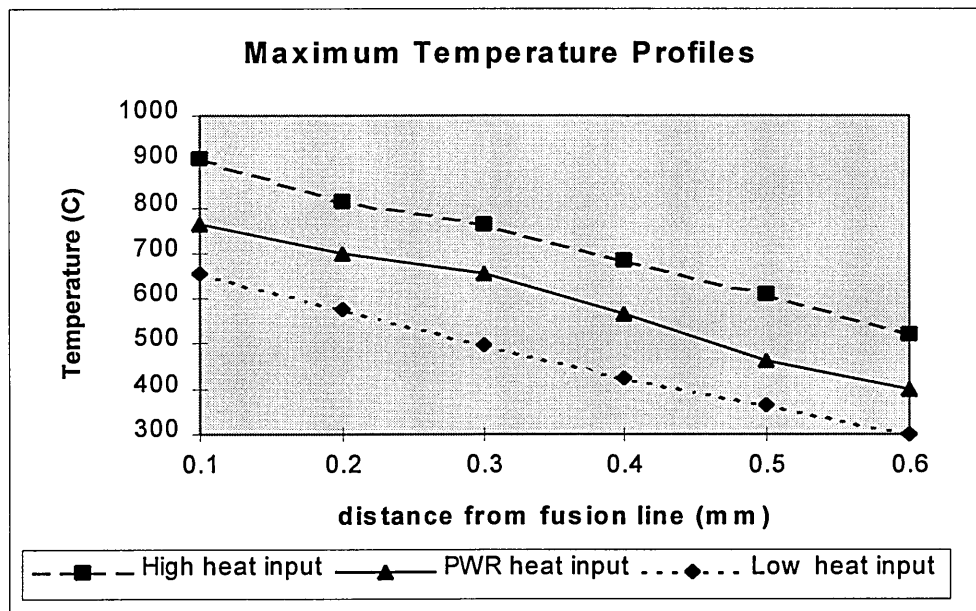
Figure 12. Graph of maximum temperature profiles with differing heat inputs
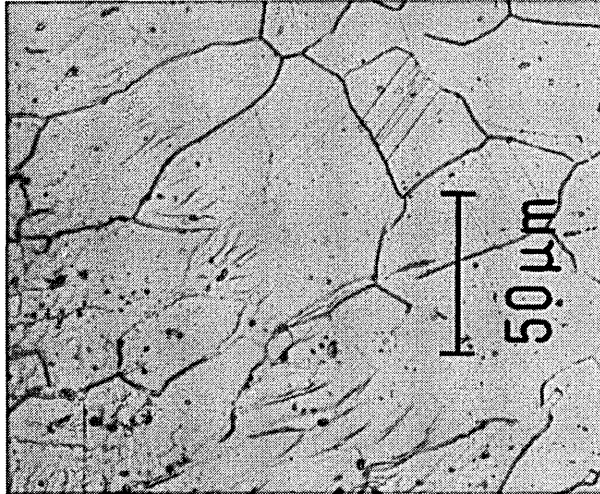
Figure 13. Laboratory welded Alloy 690 - PWR specification
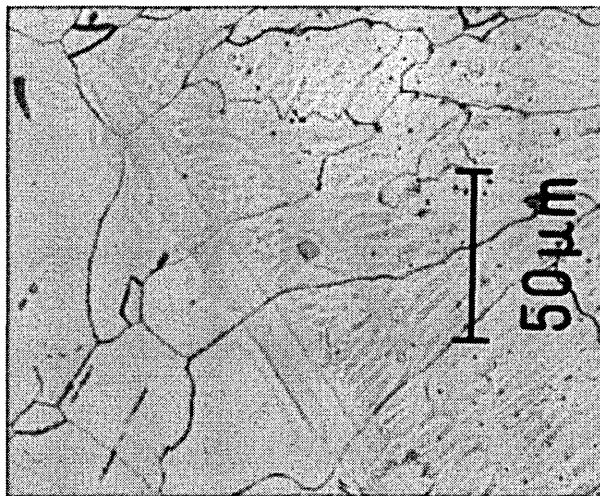

Figure 14. Archive S.G. Weld - Sizewell B project
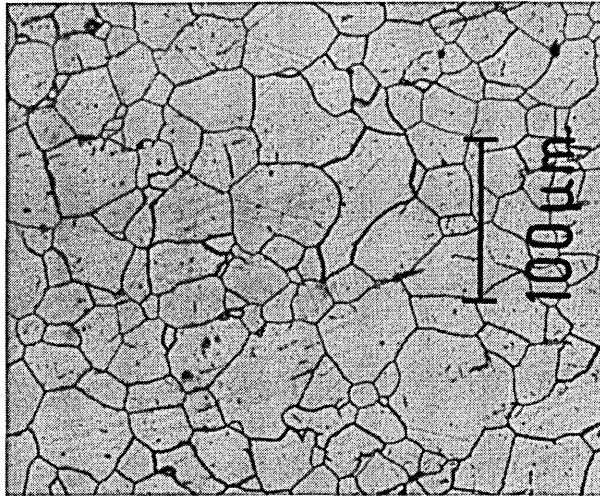
Figure 15. Alloy 690 - as received tubing material
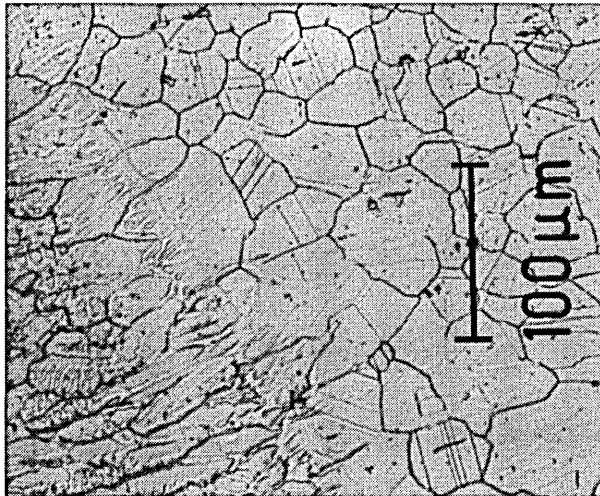
Figure 16. Alloy 690 welded to PWR specifications
but subjected to two weld thermal cycles

Figure 17. Alloy 690 welded with decreased heat input
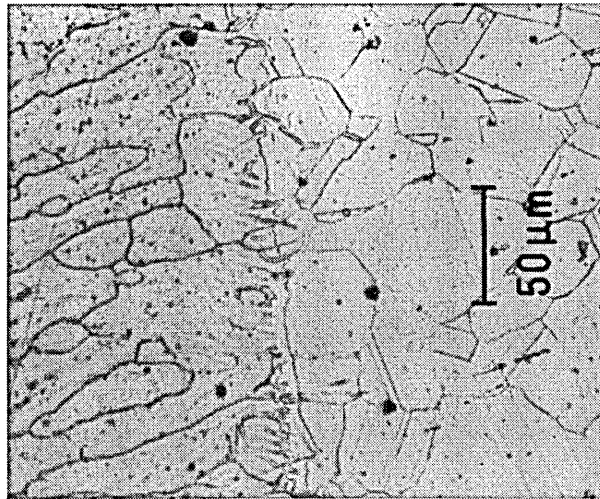
Figure 18. Alloy 690 welded with increased heat input

14
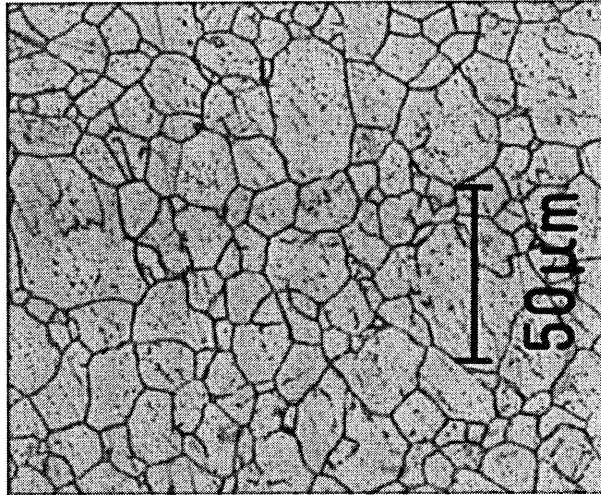
Figure 19. Alloy 600 - as received tubing material
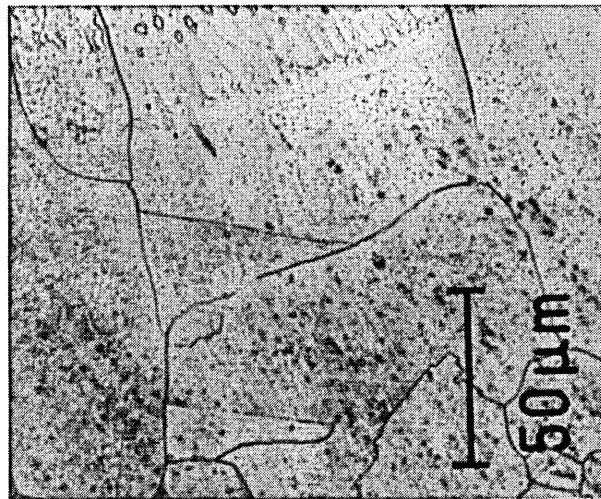
Figure 20. Alloy 600 welded to PWR specifications
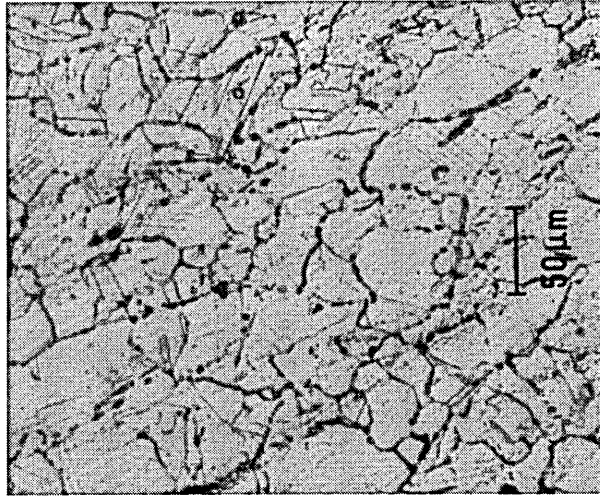
Figure 21. Alloy 800 - as received tubing material
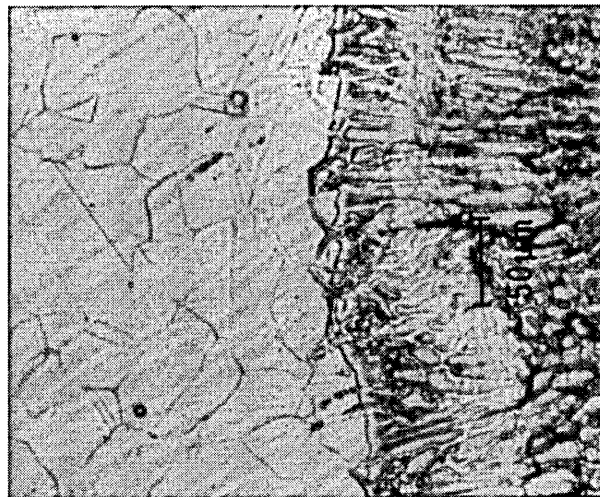

Figure 22. Alloy 800 welded to PWR specifications
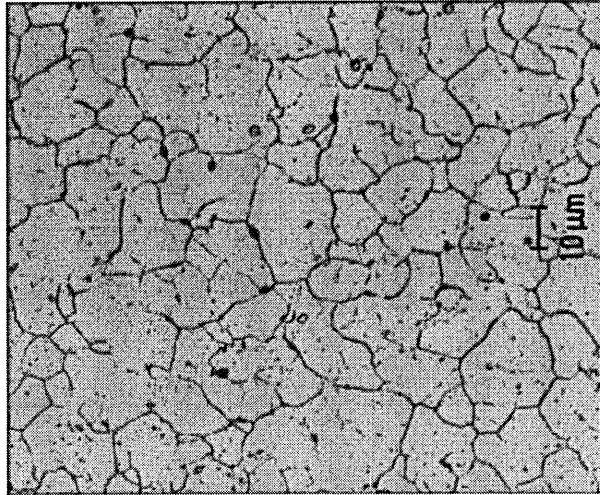
Figure 23. Experimental Melt VMA -STT condition
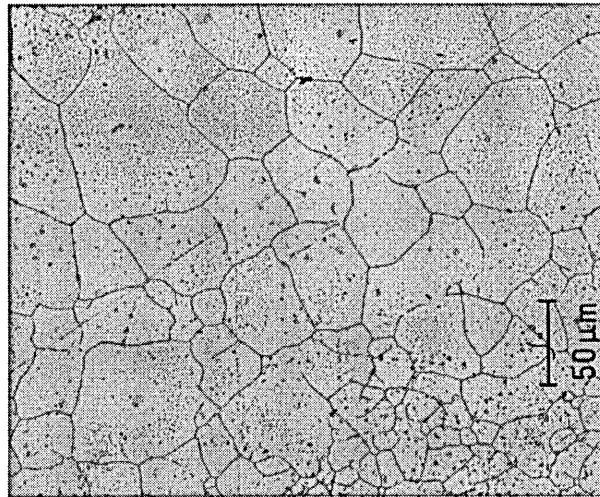
Figure 24. Experimental Melt VMA Welded to PWR specifications

17
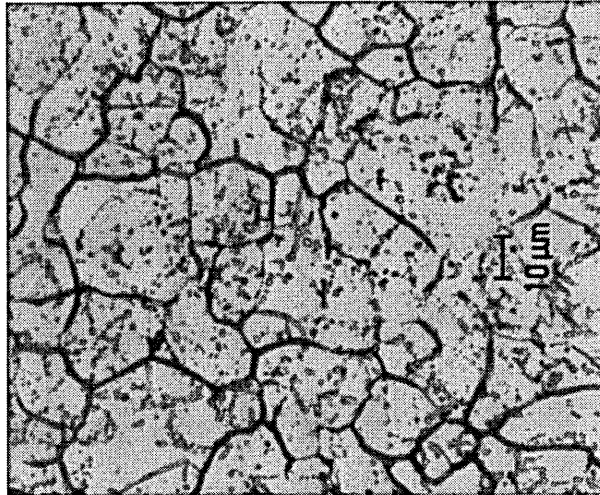
Figure 25. Experimental Melt VMB - STT condition
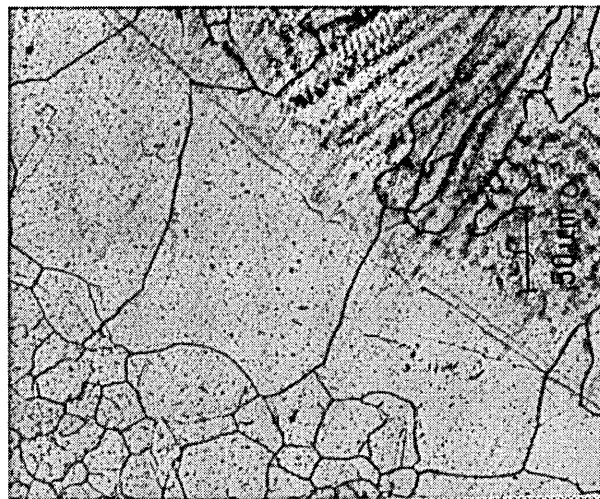
Figure 26. Experimental Melt VMB welded to PWR specifications

All HAZ Width Measurements in μm	
Sample	HAZ width
I690 PWR Spec	74
I690 Arch	74
I690/52	73
I690^Q	88
I690vQ	60
I690 Accel.	74
I690 2WTC	85
I600	70
I800	71
VMA	110
VMB	100

Key to Samples:

I690 PWR Spec = alloy 690 welded to PWR specifications

I690 Arch = alloy 690 archive weld from Sizewell B project

I690/52 = alloy 690 welded with alloy 52 cladding

I690^Q = alloy 690 welded with increased heat input

I690vQ = alloy 690 welded with decreased heat input

I690 Accel. = alloy 690 welded to spec. & aged (20yrs)

I690 2WTC = alloy 690 welded with 2 thermal cycles

I600 = alloy 600 welded to PWR specifications

I800 = alloy 800 welded to PWR specifications

VMA = experimental melt A welded to PWR specifications

VMB = experimental melt B welded to PWR specifications

Table 4. Heat Affected Zone Measurements

All Grain Size Measurements in µm		
Sample	Matrix	HAZ
I690 PWR Spec	35	45-60
I690 Arch	35	45-60
I690/52	35	45-60
I690^Q	35	45-62
I690vQ	35	45-60
I690 Accel.	35	45-60
I690 2WTC	35	45-60
I600	17	30-55
I800	40	45-60
VMA	15	35-60
VMB	15	35-50

Key to Samples:

I690 PWR Spec = alloy 690 welded to PWR specifications

I690 Arch = alloy 690 archive weld from Sizewell B project

I690/52 = alloy 690 welded with alloy 52 cladding

I690^Q = alloy 690 welded with increased heat input

I690vQ = alloy 690 welded with decreased heat input

I690 Accel. = alloy 690 welded to spec. & aged (20yrs)

I690 2WTC = alloy 690 welded with 2 thermal cycles

I600 = alloy 600 welded to PWR specifications

I800 = alloy 800 welded to PWR specifications

VMA = experimental melt A welded to PWR specifications

VMB = experimental melt B welded to PWR specifications

Table 5. Grain Size Measurements

All Grain Measurements in Vickers Microhardness				
Sample	Fusion Zone	Fusion Line	HAZ	Matrix
I690 PWR Spec	186	186	178	193
I690 Arch	184	186	180	192
I690/52	185	187	181	193
I690^Q	182	183	180	193
I690vQ	183	182	178	193
I690 Accel.	190	190	185	200
I690 2WTC	184	184	175	194
I600	201	180	177	203
I800	168	157	157	171
VMA	230	231	210	240
VMB	232	230	210	240

Key to Samples:

I690 PWR Spec = alloy 690 welded to PWR specifications

I690 Arch = alloy 690 archive weld from Sizewell B project

I690/52 = alloy 690 welded with alloy 52 cladding

I690^Q = alloy 690 welded with increased heat input

I690vQ = alloy 690 welded with decreased heat input

I690 Accel. = alloy 690 welded to spec. & aged (20yrs)

I690 2WTC = alloy 690 welded with 2 thermal cycles

I600 = alloy 600 welded to PWR specifications

I800 = alloy 800 welded to PWR specifications

VMA = experimental melt A welded to PWR specifications

VMB = experimental melt B welded to PWR specifications

Table 6. Microhardness Measurements

21

Heat input -v- HAZ Width		
Sample	J/mm	HAZ Width
I690^Q	523	88
I690 PWR spec	371	74
I690vQ	226	60
Key to Samples:		
I690^Q = alloy 690 welded with increased heat input		
I690 PWR Spec = alloy 690 welded to PWR specifications		
I690vQ = alloy 690 welded with decreased heat input		

Table 7. Data on weld heat input vs. width of HAZ in Alloy 690 samples
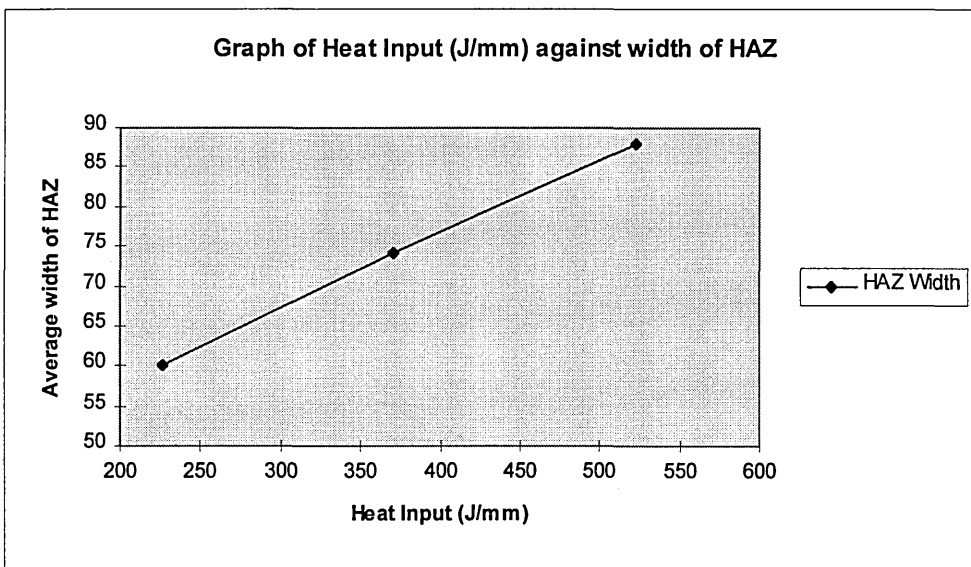
Figure 27. Graph of effect of heat input on HAZ width in Alloy 690 specimens
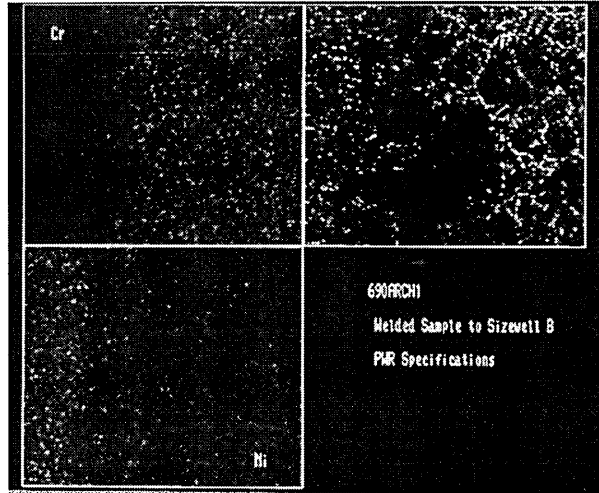
Figure 28. Ni and Cr maps of I690 welded to PWR specifications
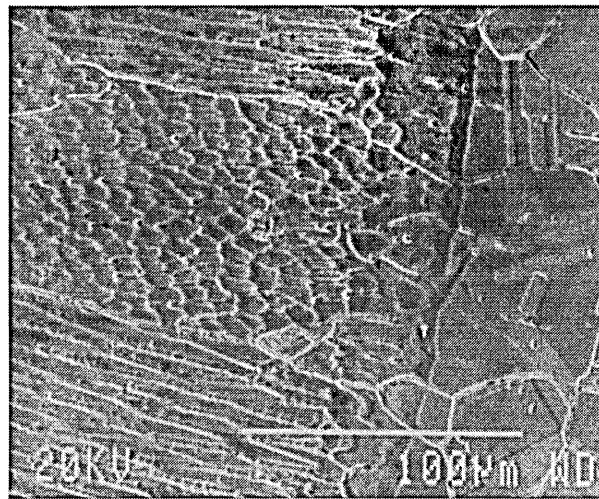
Figure 29. Microstructure across typical weld sample

23
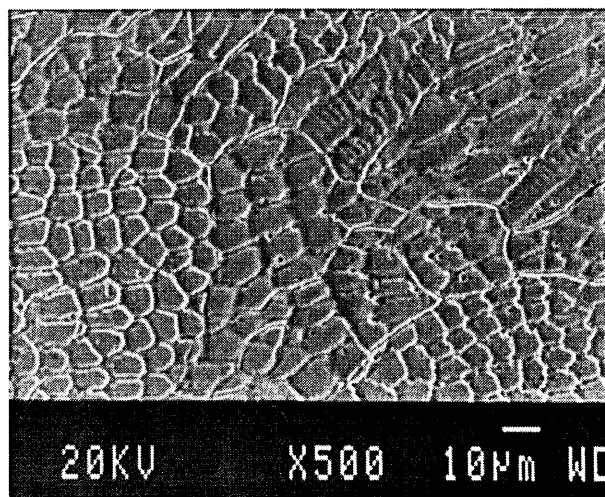
Figure 30. Fusion zone weld microstructure
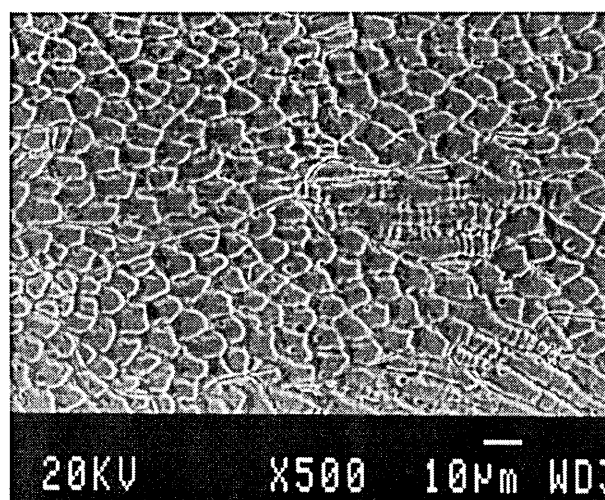
Figure 31. Fusion zone weld microstructure

Alloy 690 sample laboratory welded to PWR specifications with alloy 82 cladding							
EDX Quantitative Analysis - all figures are normalised %ages element present							
Element	Al	Si	Nb	Cr	Mn	Fe	Ni	Ti
FA Intragranular	0.01	0.22	1.19	24.3	2.01	6.28	65.5	0.50
FA Grain Boundary	0.00	0.25	1.64	23.8	2.26	5.86	65.5	0.62
HAZ Intragranular	0.00	0.23	0.16	30.4	0.29	9.39	59.2	0.25
HAZ Grain Boundary	0.01	0.24	0.32	29.1	0.44	9.39	60.7	0.09
Matrix Intragranular	0.00	0.30	0.11	30.0	0.55	9.42	59.4	0.25
Matrix Grain Boundary	0.04	0.30	0.00	33.2	0.39	8.79	57.0	0.31
Key: FA = Fusion Zone; HAZ = Heat Affected Zone; Matrix = Unaffected Zone							

Table 8. EDX analysis: Alloy 690 welded to PWR specifications

Alloy 690 welded sample - archive material from Sizewell B PWR							
EDX Quantitative Analysis - all figures are normalised %ages element present							
Element	Al	Si	Nb	Cr	Mn	Fe	Ni	Ti
FA Intragranular	0.01	0.24	1.57	26.2	1.23	6.17	64.5	0.47
FA Grain Boundary	0.02	0.25	1.23	24.4	1.34	5.44	64.5	0.63
HAZ Intragranular	0.01	0.25	0.18	29.9	0.35	9.22	60.3	0.25
HAZ Grain Boundary	0.01	0.22	0.27	30.1	0.33	9.22	61.3	0.08
Matrix Intragranular	0.01	0.31	0.14	30.2	0.43	9.31	60.3	0.25
Matrix Grain Boundary	0.02	0.30	0.01	32.5	0.47	9.07	56.7	0.33
Key: FA = Fusion Zone; HAZ = Heat Affected Zone; Matrix = Unaffected Zone							

Table 9. EDX Analysis: Alloy 690 archive weld from Sizewell B

Alloy 690 sample laboratory welded to PWR specifications - 2 weld cycles								
EDX Quantitative Analysis - all figures are normalised %ages element present								
Element	Al	Si	Nb	Cr	Mn	Fe	Ni	Ti
FA Intragranular	0.01	0.33	0.25	28.5	0.78	8.67	61.2	0.22
FA Grain Boundary	0.00	0.42	0.40	28.7	0.75	8.62	61.0	0.28
HAZ Intragranular	0.00	0.44	0.09	30.1	0.57	9.20	59.2	0.36
HAZ Grain Boundary	0.11	0.49	0.00	30.4	0.31	9.34	59.0	0.30
Matrix Intragranular	0.14	0.46	0.00	30.5	0.36	9.21	59.2	0.23
Matrix Grain Boundary	0.01	0.41	0.40	33.5	0.41	9.01	55.6	0.36
Key: FA = Fusion Zone; HAZ = Heat Affected Zone; Matrix = Unaffected Zone								

Table 10. EDX analysis: Alloy 690 welded to PWR specifications - 2 weld thermal cycles

Alloy 690 sample laboratory welded to PWR specs & accelerated aged (20yrs)								
EDX Quantitative Analysis - all figures are normalised %ages element present								
Element	Al	Si	Nb	Cr	Mn	Fe	Ni	Ti
FA Intragranular	0.09	0.30	1.32	23.3	1.98	5.00	67.5	0.32
FA Grain Boundary	0.02	0.30	1.32	23.4	1.88	5.14	67.6	0.30
HAZ Intragranular	0.03	0.46	0.03	30.3	0.43	9.23	59.1	0.29
HAZ Grain Boundary	0.04	0.51	0.00	30.3	0.47	9.23	59.6	0.25
Matrix Intragranular	0.04	0.42	0.05	30.2	0.40	9.38	59.1	0.28
Matrix Grain Boundary	0.03	0.50	0.00	32.3	0.48	8.95	57.2	0.24
Key: FA = Fusion Zone; HAZ = Heat Affected Zone; Matrix = Unaffected Zone								

Table 11. EDX analysis: Alloy 690 welded to PWR specifications - Accelerated aged (20 yrs)

Alloy 690 welded sample - increased heat input								
EDX Quantitative Analysis - all figures are normalised %ages element present								
Element	Al	Si	Nb	Cr	Mn	Fe	Ni	Ti
FA Intragranular	0.04	0.25	2.00	21.6	2.40	4.53	67.7	0.42
FA Grain Boundary	0.08	0.25	1.85	21.9	2.40	4.50	67.7	0.36
HAZ Intragranular	0.01	0.37	0.05	30.3	0.40	9.28	59.3	0.26
HAZ Grain Boundary	0.04	0.52	0.03	30.4	0.40	9.05	59.1	0.26
Matrix Intragranular	0.02	0.44	0.05	30.3	0.37	9.17	59.3	0.29
Matrix Grain Boundary	0.06	0.50	0.05	33.0	0.35	8.94	56.8	0.24
Key: FA = Fusion Zone; HAZ = Heat Affected Zone; Matrix = Unaffected Zone								

Table 12. EDX analysis: Alloy 690 welded with increased heat input

Alloy 690 welded sample - decreased heat input								
EDX Quantitative Analysis - all figures are normalised %ages element present								
Element	Al	Si	Nb	Cr	Mn	Fe	Ni	Ti
FA Intragranular	0.06	0.27	1.93	22.5	2.00	6.39	66.5	0.33
FA Grain Boundary	0.03	0.23	1.48	23.6	1.80	6.65	66.1	0.33
HAZ Intragranular	0.01	0.40	0.05	30.6	0.46	9.21	59.0	0.26
HAZ Grain Boundary	0.01	0.41	0.02	30.5	0.37	9.28	58.9	0.23
Matrix Intragranular	0.04	0.43	0.04	30.4	0.35	9.35	59.2	0.23
Matrix Grain Boundary	0.00	0.46	0.04	31.4	0.48	9.00	58.1	0.33
Key: FA = Fusion Zone; HAZ = Heat Affected Zone; Matrix = Unaffected Zone								

Table 13. EDX analysis: Alloy 690 welded with decreased heat input

Alloy 600 sample - welded to PWR specifications								
EDX Quantitative Analysis - all figures are normalised %ages element present								
Element	Al	Si	Nb	Cr	Mn	Fe	Ni	Ti
FA Intragranular	0.06	0.28	1.10	17.8	1.35	6.85	72.4	0.26
FA Grain Boundary	0.12	0.35	1.43	17.7	1.50	6.66	71.6	0.33
HAZ Intragranular	0.19	0.25	0.09	16.4	0.47	9.05	73.4	0.17
HAZ Grain Boundary	0.22	0.26	0.13	17.0	0.34	9.33	75.0	0.26
Matrix Intragranular	0.20	0.29	0.29	16.2	0.47	9.04	73.3	0.20
Matrix Grain Boundary	0.31	0.32	0.27	16.9	0.46	9.12	72.3	0.19
Key: FA = Fusion Zone; HAZ = Heat Affected Zone; Matrix = Unaffected Zone								

Table 14. EDX analysis: Alloy 600 welded to PWR specifications

Alloy 800 sample - welded to PWR specifications								
EDX Quantitative Analysis - all figures are normalised %ages element present								
Element	Al	Si	Nb	Cr	Mn	Fe	Ni	Ti
FA Intragranular	0.10	0.17	1.40	19.8	1.36	30.0	47.9	0.27
FA Grain Boundary	0.10	0.27	1.40	19.3	1.99	26.4	44.7	0.49
HAZ Intragranular	0.21	0.25	0.03	20.2	0.90	46.6	30.8	0.35
HAZ Grain Boundary	0.17	0.22	0.03	20.3	0.85	46.9	30.9	0.37
Matrix Intragranular	0.19	0.20	0.01	20.3	0.85	46.9	30.9	0.36
Matrix Grain Boundary	0.23	0.22	0.01	20.6	0.83	46.6	30.5	0.37
Key: FA = Fusion Zone; HAZ = Heat Affected Zone; Matrix = Unaffected Zone								

Table 15. EDX analysis: Alloy 800 welded to PWR specifications

Experimental melt A - welded to PWR specifications								
EDX Quantitative Analysis - all figures are normalised %ages element present								
Element	Al	Si	Nb	Cr	Mn	Fe	Ni	Ti
FA Intragranular	0.05	0.10	1.11	23.2	1.80	7.49	66.2	0.19
FA Grain Boundary	0.03	0.08	1.33	23.1	2.01	7.24	65.8	0.23
HAZ Intragranular	0.06	0.10	0.13	29.7	0.10	9.12	60.6	0.02
HAZ Grain Boundary	0.08	0.11	0.09	29.1	0.03	9.30	61.1	0.01
Matrix Intragranular	0.09	0.07	0.15	28.4	0.01	9.50	61.8	0.02
Matrix Grain Boundary	0.07	0.08	0.16	28.8	0.01	9.50	61.2	0.01
Key: FA = Fusion Zone; HAZ = Heat Affected Zone; Matrix = Unaffected Zone								

Table 16. EDX analysis: experimental melt A - welded to PWR specifications

Experimental melt B - welded to PWR specifications								
EDX Quantitative Analysis - all figures are normalised %ages element present								
Element	Al	Si	Nb	Cr	Mn	Fe	Ni	Ti
FA Intragranular	0.05	0.09	1.13	23.8	1.85	6.15	66.5	0.21
FA Grain Boundary	0.08	0.09	1.00	23.8	1.74	6.40	66.7	0.13
HAZ Intragranular	0.04	0.04	0.23	28.5	0.08	9.43	61.2	0.02
HAZ Grain Boundary	0.03	0.06	0.24	28.0	0.08	9.50	62.2	0.00
Matrix Intragranular	0.06	0.05	0.20	28.5	0.07	9.50	62.0	0.02
Matrix Grain Boundary	0.07	0.10	0.24	29.0	0.03	9.20	61.2	0.00+
Key: FA = Fusion Zone; HAZ = Heat Affected Zone; Matrix = Unaffected Zone								

Table 17. EDX analysis: experimental melt B - welded to PWR specifications

Alloy 690 sample welded to PWR specifications using Alloy 52 weld consumable								
EDX Quantitative Analysis - all figures are normalised %ages element present								
Element	Al	Si	Nb	Cr	Mn	Fe	Ni	Ti
FA Intragranular	0.13	0.26	0.01	29.5	0.36	10.0	58.7	0.45
FA Grain Boundary	0.13	0.26	0.00	30.0	0.32	10.2	58.7	0.35
HAZ Intragranular	0.02	0.38	0.02	30.3	0.31	9.30	59.3	0.26
HAZ Grain Boundary	0.08	0.29	0.03	30.0	0.34	9.90	59.1	0.25
Matrix Intragranular	0.01	0.33	0.02	30.1	0.30	9.30	59.5	0.27
Matrix Grain Boundary	0.00	0.38	0.01	30.5	0.40	9.24	59.0	0.26
Key: FA = Fusion Zone; HAZ = Heat Affected Zone; Matrix = Unaffected Zone								

Table 18. EDX analysis: Alloy 690 welded with alloy 52 cladding to PWR specifications
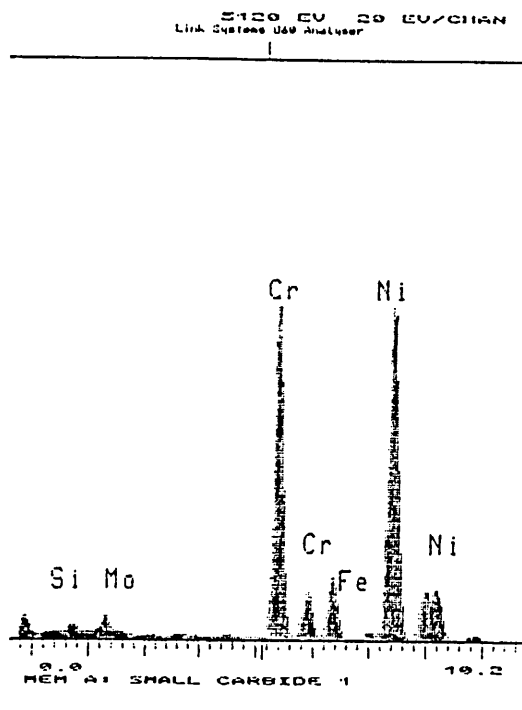
Figure 32. Spectrum of Cr rich grain boundary carbide - STT alloy 690 matrix

30
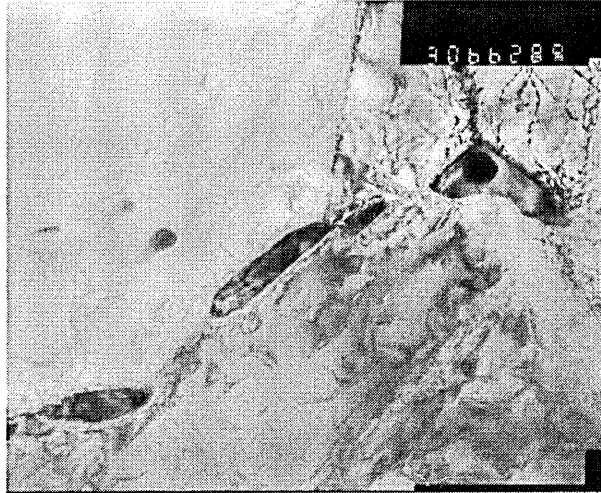
Figure 33. Grain boundary carbides - alloy 690 matrix:
66K mag. bright field image.
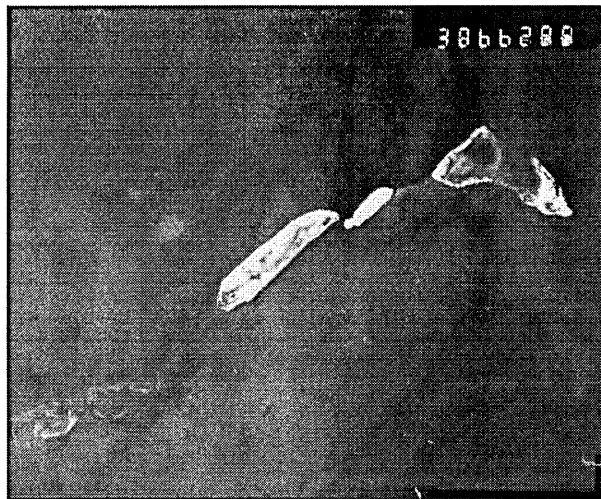
Figure 34. Grain boundary carbides - alloy 690 matrix:
66K mag. dark field image.
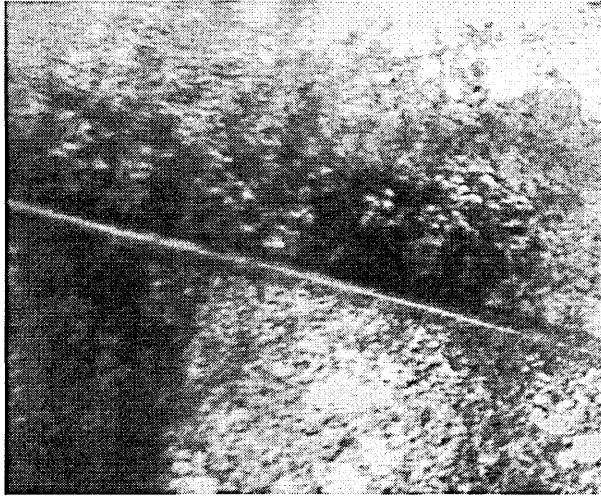
Figure 35. Precipitate free grain boundary in HAZ of Alloy 690 welded to PWR spec. - 66Kmag.

Figure 36. NbCN intragranular particle in HAZ of experimental melt A - 115K mag.
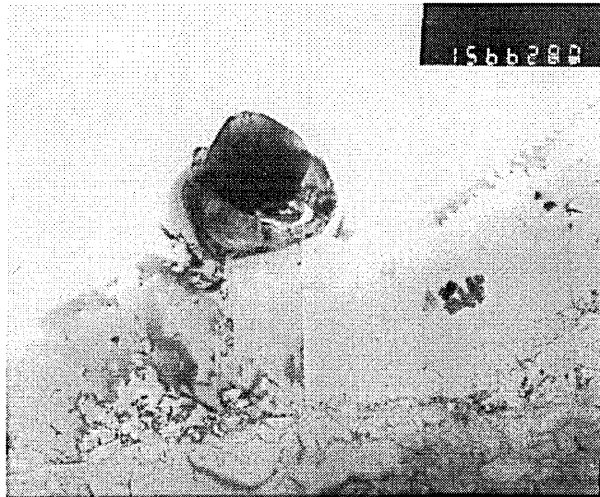
Figure 37. TiCN intragranular particle in HAZ of Alloy 690
welded to PWR spec. - 88K mag.
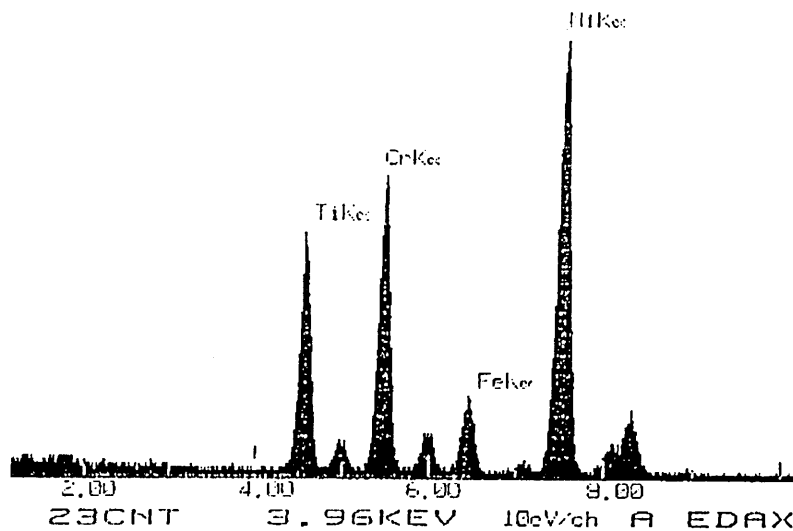
Figure 38. Spectra of intragranular Ti rich inclusion in HAZ of I690 - TiCN

33
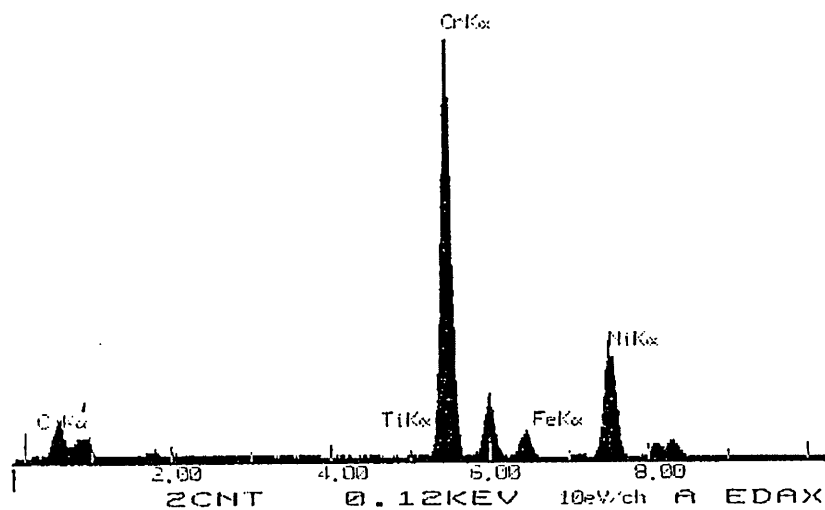
Figure 39. Spectra from Alloy 690 matrix: grain boundary $Cr_{23}C_6$ precipitate
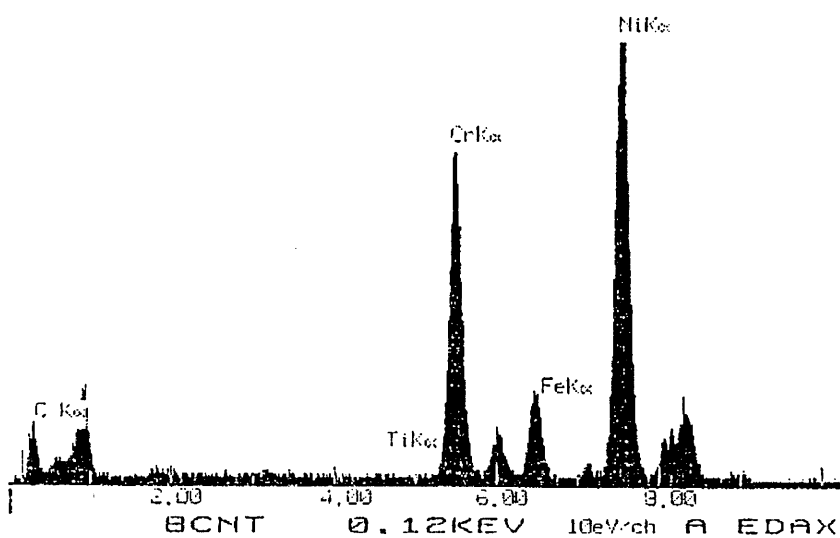
Figure 40. Spectra from welded Alloy 690: precipitate free grain boundary region in HAZ
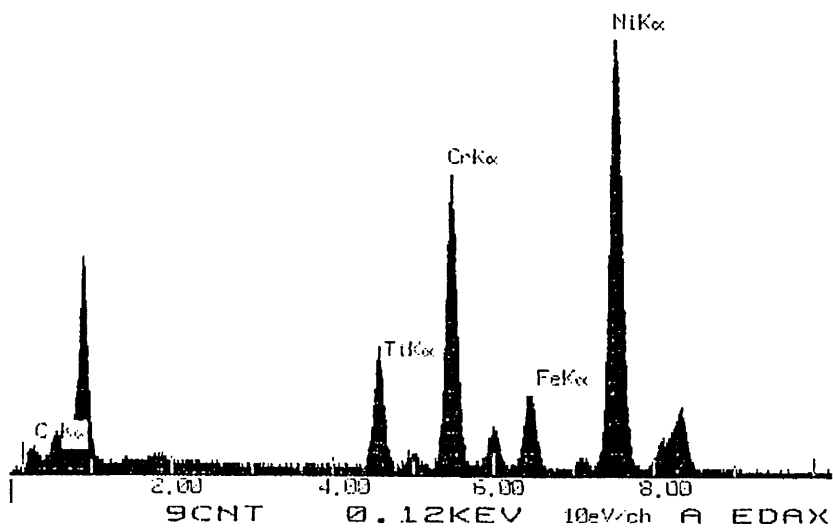
Figure 41. Spectra from welded Alloy 690: intragranular TiCN in HAZ
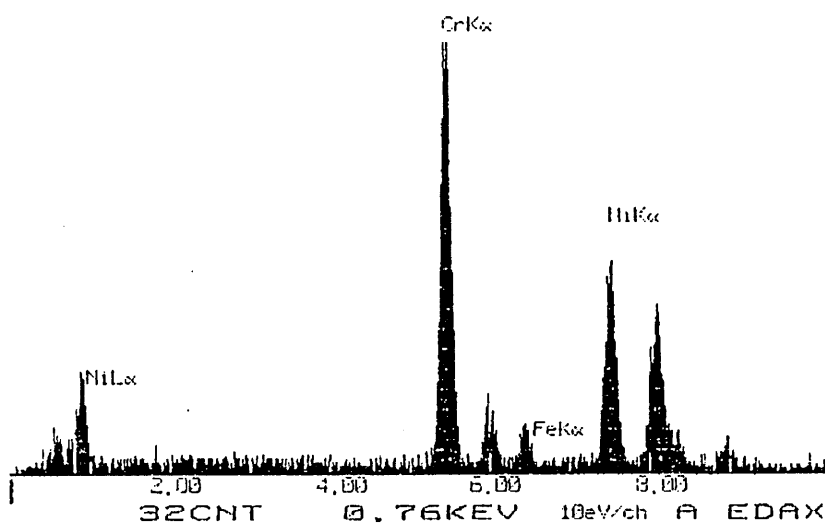
Figure 42. Spectra from Alloy 600 matrix: grain boundary $Cr_{23}C_6$ grain boundary precipitate
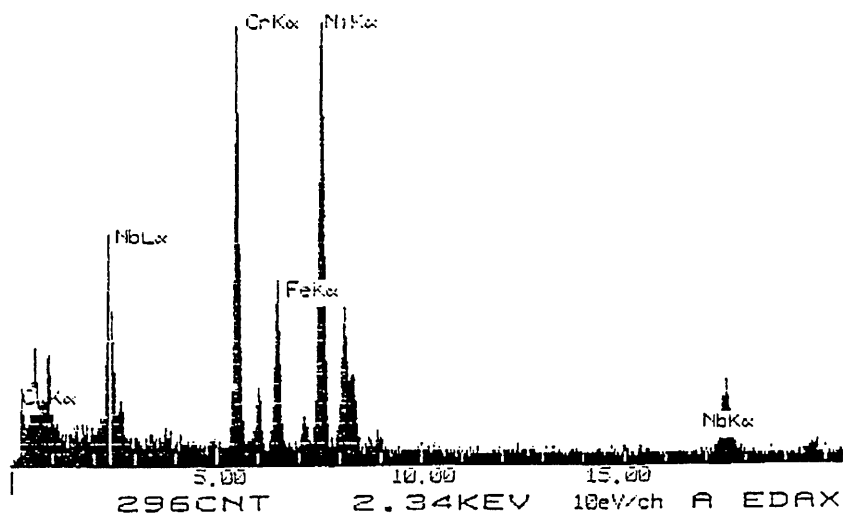
Figure 43. Spectra from welded experimental melt A: intragranular NbCN in HAZ
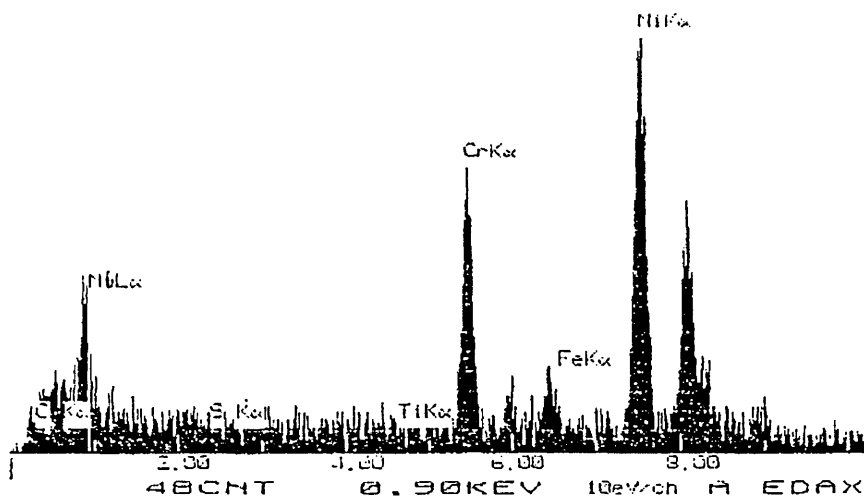

Figure 44. Spectra from welded experimental melt B: intragranular NbCN in HAZ

Modified Huey Test Results			
Sample	Fusion Zone	HAZ	Matrix
I690 PWR Spec	NA	NA	NA
I690 Arch	NA	NA	NA
I690/52	NA	NA	NA
I690^Q	NA	NA	NA
I690vQ	NA	NA	NA
I690 Accel.	NA	NA	NA
I690 2WTC	NA	NA	NA
I600	NA	LA	NA
I800	LA	SA	SA
VMA	NA	NA	NA
VMB	NA	NA	NA

NA = No Attack; LA = Light Attack; SA = Severe Attack

Key to Samples:

I690 PWR Spec = alloy 690 welded to PWR specifications

I690 Arch = alloy 690 archive weld from Sizewell B project

I690/52 = alloy 690 welded with alloy 52 cladding

I690^Q = alloy 690 welded with increased heat input

I690vQ = alloy 690 welded with decreased heat input

I690 Accel. = alloy 690 welded to spec. & aged (20yrs)

I690 2WTC = alloy 690 welded with 2 thermal cycles

I600 = alloy 600 welded to PWR specifications

I800 = alloy 800 welded to PWR specifications

VMA = experimental melt A welded to PWR specifications

VMB = experimental melt B welded to PWR specifications

Table 19. Results from Modified Huey Tests
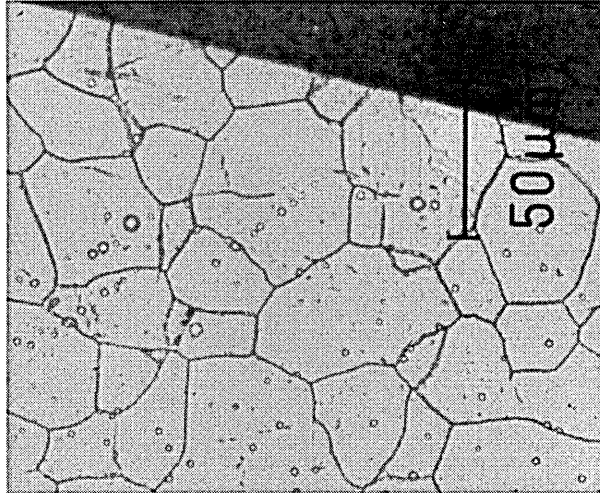
Figure 45. Modified Huey Test: Alloy 690 sample with no visible corrosive attack
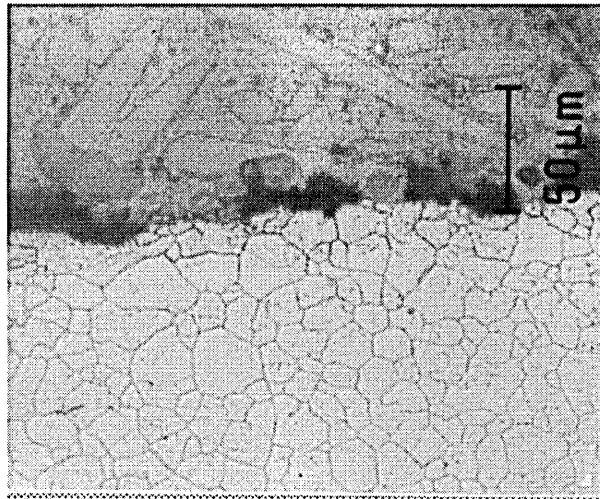
Figure 46. Modified Huey Test: Alloy 600 sample showing light attack at tube edge
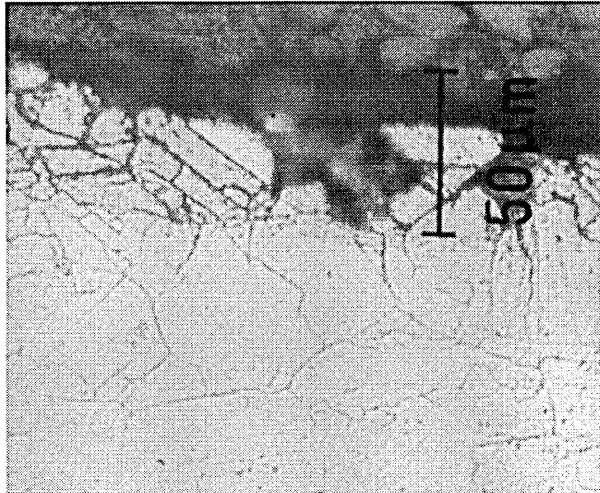
Figure 47. Modified Huey Test: Alloy 800 sample with severe corrosive attack
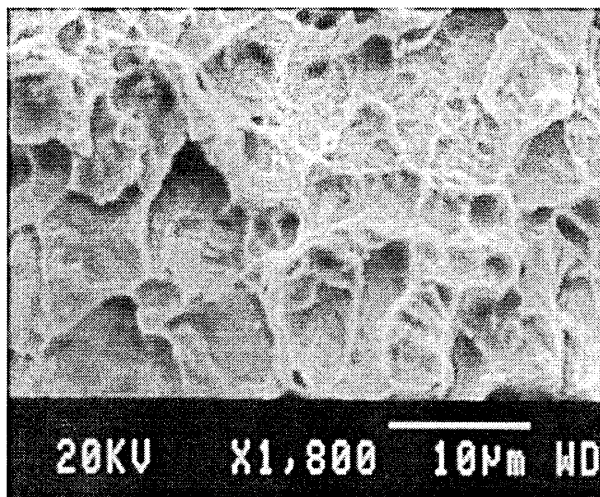
Figure 48. SEM micrograph of welded Alloy 690 sample fracture surface after CERT test
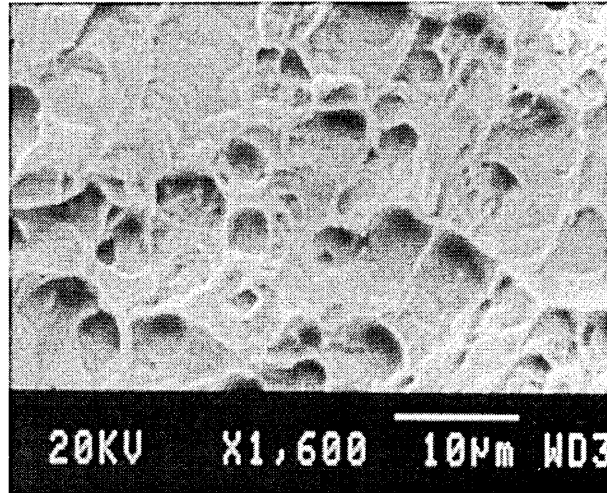
Figure 49. SEM micrograph of unwelded Alloy 690 sample fracture surface after CERT test

CERT Test Results - Mechanical Properties		
Environment: 320°C in Argon at 1.5 atmospheres - Strain rate $7x10^{-5}s^{-1}$		
Sample	0.2% Yield Strength	UTS (MPa)
Welded PWR Specification (test 1)	292	552
Welded PWR Specification (test2)	302	558
Welded PWR Specification (test 3)	285	538
Unwelded Archive Tube (test 1)	280	597
Unwelded Archive Tube (test 2)	311	620
Unwelded Archive Tube (test 3)	326	603

Comparative data from findings of Smith on archive Alloy 690 tubing material from Sizewell B project Standard Tensile Test Data at Ambient Temperature and Pressure ($\approx 20°C$ at 1 Atmosphere in Air)		
As received Archive tube from Sizewell B	335	736

Table 20. CERT Test Mechanical Property Results and Comparative Data

| Volume Fraction Precipitates - all figures percentage values		
Sample	**Regions**	
	Fusion line to HAZ Centre	Centre HAZ to Matrix
I690 PWR	0.01	0.17
I690 Arch	0.00	0.05
I690/52	0.00	0.28
I690^Q	0.00	0.11
I690vQ	0.03	1.41
I690 Accel.	0.12	0.30
I690 2WTC	0.00	0.02
I600	0.13	0.46
I800	0.05	0.35
VMA	0.05	0.05
VMB	0.00	0.01

Table 21. Volume Fraction Precipitate Results
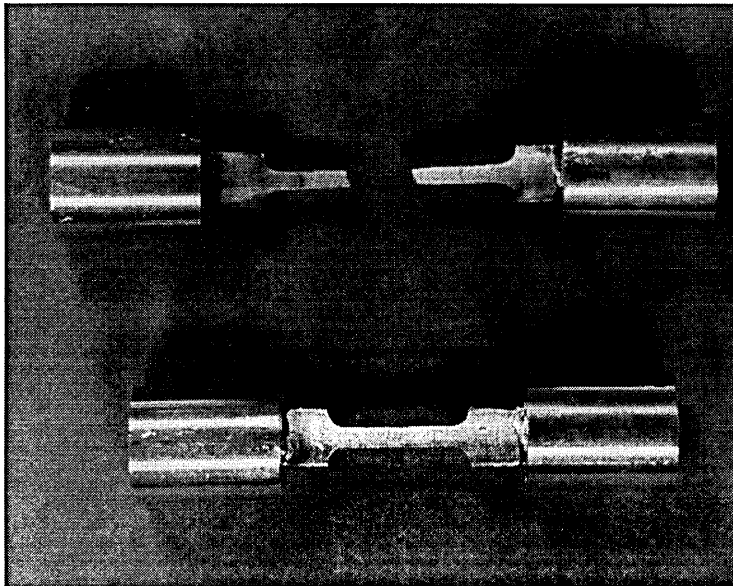
Figure 50. CERT sample before and after testing